WAVE COMPONENT IDENTIFICATION FROM SHALLOW WATER WAVES

GRACIE WATTS

WAVE COMPONENT IDENTIFICATION FROM SHALLOW WATER WAVES

by

©Gracie Watts, B.Eng.

A thesis submitted to the

School of Graduate Studies

in partial fulfillment of the requirements for the degree of

Master of Engineering

Faculty of Engineering and Applied Science

Memorial University of Newfoundland

2012

St. John's Newfoundland

ABSTRACT

The aim of this work was to develop a numerical program to decompose shallow water waves in order to properly analyze the wave induced forces on ocean vessels. The program was used in conjunction with waves generated in a model tank environment. The program identified the known waves in the tank and removed unwanted wave elevations created by imperfect model tank conditions. This will enable model testing and numerical modeling to more accurately analyze wave-ship interaction, thus improving design and prediction for vessels operating in shallow water regions.

A literature review discusses the theories required in order to create a wave splitting tool as well as the theory used to simulate the theoretical set-down wave. The results were validated in the time and frequency domain against a report from Maritime Research Institute Netherlands (MARIN) and the National Research Council (NRC) results, respectively. Results were generally acceptable; test cases became less favorable as wave frequency decreased. Potential future work on this topic includes using improved input wave data to compute wave-induced forces on vessels.

ACKNOWLEDGEMENTS

The author wishes to express sincere appreciation to Dr. Heather Peng and Dr. Wei Qui for their assistance in the preparation of this thesis. I would also like to thank the CREATE program for their assistance in funding.

As well I would like to thank Dr. Zaman for his assistance in obtaining the data to use for my trial cases in my thesis as well as results which enabled me to validate my results.

I would also like to thank Steve Forward for his helpful suggestions and preparation of my thesis. His constant support throughout the entire process of this research has been a tremendous help. Finally I would like to thank my family for their patience and support during the length of my study.

TABLE OF CONTENTS

Abstract i

Acknowledgements ii

Table of Contents iii

List of Tables v

List of Figures vi

List of Appendices x

1. Introduction 1

    1.1. Statement of Problem 1

    1.2. Thesis Structure 4

    1.3. Review of Literature 6

2. Theories 12

    2.1. Digital Methods 12

    2.2. Fourier Series 21

    2.3. Spectral Analysis 36

    2.4. Wave Splitting Theory 44

    2.5. Analytical Model of Wave Set-down 52

    2.6. Power Spectrum Estimation 56

3. Wave Generation 59

    3.1. Wave Generation Introduction 59

    3.2. Piston Type Wave Maker 60

    3.3. Basin Test Configuration 62

3.4. Physical Modeling 64

4. Computational Method 65

4.1. Band-pass Filter 65

4.2. Fast Fourier Transform 67

4.3. Newton-Raphson Method 72

4.4. Singular Value Decomposition 73

4.5. Wave Splitting Program 75

5. Results 78

5.1. Validation 78

5.2. OEB Results 85

5.3. First Order Versus Second Order Wave Generation 97

5.4. Discussion 106

6. Conclusion and Recommendations 112

References 114

LIST OF TABLES

Table 5.1 –Parameters of Model Scale and Full Scale 85

Table 5.2 –Percent Difference between Measured and Theoretical Set-down Wave 107

LIST OF FIGURES

Figure 1.1 – Wave Set-down Comparison between Shallow and Deep Water (Van Dijk 2007) 2

Figure 1.2 – Wave group versus the wave set-down (Hansen et. al. 1980) 7

Figure 2.1– Sinusoidal Wave (Beauchamp and Yen, 1973, p. 3) 13

Figure 2.2 – Wave Spectrum (Voogt 2005) 36

Figure 2.3 – A two sided line spectrum (National Instrument, 2009) 42

Figure 2.4 - Flow Diagram of Steps for Use of Wave Splitting (Dijk 2007) 51

Figure 3.1 – Piston type wave maker (Wavemaker) 60

Figure 3.2 - NRC Ocean Engineering Basin (OEB) 62

Figure 3.3 – Positions of the Fourteen Wave Probes Within the OEB. 63

Figure 4.1 – Jonswap Spectral Density Plot (Wave Spectra, FORMSYS) 65

Figure 4.2 – Decomposition of a 16 Point Signal (Smith 1997) 67

Figure 4.3 – Bit reversing algorithm (Smith 1997) 68

Figure 4.4 – Reconstructing signals in the time and frequency domain (Smith 1997) 69

Figure 4.5 – The Butterfly Calculation (Smith 1997) 70

Figure 4.6 – Total FFT Procedure (Smith 1997) 71

Figure 4.7 – Wave Splitting Code Flow Chart 77

Figure 5.1 – OEB versus MARIN: Incident Wave, Time Series, Probe 1 80

Figure 5.2- OEB versus MARIN: Incident Wave, Time Series, Probe 1 (300-500s) 80

Figure 5.3 - OEB versus MARIN: Reflected Wave, Time Series, Probe 1 81

Figure 5.4 - OEB versus MARIN: Reflected Wave, Time Series, Probe 1 (300-500s) 81

Figure 5.5 - OEB versus NRC: FO Measured Wave, Frequency Series, Probe 1 82

Figure 5.6 - OEB versus NRC: SO Measured Wave, Frequency Series, Probe 1 82

Figure 5.7 - OEB versus NRC: FO Measured Wave, Frequency Series, Probe 2 83

Figure 5.8 - OEB versus NRC: SO Measured Wave, Frequency Series, Probe 2 83

Figure 5.9 - OEB versus NRC: FO Measured Wave, Frequency Series, Probe 9 84

Figure 5.10 - OEB versus NRC: SO Measured Wave, Frequency Series, Probe 9 84

Figure 5.11 – Time Series Wave Splitting, Probe 1 87

Figure 5.12 - Time Series Wave Splitting, Probe 1 (100-150s) 87

Figure 5.13 - Time Series Wave Splitting, Probe 2 88

Figure 5.14 - Time Series Wave Splitting, Probe 2 (100-150s) 88

Figure 5.15 - Time Series Wave Splitting, Probe 3 89

Figure 5.16 - Time Series Wave Splitting, Probe 3 (100-150s) 89

Figure 5.17 - Time Series Wave Splitting, Probe 8 90

Figure 5.18 - Time Series Wave Splitting, Probe 8 (100-150s) 90

Figure 5.19 - Time Series Wave Splitting, Probe 9 91

Figure 5.20 - Time Series Wave Splitting, Probe 9 (100-150s) 91

Figure 5.21 – Frequency Domain Wave Splitting, Probe 1 92

Figure 5.22 – Low Frequency Domain Wave Splitting, Probe 1 92

Figure 5.23 - Frequency Domain Wave Splitting, Probe 2 93

Figure 5.24 – Low Frequency Domain Wave Splitting, Probe 2 93

Figure 5.25 - Frequency Domain Wave Splitting, Probe 3 94

Figure 5.26 – Low Frequency Domain Wave Splitting, Probe 3 94

Figure 5.27 - Frequency Domain Wave Splitting, Probe 8 95

Figure 5.28 – Low Frequency Domain Wave Splitting, Probe 8 95

Figure 5.29 - Frequency Domain Wave Splitting, Probe 9 96

Figure 5.30 – Low Frequency Domain Wave Splitting, Probe 9 96

Figure 5.31 – FO versus SO: Time series, Incident Wave, Probe 1, Case 1 97

Figure 5.32 - FO versus SO: Time series, Incident Wave, Probe 1, Case 2 98

Figure 5.33 - FO versus SO: Time series, Incident Wave, Probe 1, Case 3 98

Figure 5.34 - FO versus SO: Time series, Reflected Wave, Probe 1, Case 1 99

Figure 5.35 - FO versus SO: Time series, Reflected Wave, Probe 1, Case 2 99

Figure 5.36 - FO versus SO: Time series, Reflected Wave, Probe 1, Case 3 100

Figure 5.37 - FO versus SO: Time series, Theoretical Set-down, Probe 1, Case 1 100

Figure 5.38 - FO versus SO: Time series, Theoretical Set-down, Probe 1, Case 2 101

Figure 5.39 - FO versus SO: Time series, Theoretical Set-down, Probe 1, Case 3 101

Figure 5.40 - FO versus SO: Frequency Domain, Incident Wave, Probe 1, Case 1 102

Figure 5.41 - FO versus SO: Frequency Domain, Incident Wave, Probe 1, Case 2 102

Figure 5.42 - FO versus SO: Frequency Domain, Incident Wave, Probe 1, Case 3 103

Figure 5.43 - FO versus SO: Frequency Domain, Reflected Wave, Probe 1, Case 1 103

Figure 5.44 - FO versus SO: Frequency Domain, Reflected Wave, Probe 1, Case 2 104

Figure 5.45 - FO versus SO: Frequency Domain, Reflected Wave, Probe 1, Case 3 104

Figure 5.46 - FO versus SO: Frequency Domain, Set-down Wave, Probe 1, Case 3 105

Figure 5.47 - Second Order Theoretical Set-down Wave Peak Period Comparison 106

Figure 5.48 – Measured versus Theoretical Set-down Wave: Case 1, Probe 1 109

Figure 5.49– Measured versus Theoretical Set-down Wave: Case 1, Probe 2 109

Figure 5.50 – Measured versus Theoretical Set-down Wave: Case 2, Probe 1 110

Figure 5.51– Measured versus Theoretical Set-down Wave: Case 2, Probe 2 110

Figure 5.52 – Measured versus Theoretical Set-down Wave: Case 3, Probe 1 111

Figure 5.53 – Measured versus Theoretical Set-down Wave: Case 3, Probe 2 111

LIST OF APPENDICES

Appendix A – Cosine Decompositon 118

Appendix B – Model Scale Results 123

Appendix C – Full Scale Results 144

1. INTRODUCTION

1.1. Statement of Problem

Having various means to predict the performance of a vessel's interaction with the ocean environment is important for ship structure design. Full scale trial testing is expensive and time consuming but can be one of the most reliable forms of prediction. Model testing is less expensive than full scale trial testing but is conducted in a man-made environment, which can produce inaccuracies. Numerical simulation is typically the least expensive alternative, which can predict vessel performance using empirical analysis or computational method. However, numerical simulation also has associated inaccuracies in part due to the difficulty of using analytical expressions to simulate the randomness of ocean conditions.

For most companies full scale testing is not a viable option due to financial constraints and limited resources, therefore model testing and numerical simulations are favorable. However, in order to determine the performance of a vessel in a model tank environment, it is important to have a proper understanding of what types of waves are produced in the tank. When waves are measured in a tank, the total wave elevation is measured by an instrument such as a wave probe. The measured wave elevation is made up of several wave components: incident, reflected, and bound waves. Incident waves are created by a mechanical wave making device. Reflected waves are created due to the constraints of the model environment in which the incident waves are reflected from the opposite end of the tank in which they were created. The intensity of the reflected waves can be reduced if the

tank is equipped with man-made wave absorbers, which simulates a tapered beach shoreline. Bound waves, also known as wave set-down and set-up, were a phenomenon first reported by Longuet-Higgins and Steward (1964). They introduced a concept of radiation stress which explained that an individual wave component from a wave group can exert an internal compressive force in the direction of the propagated wave. The force is balanced by the water level decreasing in regions of longer wavers, known as wave set-down, and the water level increasing in shorter waves, known as wave set-up. This concept was proven experimentally by Bowen et. al. (1968).

The incident and reflected waves are comprised up from first order wave components whereas the bound waves composed of second order wave components that are more significant in shallow water depth. Van Dijk (2007) illustrates the increase in wave set-down in shallow water regions, as shown by Figure 1-1, where WD is water depth.

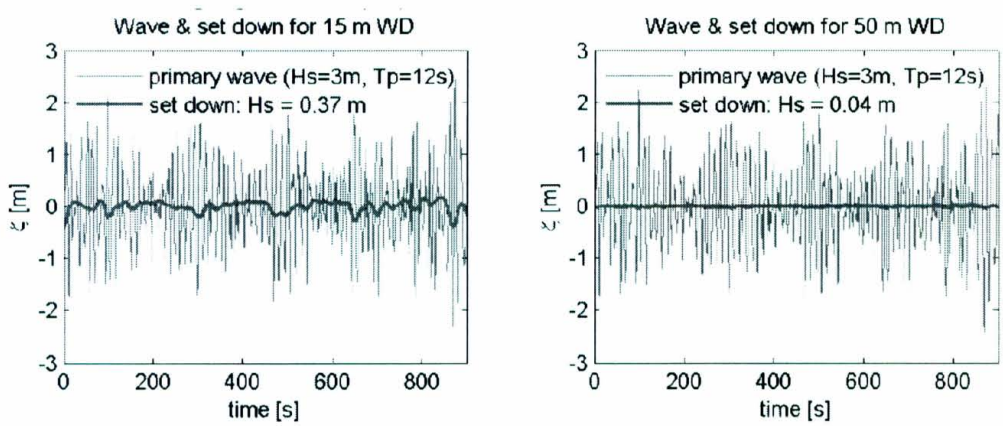

Figure 1-1 – Wave Set-down Comparison between Shallow and Deep Water (Van Dijk 2007)

Incident, reflected, and bound waves are the waves known waves types that are produced in a model tank environment. However, imperfect conditions within the tank create extra unwanted waves and need to be distinguished and removed from the deliberately generated wave types. If the unwanted waves are not removed from the known waves, large discrepancies can occur from the model testing results and full scale trial data.

Once the measured waves are split into the different wave components in the tank, a more accurate analysis can be completed for vessel design. Moored liquefied natural gas (LNG) carriers, in particular, have a fundamentally weakly damped nature and when combined with the second order waves can produce significant resonant motion and associated loads (Naciri, 2004). Therefore modeling of mooring design and ship-wave interaction in shallow water regions improves substantially by the use of this wave splitting technology.

1.2. Thesis Structure

This thesis describes the process of developing a numerical program that will identify and split the various wave components within measured waves. The results of a literature and theory review are also discussed.

Chapter 1 introduces the topic and presents a literature review. The problem and theories developed by different authors and examines why wave decomposition is needed especially when dealing with a model tank environment.

Chapter 2 presents the theories used to develop the equations that are used for the wave splitting program. This includes details on digital methods, Fourier analysis, spectral analysis, as well as the wave splitting theory.

Chapter 3 describes the environment in which the wave data was generated and used for the wave splitting program. The type of wave tank and wave maker are described as well as equations used to simulate the second order wave components.

Chapter 4 describes the computational methods that were incorporated into the wave splitting program. The band-pass filter, fast fourier transform, newton raphson, and also singular value decomposition were described.

The results are displayed and discussed in Chapter 5. The results are validated against published results from MARIN and NRC. The results are shown for the longest wave period case of 2.145s for the Offshore Engineering Basin (OEB) wave generation data, since that case shows the larger peaks. A comparison between the first order and second order wave generation is done to show the contribution of the second order wave component. A discussion is done to compare the measured wave data to the low frequency waves.

Chapter 6 consists of a summary of the results and findings from the research and future work is recommended. The research can be continued in such a way as to find the wave induced forces, from the properly split wave data, as well as the wave induced motion on a ship.

1.3. Review of Literature

The need for this research has been well documented by various authors. Hansen et. al. (1980) discuss how resonance conditions can create unacceptably large movements of moored vessels and can result in mooring failure in harbours and bays. This phenomenon can result in difficulties for the operation of ship terminals. Harbour resonance can be caused by a variety of occurrences but in particular long period waves from distant storms or wave groups (Hansen et. al., 1980). Hansen et. al. (1980) further state how generating the long period waves can be difficult in physical model, which is reiterated by many authors, such as Sand (1982) who states the importance of long waves being correctly represented in the physical model due to its influence on mooring forces and slow drift oscillations.

Recently, a higher demand for LNG carriers (Naciri, 2004) and in turn a higher development of LNG terminals (Voogt, 2005) has been noted. Due to this increase, there is a greater need for hydrodynamic modeling tools for floaters, particularly in shallow water, as most of the terminals for the LNG carriers are located near shore or in relatively shallow water. Low frequency excitation of the wave set-down increases in shallow water (Voogt, 2005). LNG carriers have inherent weakly damped nature (Naciri, 2004) and when combined with the low frequency waves can cause significant resonant motions and related mooring loads (Voogt, 2005).

Low frequency bound waves, also referred to as set-down waves, found in shallow water environment have been discussed in detail by Longuet-Higgins and Stewart (1964), Hansen

et. al. (1980), and Sand (1982), among others. Longuet-Higgins and Stewart (1964) stated that short period waves induce long period waves with periods equal to that of the wave group. They describe a 'wave group' as "…wave trains of nearly the same frequency and wavelength propagated in the same direction, resulting in the formation of 'group' of waves". These long period waves, which can also be termed low frequency waves, are bound to the group of waves propagating with group-velocity c_g (Sand, 1982). Hansen et. al. (1980) describe the long waves as "wave set-down" as the troughs of the long waves are found at the regions of the larger waves in the group, as shown in Figure 1-2.

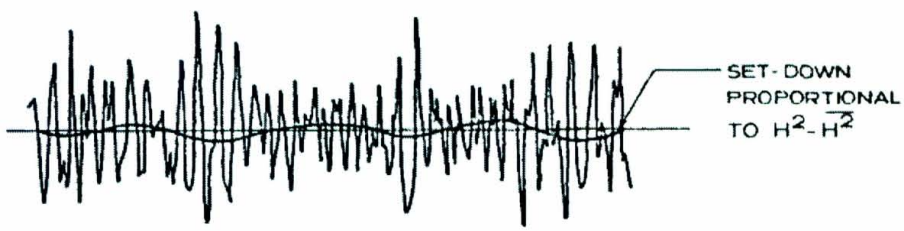

Figure 1-2 – Wave group versus the wave set-down (Hansen et. al. 1980)

The set-down long waves were discovered from radiation stress and the momentum equation (Longuet-Higgins and Stewart, 1964) but were also obtained from perturbation analysis of the Laplace equation (Hansen et. al., 1980). The latter will be explored in this work.

Hansen et. al. (1980) further describes the problems that can occur in the physical model tank environment. Although model testing has improved with the generation of natural, irregular waves, a problem still occurs when the paddle generates waves using the typical first order motion. Since the long waves are of second order approximation, the first order

approximation does not reproduce the drift velocities (Hansen et. al., 1980). The paddle will then produce natural drift velocities that will be of equal magnitude and opposite sign, which is a progressive long wave that is free and not bounded to the wave group in contrast to the set-down wave that is bounded to the wave group. Hansen et. al. (1980) also terms the free wave as a parasitic long wave, which causes the long wave effects to be exaggerated in terms of harbor resonance and slow drift ship motions. Sand (1982) further elaborates that the free long waves do not follow the dispersion relation. This parasitic wave must be identified and removed from the model testing environment in order to produce accurate results. Hansen et. al. (1980) suggest that a second order long period signal be imposed on the first order signal to produce the drift velocities required for the set-down wave. Hansen et. al. (1980) expand the boundary conditions to apply to the second order approximation as well as applying the Laplace equation with the nonlinear surface conditions (Sand 1982). Thus the position for the paddle can be corrected to apply the second order approximations.

The long waves are found by a summation of differences between each pair of frequencies of the short, or first order, wave spectrum (Hansen et. al., 1980). Hansen et al. (1980) describe the long period waves as the sum of subharmonics. They state that a regular wave group with water surface elevation η_{nm} and frequency Δf_{nm} that consist of two regular waves with water surface elevations η_n, η_m and frequencies f_n, f_m, where n and m are indices for the number of waves being considered. The wave group elevation and frequency is equal to:

$$\eta_{nm} = \eta_n + \eta_m$$

$$\Delta f_{nm} = f_n - f_m$$

Since we know that the wave group generates wave set-down, wave group η_{nm} will generate wave set-down ζ_{nm}. Hanson et. al. (1980) state that each pair of n, m components of the spectrum will contribute to the set-down. Thus by summing all the contributions of all the pairs will give:

$$\zeta = \sum_{n-m=1}^{\infty} \sum_{m=m^*}^{\infty} \zeta_{nm}$$

where $m^*=f^*/f_0$, f^* is the lowest frequency of the regular wave spectrum and f_0 is the interval of discretization of the regular wave spectrum. Further theory on the calculation is discussed in the theory section in this Thesis.

Hansen et al. (1980) and Mansard (1991) briefly discuss superharmonics corresponding to the second order correction containing a number of terms that pertaining to the sum of the a pair of frequencies in the short wave spectrum. Since this Thesis is concerned with investigating low frequency waves, superharmonics are not considered.

Voogt (2005) describes a procedure for splitting the individual wave components in order to identify the low frequency bound wave and comparing the analytical wave set-down to the separated wave set-down from the measured wave. The analytical wave set-down model is described by Sharma and Dean (1981) and is frequently referred to when calculating the theoretical wave set-down. The wave splitting program created for this research used the methods described by both Voogt (2005) and Sherman and Dean (1981) since their methods are well defined.

Stransberg (2006) presents new results for identifying the low frequency waves from bi-chromatic waves (waves having two frequencies) with and without a correction to the wave maker to remove the free waves. He uses an iterative process to find the optimal correction signal through repeated tests in a large wave basin. His findings show improvement in the corrected results in which the free waves were reduced. In the present work an attempt is made to compare a corrected second order wave generation but not in the iterative sense that Stransberg presents, but as proposed by Sand (1982) which is previously described. A large wave basin was utilized, although the NRC basin is not as big as the MARINTEK basin in which Stransberg conducted his experiments, but it is considered a large basin.

Masard and Funke (1980) describe a method to identify the incident and reflected spectra from the measured spectra from a wave tank using the least square method. It requires three simultaneous measurements within the tank that are in reasonable proximity to each other and are in parallel to each other in a line from the direction of the wave propagation. It has shown to give good agreement in comparison to incident spectra measured concurrently in a side channel. Voogt (2005) states that the least square method will give best results for three wave components: incident, reflected, and wave set-down. For this work only two components are split from the measured wave and thus the singular value decomposition formulation was used.

Mansard (1991) developed a numerical technique, based on the previously described interactions between free and bound waves, that illustrates the position in the wave tank

where waves of the same frequency would interact and either cancel or reinforce each other. The results of his research confirm the use of second order wave generation techniques reduce the parasitic free wave which produces more realistic wave profiles. He states that even when incorporating second order wave generation techniques for an irregular spectrum, rather than using monochromatic or bichromatic waves, there can be high oscillations at the tail end of the spectrum due to the interaction of free and bound components. These oscillations can cause differences in wave parameters such as significant wave height and crest front steepness (Mansard, 1991).

The experiments carried out by Zaman et. al. (2011) were done in order to identify the spurious waves in shallow water using the OEB, NRC. They generated multi-chromatic waves using first order and second order techniques. They show the differences between the first order and second order wave generation. The results from this research are validated against their results.

2. THEORIES

2.1. Digital Methods

A signal is any conversion of some property, such as temperature or pressure, from its original physical form to a related electrical quantity. A signal can be classified into two categories: deterministic and random. A deterministic signal can be predicted by mathematical relations and a random signal is not predictable, however it can be estimated through statistics and probabilities. A method of distinguishing between the two categories is to compare several sets of data obtained under identical conditions over a reasonable period of time. Sometimes a signal may appear to be random but is in fact deterministic, and can be proved to be deterministic using, for example, an auto-correlation process (Beauchamp and Yen, 1973).

The following sections describe fundamental principles of digital signal analysis with reference to Digital Methods for Signal Analysis (Beauchamp and Yen, 1973).

Deterministic Signals

A deterministic signal can be determined from time-history and is generally reproducible under identical conditions. The mathematical form of a deterministic signal can be described as periodic or transient signals. Periodic signals continuously repeat at regular intervals whereas transient signals decay to a zero value after a finite length of time. Periodic signals are comprised of one or more sinusoidal signals having an integral relationship with this period over time. The basic sinusoidal equation is described in

Equation [2.1], where A is the constant representing the peak amplitude of the wave form, ω_0 is the angular frequency and θ is the initial phase angle with respect to the time origin. Equation [2.2] describes the mathematical expression for the angular frequency ω_0, where f_0 is the cyclical frequency in Hz. Equation [2.3] describes the period, T, of the wave form. Figure 2-1 displays graphically the sinusoidal equation.

$$x(t) = A\sin(\omega_0 t + \theta) \quad \textbf{[2.1]}$$

$$\omega_0 = 2\pi f_0 \quad \textbf{[2.2]}$$

$$T = \frac{1}{f_0} \quad \textbf{[2.3]}$$

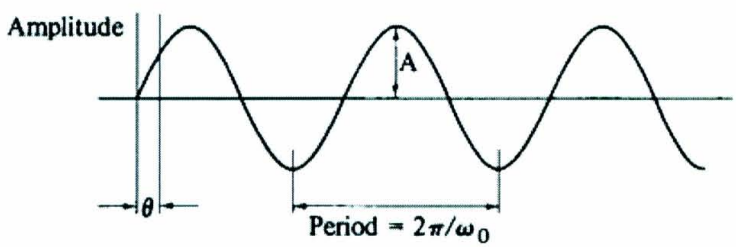

Figure 2-1– Sinusoidal Wave (Beauchamp and Yen, 1973)

The Fourier series is a means to express a general relationship for periodic signals, in which harmonic components repeat exactly for all values of t, described in Equation [2.4].

$$x(t) = A_0 + A_1\sin(\omega_0 t + \theta_1) + A_2\sin(2\omega_0 t + \theta_2) + \ldots A_n\sin(n\omega_0 t + \theta_n) \quad \textbf{[2.4]}$$

where A_0 : the mean level of the signal

A_n : the peak amplitude of the n^{th} harmonic

θ_n : the phase of the n^{th} harmonic

Deterministic signals can be a combination of several sinusoidal elements and may not be harmonically related. The deterministic signal will have similar spectral characteristics as a periodic signal.

Random Signals

A random signal is useful for obtaining new and unpredictable values that would not be guessed or estimated from previous data, although this does not mean that the values are unstructured. Since random signals cannot be determined explicitly, probabilities and statistics are the primary means of estimating a solution.

An ensemble is one random process which will produce a set of time-histories. An example of an ensemble may be an experiment which produces random data and is repeated N times (Beauchamp and Yen, 1973). The statistical value for this ensemble is obtained by considering records taken at specific instants in time. The average can be calculated at a specific time t_1, shown in Equation [2.5], as well as the average value of

the products of two different samples at different times, say t_1 and t_2, known as the auto-correlation function, described by Equation [2.6]. Note that $\tau = t_2 - t_1$.

$$\langle x(t_1) \rangle = \lim_{N \to \infty} \frac{1}{N} \sum_{k=1}^{N} x_k(t_1) \quad \textbf{[2.5]}$$

$$R(\tau) = \lim_{N \to \infty} \frac{1}{N} \sum_{k=1}^{N} x_k(t_1) \cdot x_k(t_2) \quad \textbf{[2.6]}$$

where N is the length of the record, and k is the index of summation for the ensemble.

The signal is stationary if $<x(t_1)>$ and $R(\tau)$ are constant for all values of t_1 and also if $R(\tau)$ relies only on time displacement (τ). A record can be partitioned into equal sections in order to calculate the average value of any section, as shown in Equation [2.7]:

$$\bar{x}_M = \lim_{T \to \infty} \frac{1}{T} \int_0^T x_M(t) \cdot dt \quad \textbf{[2.7]}$$

where M is a section of the record.

Properties of the Signal

The properties of a signal can be defined in a probabilistic sense in terms of amplitude, time and frequency domain.

Amplitude Domain

- Root mean-square value: shows the amplitude's effect of the signal but is

insufficient in showing the variable nature of the process. Therefore the probability of the amplitude exceeding, or lying between specified levels, must be determined. The calculation for the root mean square is given by Equation [2.8] for continuous data and by Equation [2.9] for discrete data.

$$\bar{x}_M = \sqrt{\frac{1}{T}\int_0^T x^2(t) \cdot dt} \qquad \textbf{[2.8]}$$

$$\bar{x}_M = \sqrt{\frac{1}{N}\sum_{i-1}^{N}(x_i)^2} \qquad \textbf{[2.9]}$$

- Probability density function: determines the probability that the signal will be found within a given range. It is more suitable for smaller possible numbers of discrete values of x.
- Probability distribution function: describes the probability that the variable will assume a value less than or greater than x. This case is more suitable for larger domains such as when the possible number of discrete values of x is great.

Time Domain

- Auto-correlation function: used to statistically determine information about the periodic behaviour by taking measurements of the amplitude of the signal at two

instances, separated by τ, and finding their product and averaging over the time of the record. The main value of auto-correlation is to expose any hidden periodicity within the signal.

- Cross correlation function: calculates the relation between the two signals.

Frequency Domain

- Fourier Transform: Fourier series analysis can provide peak amplitudes and related harmonics contained within a signal. But it cannot be applied to random signals as the components are not necessarily harmonically related. Therefore a Fourier Transform is used to measure the relative amplitudes of the frequency components.
- Power spectral density: calculated by finding the mean-square value of the instantaneous power at a given frequency over time T.
- Weiner-Khintchine Relationship: relates the power spectral density function and the auto-correlation function and is important for practical measurement methods.

Required Length of Record

The length of record is important for accuracy of the statistical estimates. Each method of analysis defines its own minimum length. In general, the record length is inversely proportional to twice of the bandwidth (B) multiplied by an estimation error (ϵ) as well as being proportional to a proportional constant (K) which is dependent on the measured property. For a mean square and power spectral density estimates, K is often assumed to be equal to 2.

Digitization of Continuous Information

In order to convert a continuous analog signal to a discrete form of values, sampling must be completed in the time domain, quantization in the amplitude domain, and then coding the final results into digital form. Errors can occur from the limitations of these procedures.

Sampling can be completed at a cyclic rate sampling which is a sinusoidal function that samples in accordance with a linear function of time. Another method of sampling can be done at equally spaced time intervals, known as uniform sampling. Aperture is the length of time over which data is averaged and should be small compared to the sampling period in order to prevent error.

One of the most significant difficulties arises from aliasing effects in which the measured signal is indistinguishable from other signals. For example if a high frequency signal is measured at too low a rate then the signal can be interpreted as a low frequency signal. Thus the high frequency signal looks like the low frequency signal and cannot be identified from one another, as shown by Figure 2-2.

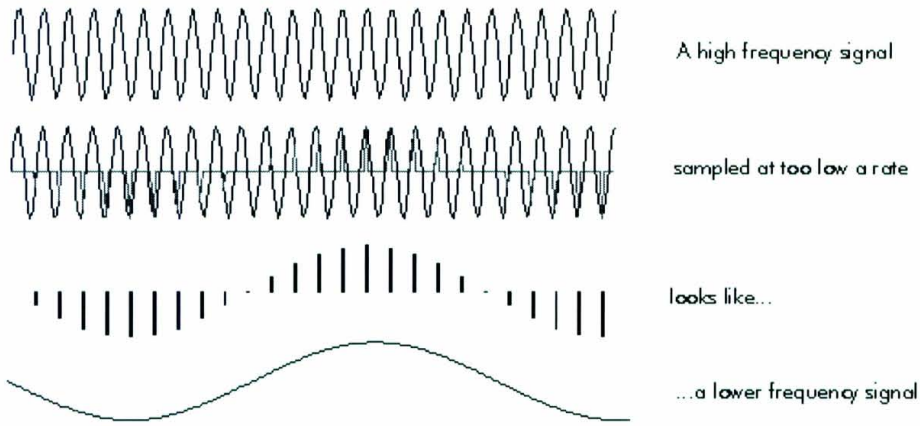

Figure 2-2 - Aliasing Effects from Signal Processing (©BORES Signal Processing 2009)

Another important parameter in signal processing is the Nyquist Frequency (f_N). It is defined as half the sampling frequency of a discrete signal. When a continuous signal is sampled, all the aliasing effects occur above the Nyquist Frequency. Additionally, if f_o is the fundamental frequency of the true signal, aliasing will not occur when frequencies range from zero to f_N.

According to the Raleigh Theorem, time T must be greater or equal to the reciprocal of twice the bandwidth, B:

$$T \geq \frac{1}{2B}$$

Signals must be subjected to band-pass filters prior to digitization. In summary, signals have to be a finite bandwidth up to B Hz and are separated by 1/(2B) seconds.

The sampling rate must be made large in order to have a practical filter in reality, and thus may be higher than the sampling theorem suggests. Proper frequency reduction may not be achieved until two octaves higher than the cut-off frequencies. Often, the sampling rate is set to 1.25 times the filter cut off frequency.

As part of the digitization process, quantization allows a set of continuous values to be represented as a limited series of discrete numbers. This is only an approximation since the original number, which has an infinite number of states, must be truncated in order to be represented digitally with a limited number a bits. This process is non-linear when representing a physical quantity numerically. The result is expressed as an integer value corresponding to the nearest whole number of units.

2.2. Fourier Series

Fourier transform is the means to which data can be transformed into the frequency domain from the time domain. Using the common trigonometric identity shown in Equation [2.10], the Fourier's theorem series shown in Equation [2.4] can be rewritten into an expanded form shown in Equation [2.11].

$$\sin(A + B) = \sin A \cos B + \cos A \sin B \qquad \textbf{[2.10]}$$

$$\begin{aligned} x(t) = A_0 &+ A_1 \sin\theta_1 \cdot \cos\omega_0 t \\ &+ A_1 \cos\theta_1 \cdot \sin\omega_0 t + \cdots \\ &+ A_n \sin\theta_n \cdot \cos n\omega_0 t \end{aligned} \qquad \textbf{[2.11]}$$

We can simplify Equation [2.11] by letting the sine and cosine terms equal to variables which can be later derived theoretically using various integrals. The variables can be written as:

$$a_k = A_n \sin\theta_n$$

$$b_k = A_n \cos\theta_n$$

$$a_0 = 2A_0$$

Note that the constant term a_0 is written as twice the original constant which is done for simplicity later on in computation since the constant is arbitrary. Inputting the above terms

into Equation [2.11] we obtain Equation [2.12] which can be simplified into the Fourier series equation notation, as shown by Equation [2.13].

$$x(t) = \frac{a_0}{2} + a_1 \cos \omega_0 t + b_1 \sin \omega_0 t + \cdots + a_n \cos n\omega_0 t + b_n \sin n\omega_0 t \quad \textbf{[2.12]}$$

$$x(t) = \frac{a_0}{2} + \sum_{k=1}^{n} a_k \cos k\omega_0 t + \sum_{k=1}^{n} b_k \sin k\omega_0 t \quad \textbf{[2.13]}$$

Using the property of orthogonality for sinusoids, the only finite value that can be obtained for the sine and cosine functions is equal to 1/2. This is obtained by squaring the sine and cosine respectively. In addition, frequencies and phase shifts must be equal, otherwise the product will be zero (Beauchamp and Yuen, 1973). Orthogonality is an important principal for the Fourier series as it will simplify the equation greatly. We can see that from Equation [2.12] all the terms will thus reduce to zero except for the first term and therefore the integral of x(t) over the period T will be:

$$\int_0^T x(t)\, dt = \int_0^T \frac{a_0}{2} dt = \frac{a_0}{2} T$$

The constant term is therefore equal to:

$$\frac{a_0}{2} = \frac{1}{T}\int_0^T x(t)\,dt \qquad \textbf{[2.14]}$$

We can solve for the variables a_k and b_k by multiplying the x(t) function by both sin $k\omega_0 t$ and cos $k\omega_0 t$. The terms will all vanish except for the $\sin^2 k\omega_0 t$ and $\cos^2 k\omega_0 t$ terms which are equal to ½ as previously stated. Therefore we have:

$$\int_0^T x(t)\sin k\omega_0 t\,dt = \int_0^T b_k \sin^2 k\omega_0 t\,dt = b_k\frac{T}{2}$$

$$\int_0^T x(t)\cos k\omega_0 t\,dt = \int_0^T a_k \cos^2 k\omega_0 t\,dt = a_k\frac{T}{2}$$

Therefore we now have equations for the variables which represent the amplitudes of the harmonics found in the original function x(t) and are known as the Fourier coefficients and are shown in Equations [2.15] and [2.16].

$$b_k = \frac{2}{T}\int_0^T x(t)\sin k\omega_0 t\,dt \qquad \textbf{[2.15]}$$

$$a_k = \frac{2}{T}\int_0^T x(t)\cos k\omega_0 t\,dt \qquad \textbf{[2.16]}$$

Complex representation of the Fourier series and integral allows for further development of the Fourier transform. Using the following identities we can expand the notations in Equation [2.13] where j=√-1:

$$\cos k\omega_0 t = \frac{1}{2}[\exp(jk\omega_0 t) + \exp(-jk\omega_0 t)] \quad \textbf{[2.17]}$$

$$j \sin k\omega_0 t = \frac{1}{2}[\exp(jk\omega_0 t) - \exp(-jk\omega_0 t)] \quad \textbf{[2.18]}$$

Incorporating Equations [2.17] and [2.18] into Equation [2.13] gives:

$$\begin{aligned}(a_k \cos k\omega_0 t + b_k \sin k\omega_0 t) \\ &= \frac{a_k}{2}[\exp(jk\omega_0 t) + \exp(-jk\omega_0 t)] \\ &+ \frac{b_k}{2}[\exp(jk\omega_0 t) - \exp(-jk\omega_0 t)] \\ &= A_k \exp(jk\omega_0 t) + B_k \exp(-jk\omega_0 t)\end{aligned} \quad \textbf{[2.19]}$$

where A_k and B_k represent complex conjugate amplitude coefficients and are equal to:

$$A_k = \frac{a_k - jb_k}{2} \quad \textbf{[2.20]}$$

$$B_k = \frac{a_k + jb_k}{2} \qquad \textbf{[2.21]}$$

Using Equations [2.15] and [2.16], as well as incorporating the identities of Equation [2.17] and [2.18], we can re-write Equations [2.20] and [2.21] into the expanded integral form, which uses the original function x(t) as shown by Equations [2.22] and [2.23]. Note that t has been changed to p for the integrations since t needs to be maintained for the exponential function.

$$\begin{aligned} A_k &= \frac{1}{T}\int_0^T x(p)[\cos k\omega_0 p - \mathrm{j}\sin k\omega_0 p]dp \\ &= \frac{1}{T}\int_0^T x(p)\exp(-jk\omega_0 p)\,dp \end{aligned} \qquad \textbf{[2.22]}$$

$$\begin{aligned} B_k &= \frac{1}{T}\int_0^T x(p)[\cos k\omega_0 p + \mathrm{j}\sin k\omega_0 p]dp \\ &= \frac{1}{T}\int_0^T x(p)\exp(jk\omega_0 p)\,dp \end{aligned} \qquad \textbf{[2.23]}$$

We can now expand the Fourier series into complex notation by incorporating Equations [2.14], [2.19], [2.22] and [2.23] into equation [2.13].

$$
\begin{aligned}
& x(t) \\
& = \frac{1}{T}\int_0^T x(p)\,dp \\
& + \sum_{k=1}^{n}\left[\frac{1}{T}\int_0^T x(p)\exp(-jk\omega_0 p)\,dp\right]\exp(jk\omega_0 t) \\
& + \sum_{k=1}^{n}\left[\frac{1}{T}\int_0^T x(p)\exp(jk\omega_0 p)\,dp\right]\exp(-jk\omega_0 t)
\end{aligned}
\qquad \textbf{[2.24]}
$$

Expression [2.24] can be simplified as there are a number of sequence of terms that are summed from k=1 to k=n as well as k=-1 and k=-n for the third term (by incorporating the negative in the exponential term) so that we can join the terms to be the summations from k=-n to k=n which includes the first term at k=0. Therefore Equation [2.24] can be rewritten as:

$$
x(t) = \sum_{k=-n}^{k=n}\frac{1}{T}\left[\int_0^T x(p)\exp(-jk\omega_0 p)\,dp\right]\exp(jk\omega_0 t) \qquad \textbf{[2.25]}
$$

Fourier Integral Transform

Since Fourier series' has limitations in that it assumes the time function is infinite and that the data is periodic, which in practice is not reality, Fourier Integral transform is used for most signal data. The data can no longer be assumed that it will repeat infinitely, therefore k

and T are extended to infinity and the fundamental frequency will lead towards zero. The separation between harmonics also tends to zero which will cause the Fourier coefficients to become continuous functions of frequency. A couple of noteworthy relations are:

$$\frac{k}{T} = f$$

$$\omega = 2\pi f$$

Therefore we can restate Equation [2.25] in terms of frequency in the complex form of a Fourier integral as shown by Equation [2.26].

$$x(t) = \int_{-\infty}^{\infty} \left[\int_{-\infty}^{\infty} x(p) \exp(-j\omega p) \cdot dp \right] \exp(j\omega t) \cdot df \qquad \textbf{[2.26]}$$

The contents within the brackets in Equation [2.26] represent the amplitude of the complex Fourier coefficients for a continuous time series. Isolating the bracketed expression we have a frequency function as shown in Equation [2.27].

$$X(f) = \int_{-\infty}^{\infty} x(p) \exp(-j\omega p) \cdot dp \qquad \textbf{[2.27]}$$

or

$$X(f) = \int_{-\infty}^{\infty} x(t) \exp(-j\omega t) \cdot dt \qquad \textbf{[2.28]}$$

to show in its original time form.

Equation [2.28] is the complex Fourier transform of the time series x(t). The absolute values of X(f) gives the frequency amplitude and the argument gives the phase. Thus Equation [2.26] becomes:

$$x(t) = \int_{-\infty}^{\infty} X(f) \exp(j\omega t) \cdot df \qquad \textbf{[2.29]}$$

which is known as the inverse complex Fourier transform. In discrete terms Equation [2.29] becomes:

$$x(t) = \sum_{-\infty}^{\infty} X_k(f) \exp(j\omega t) \cdot df \qquad \textbf{[2.30]}$$

Often ω is used in place of f, for example when a scaling factor of $1/2\pi$ is applied to a complex transform. Alternative forms of writing Fourier transform are used to quantify them in terms of cosine and sine. If the x(t) function is even, ie. x(t) is symmetric about the t=0 axis, the Fourier transform becomes known as the Fourier cosine transform $X_c(f)$ and if the function is odd the Fourier transform becomes known as the Fourier sine transform $X_s(f)$, as shown by Equations [2.31] and [2.32].

$$X_c(f) = \int_{-\infty}^{\infty} x(t)\cos \omega t \cdot dt \qquad \textbf{[2.31]}$$

$$X_s(f) = \int_{-\infty}^{\infty} x(t)\sin \omega t \cdot dt \qquad \textbf{[2.32]}$$

Discrete Fourier Series

For discrete digitized data, a finite form of Fourier series is needed to derive a discrete form of the Fourier transform. Computationally the discrete Fourier transform is identical to the complex representation of Fourier series described in the previous section but the theoretical derivation is quite different. There are quite a few more limitations to discontinuous discrete data in contrast to continuous, which occur from an attempt to preserve information when converting between continuous and discontinuous data.

A number of conditions must be included in order to derive the Fourier transform. For a sample record of length T seconds, it is divided into N equally spaced points by h length, also known as the time step. The sampling rate, f_S, of the record is 1/h. There are a limited number of frequencies that can represent the time series and is established by the Nyquist frequency, f_N. The Nyquist frequency is half the sampling frequency and is thus equal to:

$$f_N = \frac{1}{2h}$$

Since the record length for the time series has N number of values to compute, but in the frequency domain the Fourier coefficient contains a real and imaginary value, the frequency components must be limited to N/2 discrete values.

Now to expand the Fourier series shown in Equation [2.13], we will use i to describe the time series summation and n for frequency domain. Therefore:

$$t = i \cdot h \quad (i = 1,2,3 \ldots,\mathrm{N})$$

$$f = f_n \quad (n = 1,2,3 \ldots, \frac{N}{2})$$

Replacing ω_0 by $2\pi/T$ and k by n, Equation [2.13] will become Equation [2.33].

$$x_i = \frac{a_0}{2} + \sum_{n=1}^{N/2} a_n \cos\frac{n2\pi ih}{T} + \sum_{n=1}^{N/2} b_n \sin\frac{n2\pi ih}{T} \qquad \textbf{[2.33]}$$

Since T=h*N and to show the special case where the constant term in Equation [2.33] can be removed, when considering the mean value case when n=0, we can rewrite Equation [2.33] to:

$$x_i = \sum_{n=0}^{N/2} a_n \cos\frac{n2\pi i}{N} + \sum_{n=0}^{N/2} b_n \sin\frac{n2\pi i}{N} \qquad \textbf{[2.34]}$$

Equation [2.33] and [2.34] are the main expressions used to define discrete Fourier series. Similarly, the coefficients can be derived from Equations [2.14], [2.15] and [2.16] to be:

$$\frac{a_0}{2} = \frac{1}{N}\sum_{i=1}^{N} x_i$$

$$a_n = \frac{2}{N}\sum_{i=1}^{N} x_i \cos\frac{n2\pi i}{N}$$

$$b_n = \frac{2}{N}\sum_{i=1}^{N} x_i \sin\frac{n2\pi i}{N}$$

Discrete Fourier Transform

Since there are limitations implemented on discrete data, we know that integrals must be replaced with summations and that the limits on the summations cannot be infinite. In order to use the discrete Fourier series derived in the previous section, the transform X(f) must be complex so that it would contain both negative and positive frequencies such as:

$$X_n = a_n + jb_n$$

where j signifies the complex component. Therefore we can rewrite Equation [2.34] as

$$x_i = \sum_{n=-\frac{N}{2}}^{\frac{N}{2}} X_n \exp\left(\frac{jn2\pi i}{N}\right) \quad (i = 1,2,3,\dots,N) \qquad \textbf{[2.35]}$$

Due to the fact that two spectrum components are generated for each real frequency, the summation of the two components will cause a doubling of amplitude of the spectral series produced. Therefore a scaling factor of 1/N must be included to properly account for the increase, which allows the transform to be written as:

$$X_n = \frac{1}{N} \sum_{i=-\frac{N}{2}}^{\frac{N}{2}} x_i \exp\left(-\frac{jn2\pi i}{N}\right) \quad \textbf{[2.36]}$$

Equations [2.35] and [2.36] can be further simplified by noting that they are symmetrical for the positive and negative values of N. Therefore x_i and X_n become:

$$x_i = \sum_{n=0}^{N-1} X_n \exp\left(\frac{jn2\pi i}{N}\right) \quad (i, n = 0,1,2, \dots, (N-1)) \quad \textbf{[2.37]}$$

$$X_n = \frac{1}{N} \sum_{i=0}^{N-1} x_i \exp\left(-\frac{jn2\pi i}{N}\right) \quad \textbf{[2.38]}$$

Equation [2.37] and [2.38] are the discrete Fourier transform and inverse discrete Fourier transform, respectively.

Fast Fourier Transform

Due to the slow computational time of the Fourier transform, which is a 1:1 conversion of a data sequence, a method called the fast Fourier transform (FFT) is often used instead. It was described by Cooley and Turkey in 1965 (Beauchamp and Yuen, 1973) in a method to ease

machine calculation and also independently discovered by Danielson and Lanczos in 1942 (Press et. al., 1992) who were not able to see much use of it when the most advance technology was a hand calculator.

The Cooley-Tukey method reduces a large process of matrix multiplication and addition to a series of sparse matrices. This eliminates much of the redundancy that occurs using discrete Fourier transforms (DFT), where many of the products are repeated. The matrix multiplication requires N^2 complex multiplications for a DFT but a FFT can be done using $N\log_2 N$ which makes a large difference in terms of computation time. For example (Press et. al., 1992) $N=10^6$ will take roughly 30 seconds for $N\log_2 N$ and 2 weeks for N^2 computation time on a microsecond cycle time computer.

Danielson and Lanczos (Press et. al., 1992) provide one of the clearest derivations of the FFT algorithm. They describe the length T of a signal x_i can be split into two discrete Fourier Transforms of length T/2, one being an even-indexed (i=2m) points, x_{2m}, and the other being odd-indexed (i=2m+1), x_{2m+1}. After the two DFTs are computed, they are combined to produce the full sequence as shown in Equation [2.39], which is expanded from Equation [2.38], noting that the scaling factor is not shown for simplicity.

$$X_n = \sum_{m=0}^{N/2-1} x_{2m} \exp\left(-\frac{jn2\pi(2m)}{N}\right) + \sum_{m=0}^{N/2-1} x_{(2m+1)} \exp\left(-\frac{jn2\pi(2m+1)}{N}\right) \quad \textbf{[2.39]}$$

Taking out the common multiplier $\exp\left(-\frac{2\pi jn}{N}\right)$ of the odd-indexed summation, using the $e^{(a+b)}=e^a e^b$ identity, and simplifying we can clearly see the even and odd indexed parts that make up the x_i function:

$$X_n = \sum_{m=0}^{\frac{N}{2}-1} x_{2m} \exp\left(-\frac{2\pi jnm}{\frac{N}{2}}\right) + \exp\left(-\frac{2\pi jn}{N}\right) \sum_{m=0}^{\frac{N}{2}-1} x_{(2m+1)} \exp\left(-\frac{2\pi jnm}{\frac{N}{2}}\right) \quad \textbf{[2.40]}$$

$$= F_{even} + \exp\left(-\frac{2\pi jn}{N}\right) \cdot F_{odd}$$

One of the easiest ways to compute the FFT is to use a radix of 2 for the number of inputs N, ie. $N=2^P$ where P=1,2,3…∞. The advantage of the radix of 2, as described by

Beauchamp and Yuen (1973), is due to some of the terms of the common multiplier, shown in Equation [2.40], reduce to either 1 or -1 which avoids even further complex arithmetic. The structure of the computation of the FFT is described in section 4.2.

2.3. Spectral Analysis

The previous section describes the value of working in the frequency domain using a series of values. This section develops the usefulness of the frequency domain in terms of an electronic signal.

Amplitude and the power of the signal are the most frequently used and useful characteristics of a signal in the frequency domain and were defined in section 2.1. Each characteristic pertains to a certain frequency and when combined create a wave spectrum as shown in Figure 2-3. The characteristics of a signal create what is known as a power spectrum and is an average quantity which describes the energy that is allocated at assorted frequencies.

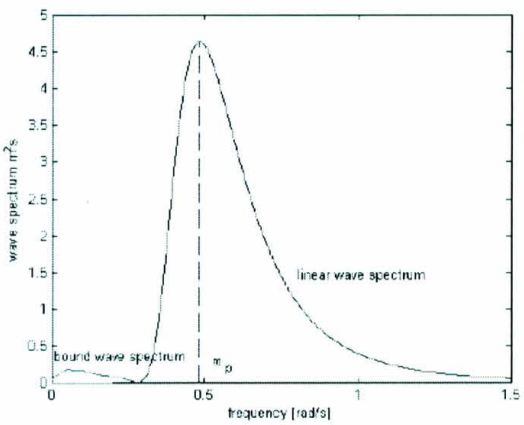

Figure 2-3 – Wave Spectrum (Voogt 2005)

Spectral Analysis allows certain characteristics of a signal to be calculated which would otherwise be quite difficult. For example, as noted by Beauchamp and Yuen (1973), the difficulty of calculating the total energy of signals can be reduced by integrating the power spectral density since the power at individual frequencies can be easily found. Another

useful application of spectral analysis is determining the relationship between correlation and spectral density, in which one quantity can be found from one another, even if the signal is immeasurable in the time domain. The link between the two quantities has been useful for finding analogies of theories in the subject of signal analysis. Beauchamp and Yuen (1973) note that we cannot measure visible light as a time series, but it is possible to measure the spectrum of a light source. This trait becomes particularly useful when incorporating fast Fourier transform algorithms.

Beauchamp and Yuen (1973) note several techniques used for determining the power spectral density:

- Direct Fourier transform: Computes Fourier transform of the time series and then the mean-square value is calculated.
- Indirect method: The Fourier transform of the auto-correlation function is calculated and then the spectral density function is derived.
- Band-pass filtering: A method of filtering out unwanted data from a range of frequencies.

The direct method was used in this research as is more common after the development of the FFT subroutines since this allowed for a much faster computational time. A band-pass filter was used to smooth the spectral density curve to produce reliable estimates.

Power Spectrum Estimation

The square of a random signal will calculate its energy content and the square of Fourier transform at a frequency f will give the energy content at f. Since we are dealing with a random process, the values at the Fourier transform will fluctuate at any frequency. Therefore two pieces of a random signal at different times would produce different Fourier transforms, thus the square of a Fourier transform cannot describe its energy content in general. But the use of an ensemble average, as described in section 2.1, of a Fourier transform square can be used to describe the importance of the Fourier transform at any frequency. Therefore we can describe the power spectrum, or auto-spectrum, as:

$$S(f) =< |X(f)|^2 >$$

where X(f) is the Fourier transform as derived in the previous section. In order to prove that the total power contained in X(f) is equal to that of x(t), Parseval theorem is derived. Real functions x(t) and y(t) are multiplied and are expressed in terms of Fourier transform using Equation [2.30]:

$$x(t)y(t) = x(t) \int_{-\infty}^{\infty} Y(f) \exp(j\omega t) \cdot df \qquad \textbf{[2.41]}$$

Taking the integral of Equation [2.41] we get:

$$\int x(t)y(t)\, dt = \int \left\{ \int x(t)Y(f) \exp(j\omega t)\, df \right\} dt \qquad \textbf{[2.42]}$$

And rearranging Equation [2.42] we get:

$$\int x(t)y(t)\,dt = \int Y(f)\left\{\int x(t)\exp(j\omega t)\,dt\right\}df \qquad \textbf{[2.43]}$$

where the bracketed part in Equation [2.43] is the complex conjugate of X(f) and thus Equation [2.43] can be rewritten as Equation [2.44].

$$\int x(t)y(t)\,dt = \int X^*(f)Y(f)df \qquad \textbf{[2.44]}$$

Letting x(t)=y(t) and X(f)=Y(f) then equation becomes:

$$\int x^2(t)\,dt = \int X^*(f)X(f)df = \int |X(f)|^2\,df \qquad \textbf{[2.45]}$$

When the ensemble averages are taken on both sides in Equation [2.45], we get:

$$\int \langle x^2(t)\rangle\,dt = \int S(f)df \qquad \textbf{[2.46]}$$

Equation [2.46] proves that the power spectral density added up for all frequencies equals the average power of x added up over time.

Auto-Spectrum and Amplitude Spectrum

The auto-spectrum and the amplitude spectrum are important properties of signals that use the DFT coefficients to calculate one of the other. The auto-spectrum was described earlier as the power spectrum and the amplitude spectrum is the spectrum of modulus of the coefficients obtained from the FFT. The FFT produces a two-sided spectrum in complex form and must be converted to polar and scaled by the length of the record in order to obtain the magnitude and phase (National Instrument, 2009). To illustrate this relationship

the wave profile, ζ_p, observed at a wave probe is shown in Equation [2.47] (Mansard and Funke, 1980).

$$\varsigma_p = \sum_{k=1}^{N} A_{p,k} \cdot \sin\left[\frac{2\pi kt}{T} + \alpha_{p,k}\right] \quad \textbf{[2.47]}$$

which looks similar to Equation [2.37], except it is denoted using the sine notation. $A_{p,k}$ is the Fourier coefficient for frequency, T is the length of the wave profile, $\alpha_{p,k}$ is the phase relative to the time origin, and N is the upper limit of the summation which is related to the maximum significant frequency component. The Fourier coefficients and their phases can be expressed in polar or rectangular form as indicated in equations and are stated as in Equation [2.48] and [2.49], respectively:

$$B_{p,k} = A_{p,k} \cdot e^{-i\alpha_{p,k}} \quad \textbf{[2.48]}$$

$$B_{p,k} = A_{p,k} \cdot \cos\alpha_{p,k} + i\, A_{p,k} \cdot \sin\alpha_{p,k} \quad \textbf{[2.49]}$$

where $B_{p,k}$ is the Fourier Transform of $\zeta_{p,k}$. The FFT subroutine that is used for this research uses the rectangular form, and thus using the property of $\cos^2\theta+\sin^2\theta=1$, scaling by T, and renaming $B_{p,k}$ to be the amplitude spectra $A_S(k,f)$ we get:

$$A_s(k,f) = \frac{\sqrt{(A_{p,k})_{real}{}^2 + (A_{p,k})_{imag}{}^2}}{T}$$

The phase spectrum is calculated as:

$$\varepsilon_S = \tan^{-1}\left[\frac{(A_{p,k})_{imag}}{(A_{p,k})_{real}}\right] (-\pi \ldots \pi) \quad \textbf{[2.50]}$$

The magnitude and phase spectrum are in radians. The auto-spectra can now be used to calculate the auto-spectra $S_a(k,f)$ using Equation [2.50]:

$$S_a(k,f) = \frac{A_S(k,f)^2}{2 \cdot df} \quad \textbf{[2.51]}$$

or using angular frequency ω we have

$$S_a(k,\omega) = \frac{A_S(k,\omega)^2}{2 \cdot d\omega}$$

When the auto-spectrum is calculated through alternative means, for example using the indirect method, the magnitude spectrum can be calculated by the inverse of Equation [2.51] or as shown by:

$$A_S(k,\omega) = \sqrt{2 \cdot S_a(k,\omega) \cdot d\omega}$$

Since the FFT is producing a two sided spectrum, the amplitude spectrum is only showing the half peak of the energy spread out over the positive and negative frequencies to produce a mirror image, as shown in Figure 2-4.

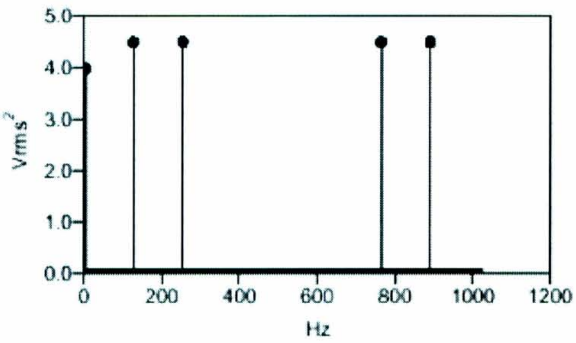

Figure 2-4 – A two sided line spectrum (National Instrument, 2009)

To correct the mirroring effect, the amplitude must be multiplied by 2 for half of the frequencies, ie. frequency of i=1 to N/2-1, and amplitudes at i=0 and N/2 to their original amplitudes and discard the rest of the amplitudes by letting them equal to 0 (National Instrument, 2009).

The spectral characteristics can be related to the time series with the use of the previously mentioned root mean square, shown by Equation [2.52], and the spectral moment, m^n. The spectral moment to the n^{th} power has the following formulation (Wave Spectra, FORMSYS):

$$m_n = \int_0^\infty \omega^n S_\varsigma(\omega) d\omega \ \ (n = 0,1,2, \dots) \qquad \textbf{[2.52]}$$

The zeroth moment, m_0, is the most important as it gives the equivalent to the area under the wave spectrum curve and it is equal to the variance of the time series, or the root mean square, as shown by Equation [2.54]. Equation [2.52] becomes Equation [2.53] for m_0.

$$m_0 = \int_0^\infty \omega^0 S_\varsigma(\omega) d\omega = \int_0^\infty S_\varsigma(\omega) d\omega \ \ (n = 0,1,2, \dots) \qquad \textbf{[2.53]}$$

$$rms_0 = \sqrt{m_0} \qquad \textbf{[2.54]}$$

2.4. Wave Splitting Theory

Introduction

Wave splitting is done by first measuring the waves at an assortment of locations in a model basin and then using of a wave model with regression techniques to distinguish how much energy is coming from the wave maker to the beach and vice versa. The low frequency wave, associated with the second order wave, can be identified by the wave model. The device used to record the wave is a wave probe in which there can be many placed at various locations in the basin.

The following environmental basin effects cause low frequency waves (Voogt, 2005):

1) Generating waves using a Flat Wave Flap. This type of wave flap can cause a mismatch between generated water velocities in a generated wave at the wave flap. This error can be minimized by applying a second order correction to the wave which is further discussed in Chapter 3.
2) Reflections of the waves due to the finite size of the basin. Minimized by inputting a parabolic beach but does not sufficiently dampen the long wave components.
3) Shoaling effects created by the bathymetry of the basin bottom. Significant in modeling shallow water situations as wave set-down will reflect as free waves from the parabolic beach.

The wave can be split into four different categories: incident free, incident bound, reflected free wave, and reflected bound wave, as shown by Equation [2.55]. The reflected bound

wave is neglected due to its insignificant size as compared with other wave categories (Voogt, 2005).

$$\varsigma = \varsigma_{inc,free} + \varsigma_{inc,bound} + \varsigma_{ref,free} + \varsigma_{ref,bound} \quad \textbf{[2.55]}$$

where:

ς: The total wave elevation.

$\varsigma_{inc,free}$: Incident free waves, propagating from the wave flaps to the beach.

$\varsigma_{inc,bound}$: Wave found bound to the incident free waves, also known as wave set-down.

$\varsigma_{ref,free}$: Reflected free wave from the wave flap to the beach.

$\varsigma_{ref,bound}$: Wave bounded to the reflected wave. As previously mentioned this term is neglected in the final wave elevation calculation.

The speed of the free waves differs from the bound waves and they have different directions. This allows the wave components to be distinguished from one another. Equations [2.56] and [2.57] describe the wave velocities for the free and bound waves, respectively, in which the bound uses the difference of the frequency (ω) and wave number (k).

$$c_{free} = \frac{\omega}{k} \quad \textbf{[2.56]}$$

$$c_{bound} = \frac{\delta\omega}{\delta k} \quad \textbf{[2.57]}$$

where

c_{free}: Speed of the free waves

c_{bound}: Speed of the bound waves

ω: Wave frequency

k: Wave number

$\delta\omega$: Partial wave frequency

δk: Partial wave number

Splitting the waves must be done for each wave frequency and the wave elevation for at least 3 spatial positions (Voogt, 2005). The incident and bound free waves at one specific frequency are shown in Equations [2.58], [2.59], and [2.60].

$$\varsigma_{inc,free} = \varsigma_{if} \cos(\omega t - k_{inc}x + \varepsilon_{if}) \quad \textbf{[2.58]}$$

$$\varsigma_{ref,free} = \varsigma_{rf} \cos(\omega t + k_{ref}x + \varepsilon_{rf}) \quad \textbf{[2.59]}$$

$$\varsigma_{inc,bound} = \varsigma_{ib} \cos(\Delta\omega t - \Delta k x + \varepsilon_{ib}) \quad \textbf{[2.60]}$$

where ε refers to a random phase angle between $-\pi$ and π for each wave type.

In order to find the frequency, ω, and wave number, k, the dispersion relationship can be used as shown by Equation [2.61]. Note that the difference frequency, $\Delta\omega$, and difference

wave number, Δk, do not satisfy the dispersion equation. The term g refers to gravity ($9.81 m/s^2$).

$$\omega^2 = gk \tan kh \qquad \textbf{[2.61]}$$

The Newton-Raphson method was the numerical method used to solve the wave number from the dispersion equation, which is described in section 4.3. Since the information pertaining to the wave components is limited, it is assumed that the bound wave propagates with a group speed that corresponds to the peak period of the energy spectrum (ie. $\omega = \omega_p$). This is reasonable with the further assumption of a narrow banded spectrum (Voogt, 2005). A Fourier transform will give the individual frequency components of the wave. Each frequency component can be written as Equation [2.62] where A and B are known coefficients.

$$\varsigma(x = x_n, \omega = \omega_j) = A\cos(\omega_j t) + B\sin(\omega_j t) \qquad \textbf{[2.62]}$$

Substituting Equations [2.62], [2.58], [2.59], and [2.60] into Equation [2.55], the total wave elevation equation is found:

$$
\begin{aligned}
A\cos(\omega_j t) + B\sin(\omega_j t) & \\
&= \varsigma_{if}\cos(\omega_j t - k_j x_n + \varepsilon_{if}) \\
&+ \varsigma_{ib}\cos(\Delta\omega_j t - \Delta k_j x_n + \varepsilon_{rf}) \\
&+ \varsigma_{rf}\cos(\omega_j t + K_j x_n + \varepsilon_{rf})
\end{aligned}
\qquad \textbf{[2.63]}
$$

The terms in Equation [2.63] can be collected and the unknown terms can be isolated and shown in Equation [2.64] as vector $\vec{y}$:

$$
\vec{y} = \begin{pmatrix} \varsigma_{if}\cos\varepsilon_{if} \\ \varsigma_{if}\sin\varepsilon_{if} \\ \varsigma_{rf}\cos\varepsilon_{rf} \\ \varsigma_{rf}\sin\varepsilon_{rf} \\ \varsigma_{ib}\cos\varepsilon_{ib} \\ \varsigma_{ib}\sin\varepsilon_{ib} \end{pmatrix} \qquad \textbf{[2.64]}
$$

Collecting the cosine and sine terms, two equations can be found for A and B as shown by Equations [2.65] and [2.66] and is proved in Appendix A.

$$
A = \begin{bmatrix} \cos(k_j x_n) & \sin(k_j x_n) & \cos(K_j x_n) & -\sin(K_j x_n) & \cos(\partial k_j \partial x_n) & \sin(\partial k_j \partial x_n) \end{bmatrix} \cdot \vec{y} \qquad \textbf{[2.65]}
$$

$$B = \left[\sin(k_j x_n) \quad -\cos(k_j x_n) \quad -\sin(K_j x_n) \quad -\cos(K_j x_n) \quad \sin(\partial k_j \partial x_n) \quad -\cos(\partial k_j \partial x_n)\right] \cdot \vec{y} \qquad \textbf{[2.66]}$$

Equations [2.65] and [2.66] are well conditioned then the solution can be found by matrix inversion. Singular Value Decomposition was the computational method used for matrix inversion and is described in section 4.4. The distance to which the wave probes are separated relative to the wavelength has great influence on the condition number, the ease of digital computation. The conditioning worsens (ie. the condition number will increase) when the distance between two probes are integer multiple of half the wavelength. Voogt (2005) discuses that the optimum spacing of the wave probes is 0.25 times the wavelength. When there are large distances between the probes, aliasing effects can occur where the signal from the probes becomes indistinguishable. Therefore the distances between the probes must be limited but must also be large enough to separate the free and bound waves travelling in the same direction.

Applying Wave Splitting Theory

When applying the wave splitting theory to a model test basin, there is a procedure that can be followed as discussed below shown in Figure 2-5 (Dijk 2007).

Step 1: Install wave probes in optimum locations

Step 2: Commence measurement of wave data during calibration; including start of wave marker to sometime after waver maker is shut down

Step 3: Prepare input for wave splitting tool

Step 4: Run wave splitting tool

Step 5: Check data from wave splitting results

Step 6: Attain wave forces of incident and reflected waves which are based on reflected database

Step 7: Solve equations of motion in the time domain

Step 8: Do comparison between numerical and measured vessel response in the basin

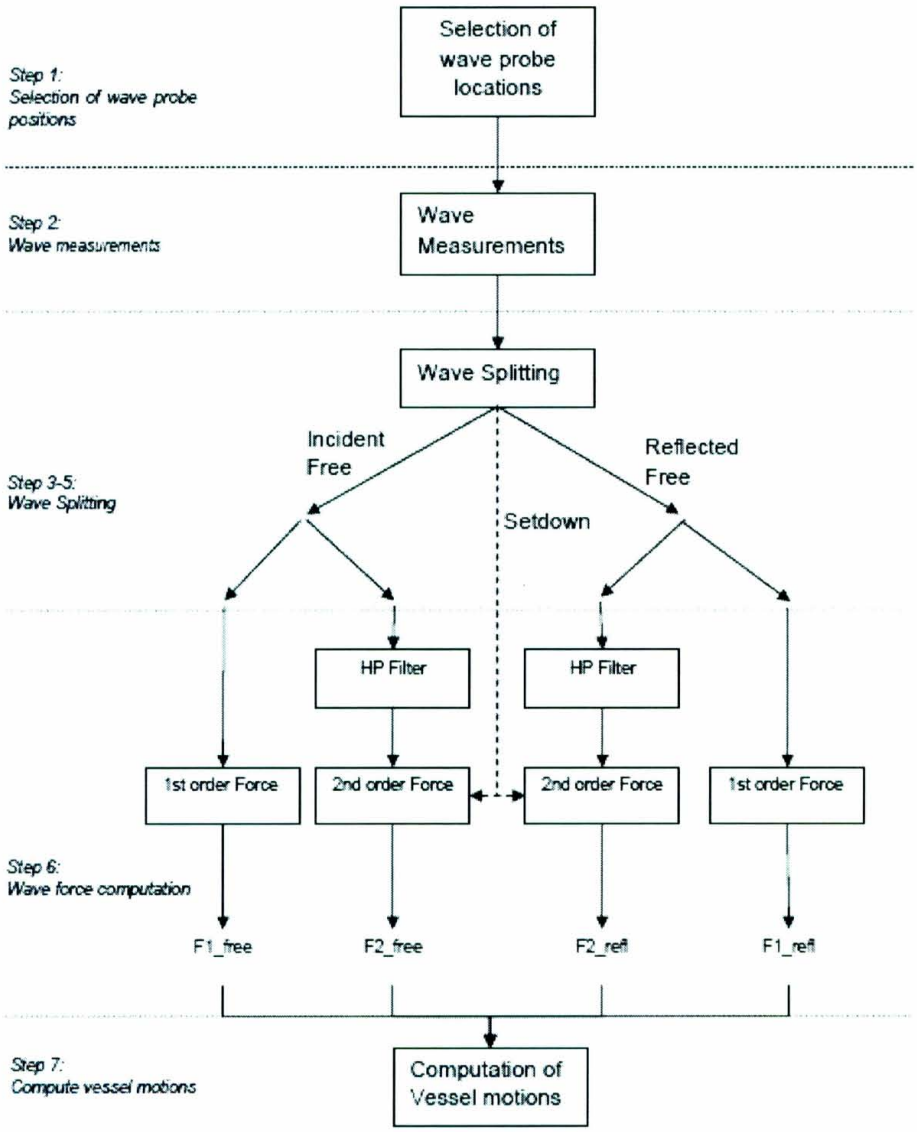

Figure 2-5 - Flow Diagram of Steps for Use of Wave Splitting (Dijk 2007)

It should be noted that attention must be paid to the damping values of the floating vessel to ensure that the numerical results match up with the measured results.

2.5. Analytical Model of Wave Set-down

An analytical model is used to calculate the theoretical set-down in the waves as an alternate method of calculating set-down and can also be compared to the set-down that was decomposed from the measured wave using the wave splitting tool.

As previously stated, the second order component of the waves contains a low frequency component known as wave set-down. It is a quadratic function of the wave amplitudes and can be found using a quadratic transfer function which gives the wave amplitudes and phases of the set-down in a travelling wave group (Huijsmans, 2002). In order to develop the analytical equations, potential theory is assumed.

The velocity potentials of fluid flow in waves are a summation of the different approximation orders that make up a wave and can be described as:

$$\phi = \phi^{(1)} + \phi^{(2)} + \cdots$$

The first order approximation of the equation, $\phi^{(1)}$, is usually the most significant component, especially in deep water situations. Huijsmans (2002) describes the boundary conditions for the first order approximation:

- The continuity equation states that the gradient of the first order approximation is equal to zero everywhere in the fluid domain.

$$\Delta\phi^{(1)} = 0,$$

- The free surface condition: the bottom potential added with the top potential must be equal to zero at the free surface.

$$g\phi_z^{(1)} + \phi_{tt}^{(1)} = 0$$

- The botton condition:

$$g\phi_z^{(1)} = 0 \text{ , at z=-h}$$

Using the previously stated boundary condition for a regular plane wave progression we can get an expression for the first order wave potential (Huijsmans, 2002), shown by Equation [2.67].

$$\phi^{(1)} = -\frac{\zeta^{(1)} gi}{\omega} \frac{\cosh \kappa(z+h)}{\cosh \kappa h} \exp(i\kappa x \cos\mu + i\kappa y \sin\mu - i\omega t) \qquad \textbf{[2.67]}$$

For the second order approximation, Huijsmans (2002) states the boundary conditions as:

- The continuity equation states that the gradient of the second order approximation is equal to zero everywhere in the fluid domain.

$$\Delta\phi^{(2)} = 0$$

- The free surface condition, shown by Equation [2.68], shows that the second order potential is dependent on the first order potential.

$$g\phi_z^{(2)} + \phi_{tt}^{(2)} = -2\nabla\phi^{(1)} \cdot \nabla\phi_t^{(1)} + \phi_t^{(1)}\left(\phi_{zz}^{(1)} + \frac{1}{g}\phi_{ttz}^{(1)}\right) \qquad \textbf{[2.68]}$$

- The bottom boundary condition:

$$\phi_z^{(2)} = 0, \text{ at z=-h}$$

To use the boundary conditions to derive an expression for the second order potential, we can first derive the first order potential associated with a regular wave group that consists of

two regular waves coming from two different directions (Huijsmans, 2002) shown by Equation [2.69].

$$\phi^{(1)} = \sum_{i=1}^{2}\sum_{k=1}^{2} \zeta_{ik}^{1} \frac{\cosh \kappa_i (z+h)}{\cosh(\kappa_i)\, h} \cos(\kappa_i x \cos \mu_k + \kappa_i y \sin \mu_k - \omega_i t) \qquad \textbf{[2.69]}$$

where i cannot equal k.

Huijsmans (2002) then describes the low frequency component of the second order potential between the two regular waves from different directions as shown by Equation [2.70].

$$\phi^{(2)} = \sum_{i=1}^{2}\sum_{j=1}^{2}\sum_{k=1}^{2}\sum_{l=1}^{2} \zeta_{ik}^{(1)} \zeta_{jl}^{(1)} A_{ijkl}^{-} \frac{\cosh(\kappa_i - \kappa_j)(z+d)}{\cosh(\kappa_i - \kappa_j) d} \exp i \Big((\kappa_i \cos \mu_k - \kappa_j \cos \mu_l) x + (\kappa_i \sin \mu_k - \kappa_j \sin \mu_l) y - (\omega_i - \omega_j) t \Big) \qquad \textbf{[2.70]}$$

The unknown A_{ijkl}^{-} term can be found by utilizing the free surface condition for the second order potential, shown in Equation [2.68]. Thus for A_{ijkl}^{-} we get:

$$A_{ijkl}^{-} = \frac{1}{2} \frac{B_{ijkl}^{-} + C_{ijkl}^{-}}{(\omega_i - \omega_j)^2 - (\kappa_i - \kappa_j) g \tanh(\kappa_i - \kappa_j) h} g^2$$

$$B_{ijkl}^{-} = \frac{\kappa_i^2}{\omega_i (\cosh \kappa_i h)^2} - \frac{\kappa_j^2}{\omega_j (\cosh \kappa_j h)^2}$$

$$C_{ijkl}^{-} = \frac{2\kappa_i\kappa_j(\omega_i - \omega_j)\left(\cos(\mu_k - \mu_l) + \tanh\kappa_i h \tanh\kappa_j h\right)}{\omega_i\omega_j}$$

The wave set-down is the low frequency component of the second order wave height on the free surface, given by Equation [2.71].

$$\zeta^{(2)} = -\frac{1}{g}\phi_t^{(2)} - \frac{1}{2g}\left|\nabla\phi^{(1)}\right|^2 - \frac{1}{g}\zeta^{(1)}\phi_{tz}^{(1)} \qquad \textbf{[2.71]}$$

Therefore the wave set-down is obtained as Equation [2.72].

$$\begin{aligned}\zeta^{(2)} = \sum_{i=1}^{2}\sum_{j=1}^{2}\sum_{k=1}^{2}\sum_{l=1}^{2} 2\zeta_{ik}^{(1)}\zeta_{jl}^{(1)}D_{ijkl}^{-}\cos\Big(&\big(\kappa_i\cos\mu_k \\ &- \kappa_j\cos\mu_l\big)x \\ &+ \big(\kappa_i\sin\mu_k - \kappa_j\sin\mu_l\big)y \\ &- \big(\omega_i - \omega_j\big)t\Big)\end{aligned} \qquad \textbf{[2.72]}$$

where $D_{ijkl}^{-}$is a transfer function that includes A_{ijkl}^{-}, B_{ijkl}^{-}, and C_{ijkl}^{-}components. $D_{ijkl}^{-}$is expressed as:

$$\begin{aligned}D_{ijkl}^{-} = \frac{A_{ijkl}^{-}(\omega_i - \omega_j)}{2g} - \frac{\kappa_i\kappa_j g}{4\omega_i\omega_j}\left(\cos(\mu_k - \mu_l) + \tanh\kappa_i h\tanh\kappa_j h\right) \\ + \frac{1}{4}\left(\kappa_i\tanh\kappa_i h + \kappa_j\tanh\kappa_j h\right)\end{aligned}$$

2.6. Power Spectrum Estimation

A power spectrum estimation theory was used in order to produce smooth power spectra since the wave splitting method produced noisy spectra graphs and made the real properties of the graphs difficult to distinguish. A method to reduce large variance from a $|X(f)|^2$ set of data is to multiply it by a weighting function W(f) (Beauchamp and Yuen, 1973). The process is typically called windowing and the weighting function is called the window, which produces a smoothed version of a spectrum. The type of window is discussed later in this section.

The method used to produce the spectra is based on the Welch method (Welch 17). The length of the record was sectioned into overlapping segments and a modified periodogram was found for each section by windowing the original record. Then the modified periodogram was then averaged. This method requires less iterations than other methods (Welch 17), due to the shorter record segments for computations.

For this method, a record has a length of:

$$X(j), j = 0, \dots, N-1$$

where N is the total number of record points. Overlapping segments, with a length of L, are separated by distance M. There are a total of K segments. The first few segments will have the form:

$$X_1(j) = X(j), j = 0, \dots, L-1$$

$$X_2(j) = X(j+M), j = 0, \dots, L-1$$

$$X_3(j) = X(j+2*M), j = 0, \dots, L-1$$

Therefore a general formula can be stated as

$$X_K(j) = X(j + (K-1)M), j = 0, \dots, L-1$$

Note that L+(K-1)M=N.

For each of the segments, the modified periodogram, another term for estimating the spectral density of a time series, can be found by multiplying it by a windowing function. A hanning function, or window, was used which has a cosine shape and has the following formulation:

$$W(f) = \frac{1}{2} + \frac{1}{2}\cos\left(\frac{\pi f}{N}\right)$$

where N is the total number of points (Beauchamp and Yuen, 1973).

In order to determine the total number of segments K, the length of M was first calculated, which was based on the Nyquist frequency and the frequency resolution dw. The frequency resolution was assumed in order for the resolution to be low enough to smooth the fluctuations but high enough not to underestimate the properties of the spectra. The Nyquist frequency, as previously mentioned, is based on the time step and π. Thus M was calculated to be the Nyquist frequency divided by the resolution (Dijk, 2007). K can then be found as N/M-1. The overlapping length L is calculated as 2*M.

For each segment of length L the modified periodogram is calculated and then the finite Fourier transforms are found as shown in Equation [2.73].

$$A_K(n) = \frac{1}{L}\sum_{j=0}^{L-1} X_K(j)W(j)e^{-2kijn/L} \quad \textbf{[2.73]}$$

We can thus calculate the modified periodograms as:

$$I_k(f_n) = \frac{1}{L * f_N}|A_k(n)|^2, k = 1,2, \dots, K$$

which is a modified equation based on Welsh (1976) and Dijk (2007). The spectral estimate is the average of the periodograms as shown in Equation [2.74].

$$\hat{P}(f_n) = \frac{8}{3K}\sum_{k=1}^{K} I_k(f_n) \quad \textbf{[2.74]}$$

where 8/3 is an averaging function as recommended by Dijk (2007).

3. WAVE GENERATION

3.1. Wave Generation Introduction

Wave generation was done at the National Research Council (NRC) Offshore Engineering Basin (OEB) in St. John's, NL. 56 piston-type segmented wave makers were used to generate the waves. The wave data in the OEB was measured using fourteen wave probes.

The waves were generated by two methods: the first method generated waves containing only first order waves and the second method contained both first order components as well as second order components, as outlined in Section 1.3. Second order wave components are naturally created in the shallow water environment and thus generating waves with second order components should allow for better correlation with results from the wave splitting program. The measured data should better align with the theoretical wave set-down that was generated using the analytical model in the low frequency domain. The addition of the second order wave generation should also correct the mismatch between the wave velocities that the first order wave generation can cause.

3.2. Piston Type Wave Maker

A piston type wave maker, as shown in Figure 3-1, has multiple pistons that displace the water by repeatedly moving horizontally back and forth. Figure 3-1 shows that there can be a large number of pistons moving the water forward to create the water waves.

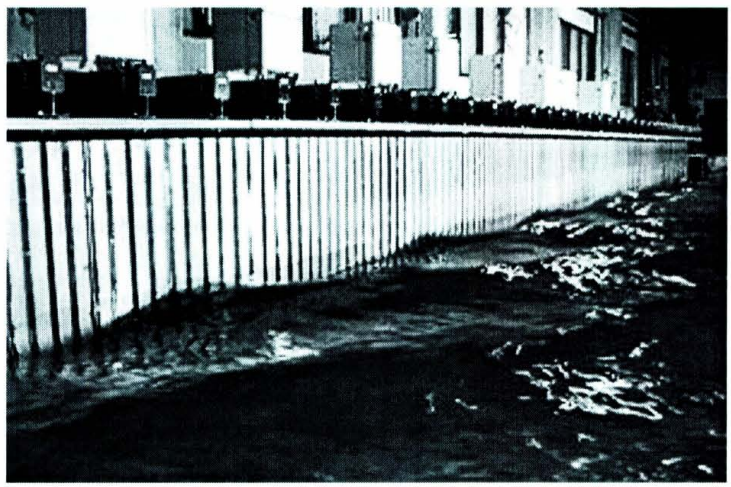

Figure 3-1 – Piston type wave maker (Wavemaker)

The piston type wave maker is one of the more simplified wave makers in terms of boundary conditions as there is only translational motion, with no rotational motion (Schäffer, 1994). The wave maker oscillates with varying velocities and stroke lengths. The range of the frequencies of the oscillations corresponds to the desired frequency range of the generated irregular sea state. Software equipped into the wave maker take into account the second order wave theory in shallow water. Therefore there is a second order correction for the linear motion of the piston that differs slightly from the motions of the water particles in shallow water. The linear motion of the piston causes the motion of the free waves to be circular in shape and is not representative of ocean going waves as they are

typically oval shaped particles of motion. Therefore an added signal is incorporated to the unwanted free waves that is opposite in sign and will eliminate them.

3.3. Basin Test Configuration

The shallow water model testing took place at NRC in the OEB. The basin is 75 meters length and 32 meters in width (Zaman et. al., 2011), as shown in Figure 3-2.

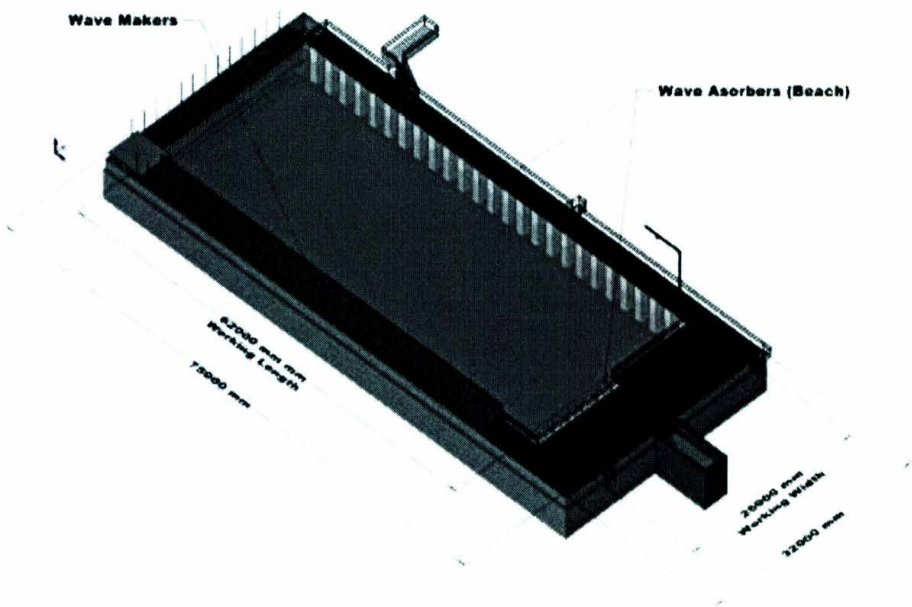

Figure 3-2 - NRC Ocean Engineering Basin (OEB)

The basin has wave makers in both longitudinal and transverse directions, but only longitudinal waves were used. There are also wave absorbers, or beaches, opposite of the wave maker. The basin also has capabilities to create environmental conditions such as current and wind, but only wave generation was used. In order to replicate shallow water depths of 15m in the basin, a scale of 1:50 was used to result in a depth of 0.3m and 0.6m. The piston wave maker oscillates with varying velocities and strokes to generate the waves. A different range of frequencies were used and input into the software equipped to the wave maker. Fourteen capacitance type wave probes were used to read the encounter frequency

of the waves. As waves contact the wave probes, the changing internal resistance within wave probes allows the frequency of the waves to be measured. Figure 3-3 shows the positions of the wave probes within the OEB.

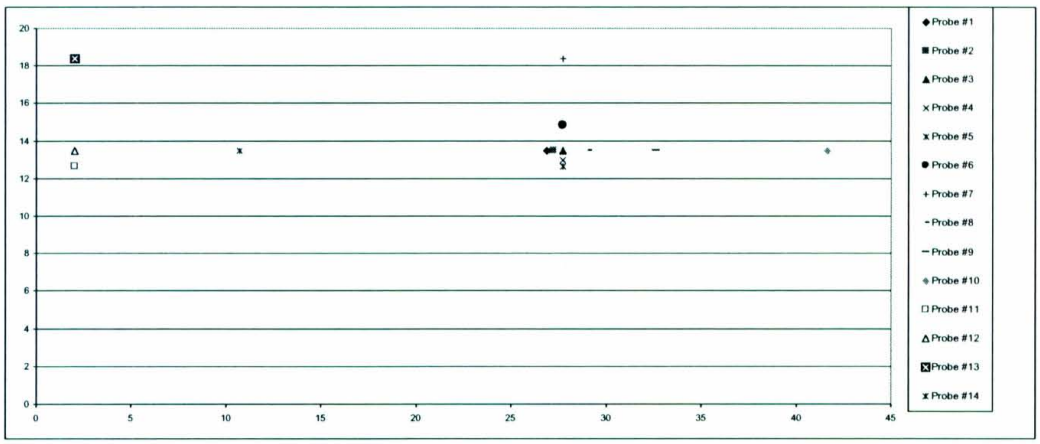

Figure 3-3 – Positions of the Fourteen Wave Probes Within the OEB.

3.4. Physical Modeling

Certain properties of the long waves are dominant at different frequency ranges which have an effect of the wave generators. For a piston type wave generator, a method to find the accurate second order piston position, $X^2(t)$, is to extend the boundary conditions to second order and apply the Laplace equations with nonlinear surface conditions. Free waves are excluded from $X^2(t)$ equation. Sand (1982) discusses how if only first order wave generation was utilized for the model tests of a moored bulk carrier, the mooring forces would greatly differ from the prototype. It is important to know the amplitude of the second order long waves, ξ_a, and the amplitude of the second order control signal, $X_a^{(2)}$, before doing the model test. ξ_a and $X_a^{(2)}$ can be estimated through the use of a transfer function, as shown by Equations [3.1] and [3.2].

$$\xi_a = \frac{G_{nm} h A_n A_m}{h} \qquad \textbf{[3.1]}$$

$$X_a^{(2)} = \frac{F_1 h A_n A_m}{h} \qquad \textbf{[3.2]}$$

where:

G_{nm}: a transfer function

F_1:a transfer function

h: water depth

A_n,A_m: the amplitudes of the terms in the respective transfer function

4. COMPUTATIONAL METHOD

4.1. Band-pass Filter

A band-pass filter was used to reduce the noise of the data. Band-pass values were assumed from typical values of typical spectral density plots, specifically the JONSWAP wave spectral density plot as shown in Figure 4-1.

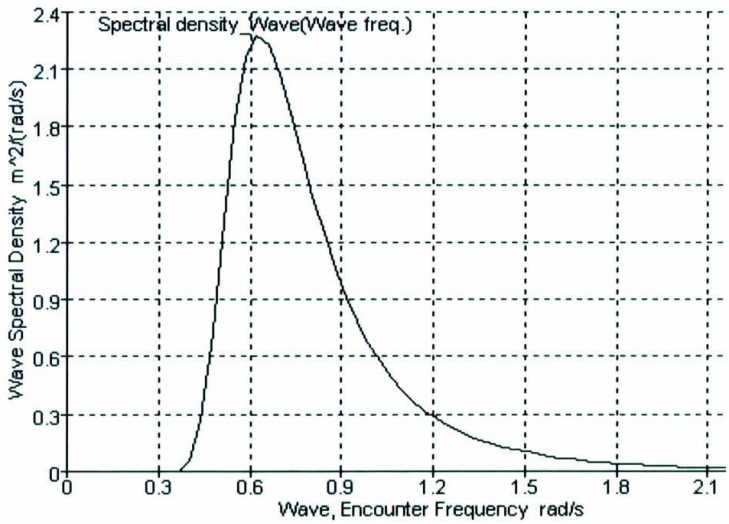

Figure 4-1 – JONSWAP Spectral Density Plot (Wave Spectra, FORMSYS)

The high pass frequency filter sets a lower limit for acceptable frequencies to be used within the program so that frequencies higher than the limit can pass. The low pass frequency filter sets an upper limit for acceptable frequencies to be used within the program so that frequencies lower than the limit can pass. Values assumed for the high pass filter were 0.2 rad/s. For the low pass filter the Nyquist frequency was used to avoid aliasing

effects. An absolute maximum of 6 rad/s is also imposed in order to reduce noise if the Nyquist frequency determined to be too large.

4.2. Fast Fourier Transform

The FFT is a complex algorithm that few scientists and engineers could write themselves. There are two main steps to an FFT computation: first the FFT breaks down an N point time domain signal into N single transforms, to which it then calculates the N frequency spectra. Secondly it synthesizes the N spectra into single frequency spectrum. Using an example illustrated by Smith (1997) it can be shown exactly how it is broken down.

A 16 point signal can be decomposed four times until each signal is down to a single point, as shown in Figure 4-2.

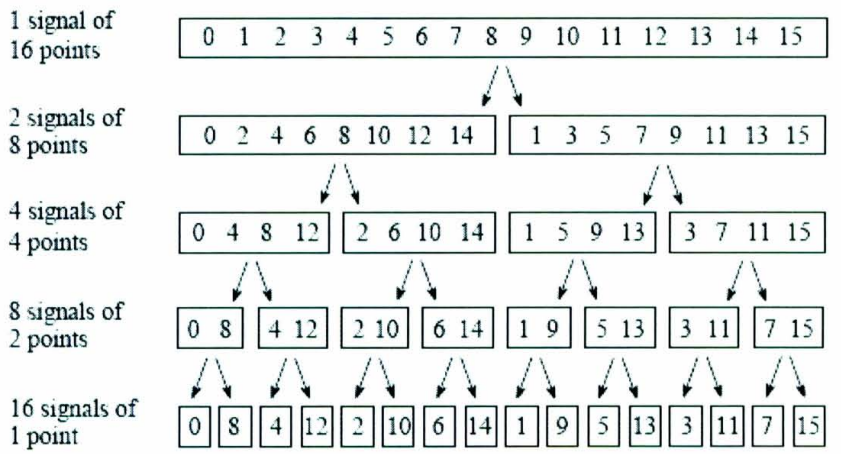

Figure 4-2 – Decomposition of a 16 Point Signal (Smith 1997)

The decomposition is done by converting each decimal number into a binary number so that the numbers are separated into even and odd categories or what is known as interlaced decomposition. This process is often done using a bit reversing algorithm that rearranges the points with the bits flipped left to right, shown in Figure 4-3.

Sample numbers in normal order			Sample numbers after bit reversal	
Decimal	*Binary*		*Decimal*	*Binary*
0	0000		0	0000
1	0001		8	1000
2	0010		4	0100
3	0011		12	1100
4	0100		2	0010
5	0101		10	1010
6	0110	⇨	6	0100
7	0111		14	1110
8	1000		1	0001
9	1001		9	1001
10	1010		5	0101
11	1011		13	1101
12	1100		3	0011
13	1101		11	1011
14	1110		7	0111
15	1111		15	1111

Figure 4-3 – Bit reversing algorithm (Smith 1997)

After the points have been rearranged, the next step is to find the frequency spectra of a one point time domain signal, which is simply equal to itself. Therefore there is no work required to do this step and all time domain points are now frequency domain points.

For the final step in the FFT procedure, the N frequency spectra must be recombined in the exact opposite manner in which it was decomposed in step one. This is the most complex of all the steps. Since bit reversal cannot be used for this stage, the process is reversed one level at a time. A 16 frequency spectra (1 point each) is divided into two 8 frequency spectra (2 points each) and then each 8 point spectra are subdivided into 4 point spectra, etc, until a 16 point frequency spectrum is created. Therefore in order to build the frequency domain points back so that they correspond the time domain points, two signals must be

interlaced to make one. For example, to obtain an 8 point signal from two 4 point signals, each 4 point signal must be diluted with zeros and added together to obtain the original signal, as shown in Figure 4-4.

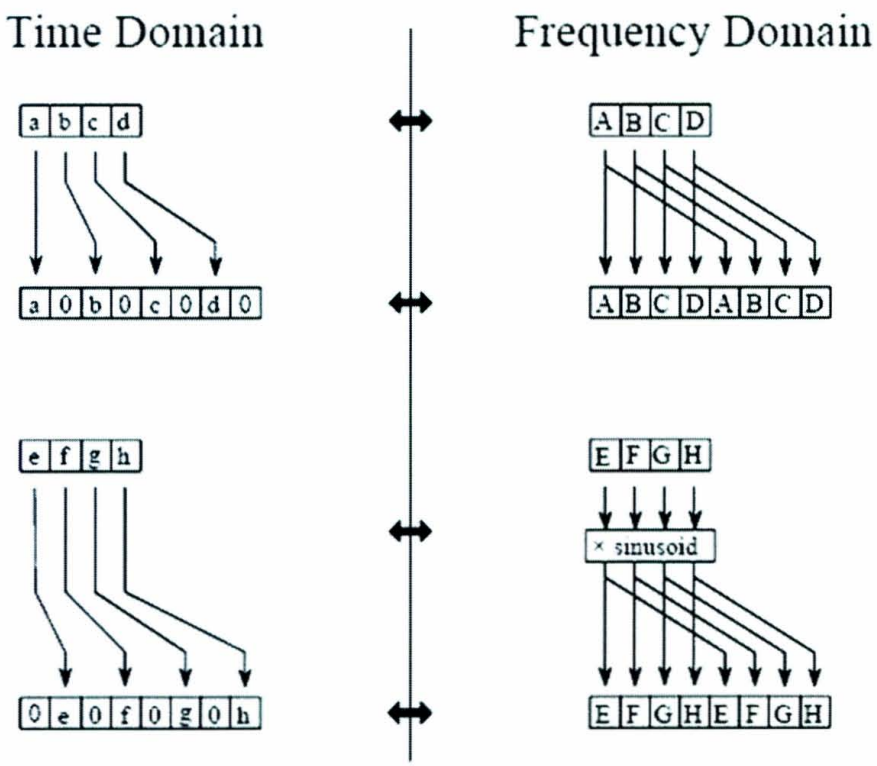

Figure 4-4 – Reconstructing signals in the time and frequency domain (Smith 1997)

It can also be noted from Figure 4-4 that in order to appropriately add the two 4 point signals, one of the signals must be shifted. This will allow a0b0c0d0 and 0e0f0g0h to become aebfcgdh. In the frequency domain, the dilution from the time domain becomes duplication in the frequency domain, as can be seen in Figure 4-4. The duplicated spectra

are then added together in order to form the new spectra. The shift that is done in the time domain corresponds to multiplying the spectrum by a sinusoid.

The most basic calculation within the FFT subroutine is called a butterfly, termed after its appearance, where two complex points are converted to two other complex points and is shown in Figure 4-5.

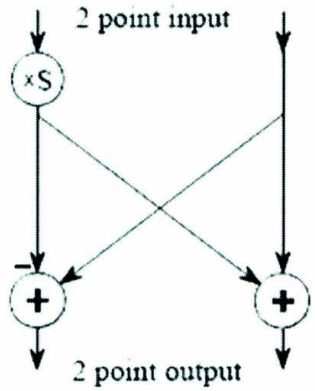

Figure 4-5 – The Butterfly Calculation (Smith 1997)

This pattern is repeated for each step of the process of recreating the full frequency spectrum, as shown by Figure 4-6.

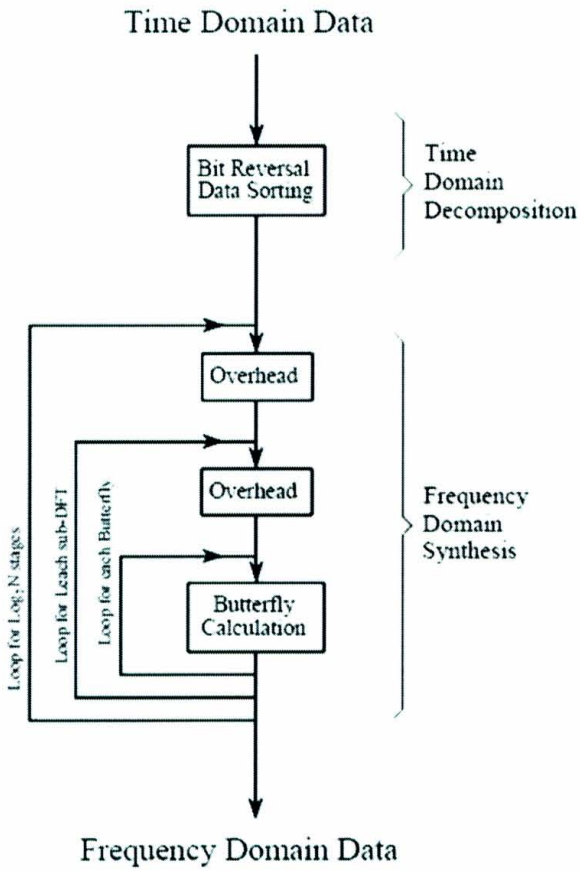

Figure 4-6 – Total FFT Procedure (Smith 1997)

Figure 4-6 illustrates the three loops that are needed in order to recreate the frequency domain data. The outer loop repeats for Log_2N stages, the middle loop repeats for each of the levels of frequency spectra that are being added, and the inner loop repeats the butterfly for each individual frequency spectra. The overhead boxes calculate the level of the interlacing to determine what is left to be calculated.

4.3. Newton-Raphson Method

The Newton-Raphson method is used for solving the dispersion equation. It uses an initial guess for the value of k, described here as x_i, in order to create a tangent line to the function $f(x_i)$, where the tangent line is the derivative of the function $f(x_i)$, and is extrapolated down to the x axis which provides an estimate of the root x_{i+1} (Chapra 2006). Thus the Newton-Raphson can be derived on the basis of geometrical analysis and can be shown in the form of Equation [4.1].

$$x_{i+1} = x_i - \frac{f(x_i)}{f'(x_i)} \qquad \textbf{[4.1]}$$

4.4. Singular Value Decomposition

Singular value decomposition (SVD) is a method in linear algebra that factorizes a real or complex matrix. The form that SVD takes in shown below:

$$M_{mn} = U_{mm}S_{mn}V_{nn}^{T}$$

where: M is the initial rectangular matrix

U is an orthogonal matrix. The columns are orthonormal eigenvectors of AA^T.

S is a diagonal matrix that contains the singular values, or the square roots of eigenvalues, of U

V^T is the transpose of the orthogonal matrix V. The columns of V are the orthonormal eigenvectors of A^TA

m is the number of rows in the matrix

n is the number of columns in the matrix

The orthogonal matrices multiplied by their transpose matrix must equal the identity matrix, such that $U^TU = I$ and $V^TV = I$.

SVD has many advantages, which include revealing many important properties of the matrix, such as the eigenvectors, and determining a form of matrix inversion. For this research, SVD was used to solve the unknown matrix y stated in Section 2.4. Finding the inverse of a matrix can be easily completed for a square matrix. Since the matrices in this research are rectangular matrices, an alternative method is required. The SVD method becomes useful as it can solve a pseudo-inverse matrix for a non-square matrix. The SVD

method also provides a numerically stable method for solving linear equations which is important for a highly numerical process. In order to complete the matrix inversion, the three matrices that make up the original matrix M are used to find the inverse as shown in Equation [4.2].

$$M_{mn}^{-1} = V_{nn} S_{mn}^{-1} U_{mm}^{T} \quad \textbf{[4.2]}$$

4.5. Wave Splitting Program

The wave splitting program, created using FORTRAN 77 is described by the flow chart shown in Figure 4-7. The program starts by having the user input select variables which includes:

- Peak period of the wave data in seconds
- Water depth in meters
- Desired number of wave components to be split.

This gives the option for the user to run a variety of different wave data sets and easily change the important input parameters.

The program then reads in the files containing the time, wave amplitudes, and wave probe positions. The user must verify the files are named in correspondence to what they are named the program, which can be left to the discretion of the user.

The program then will set up all the variables in a relative manner, ie. setting everything in relation to the first probe so that the first probe is at longitudinal position x=0. The subroutine then calls the 'Specsmooth' subroutine which will create smooth spectra for the measured data from each wave probe.

The signal is then filtered using a band-pass filter subroutine to eliminate low and high frequencies that is beyond the desired spectrum to eliminate aliasing effects. The filtered

signal is called into a subroutine that will calculate the theoretical wave set-down. The theoretical wave set-down is removed from the original measured signal.

The signal is then converted from the time domain to the frequency domain in order to split the wave into its individual components in the wave splitting subroutine. A Newton-Raphson subroutine is used to solve the dispersion relation in order to solve the wave numbers. The frequency domain information is read into the wave splitting subroutine where the wave components are individualized as required by the user. The wave splitting subroutine uses the 'SVD' subroutine to do the matrix decomposition.

The individual components are converted back to the time domain and the 'Spectral Smoothing' subroutine creates smooth spectra for each of the wave components data for each wave probe. The 'output' subroutine creates eight data files for the each individual wave component in the time and frequency domain.

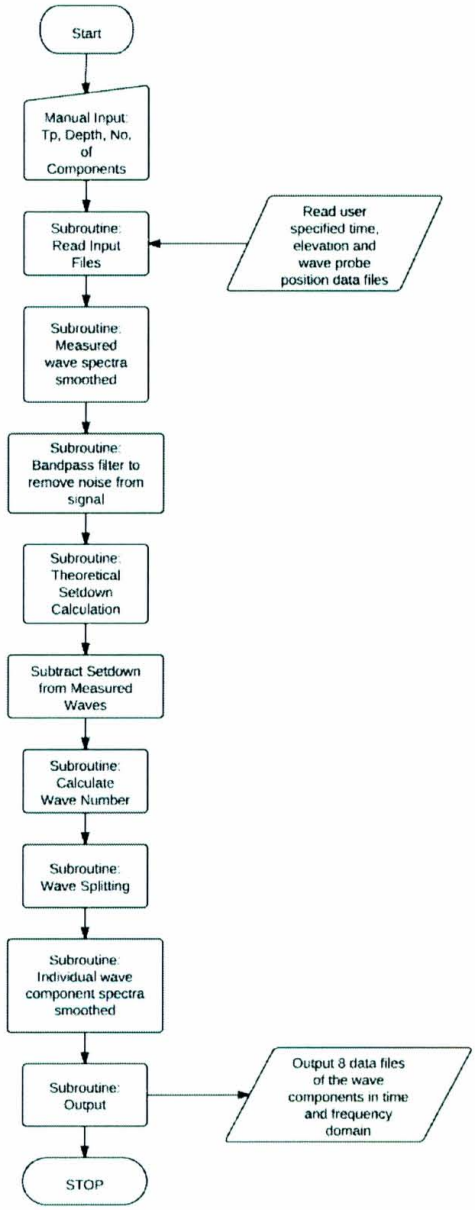

Figure 4-7 – Wave Splitting Code Flow Chart

5. RESULTS

5.1. Validation

Theoretical Set-down

The theoretical wave set-down was validated using published results reported by Huijmans (2002). Huijmans (2002) reports the transfer function of the wave set-down for a water depth at 19 m using frequencies from 0.5 rad/s to 0.8 rad/s.

Wave Splitting

The wave splitting code in FORTRAN was validated against the wave splitting program reported by MARIN (Djik 2007) for the time domain results shown in Figure 5-1 to Figure 5-4, which show a full scale comparison using peak period 1.705s. The current results were also validated against published experimental NRC data and numerical results (Zaman et. al., 2011) in the frequency domain shown in Figure 5-5 to Figure 5-10 for wave probes 1,2,9 for peak period 1.133s. The frequency domain plots illustrate the measured data from the wave probes and results for both the first order (FO) and second order (SO) wave generation are reported. The time domain results were shown to be quite similar to the MARIN results. Due to the high degree of similarity between the plots of Figure 5-1 to Figure 5-4, the results for this research and MARIN, for the most part, overlay each other.

The frequency domain results were only satisfactory but deemed passable as there are many different methods for approximating the power spectrum and thereby makes it difficult to conduct a meaningful comparison. For instance, the resolution chosen for the spectral

approximation had a significant effect on the spectral density function when computing the results. Since the parameters for computing the spectra chosen by NRC are unknown, including the resolution, it is difficult to speculate the reasons for differences.

Figure 5-5 to Figure 5-10 also show that there is some fluctuation at the higher frequencies. This appears to reiterate the observation by Mansard (1991) who stated that even with the use of a second order correction, which was applied to the irregular wave data from NRC, oscillations can still occur in the high frequency tail end of the spectrum from free waves and locked waves.

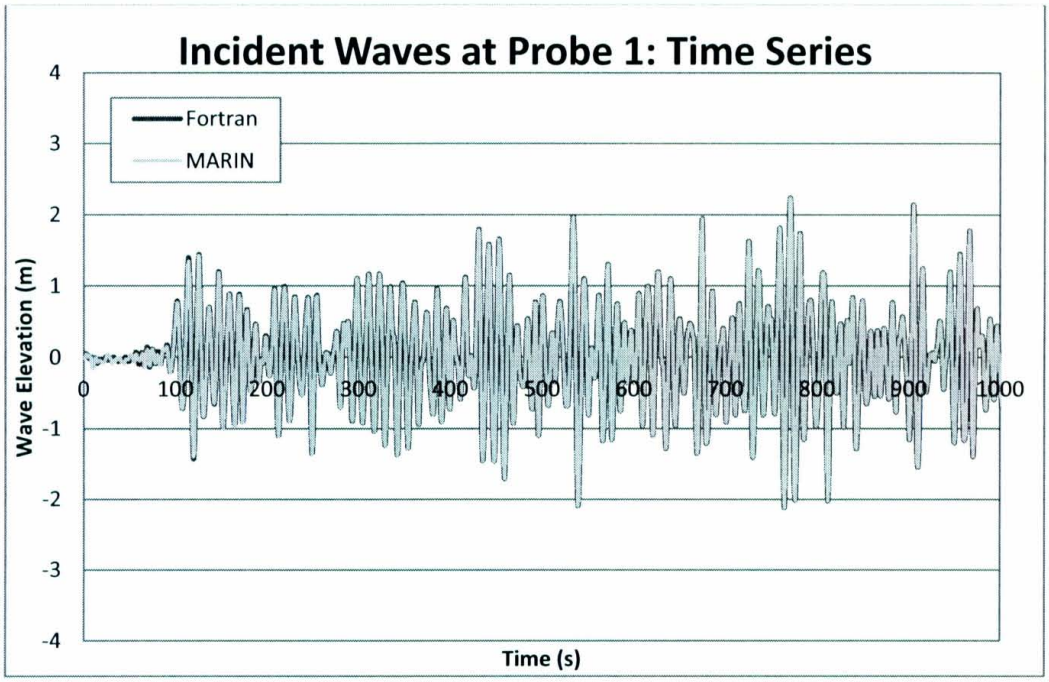

Figure 5-1 – Current Method versus MARIN: Incident Wave, Time Series, Probe 1

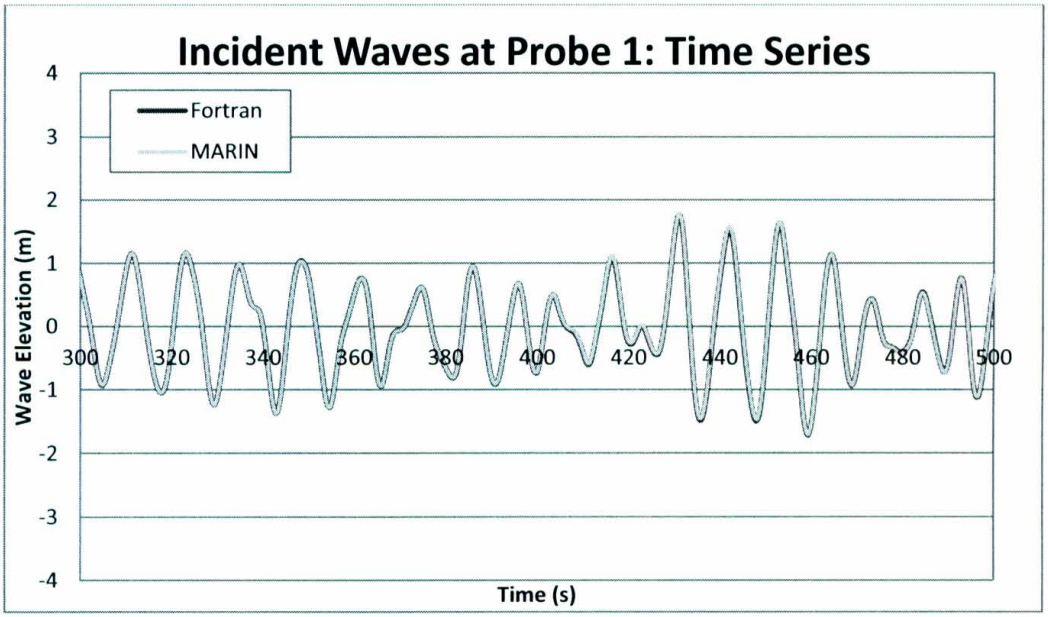

Figure 5-2- Current Method versus MARIN: Incident Wave, Time Series, Probe 1 (300-500s)

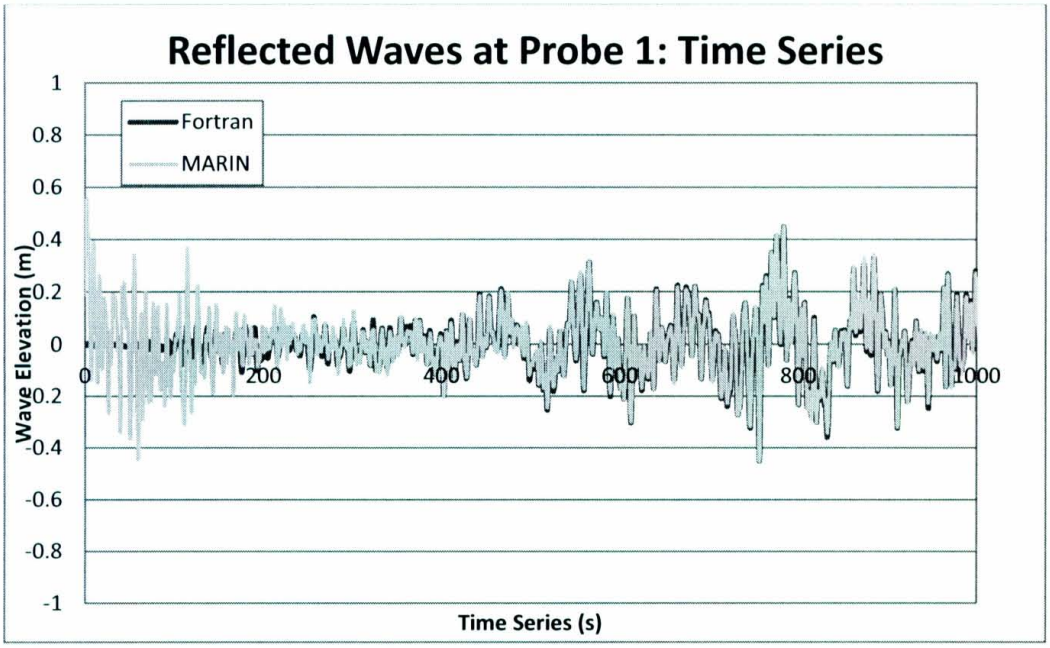

Figure 5-3 – Current Method versus MARIN: Reflected Wave, Time Series, Probe 1

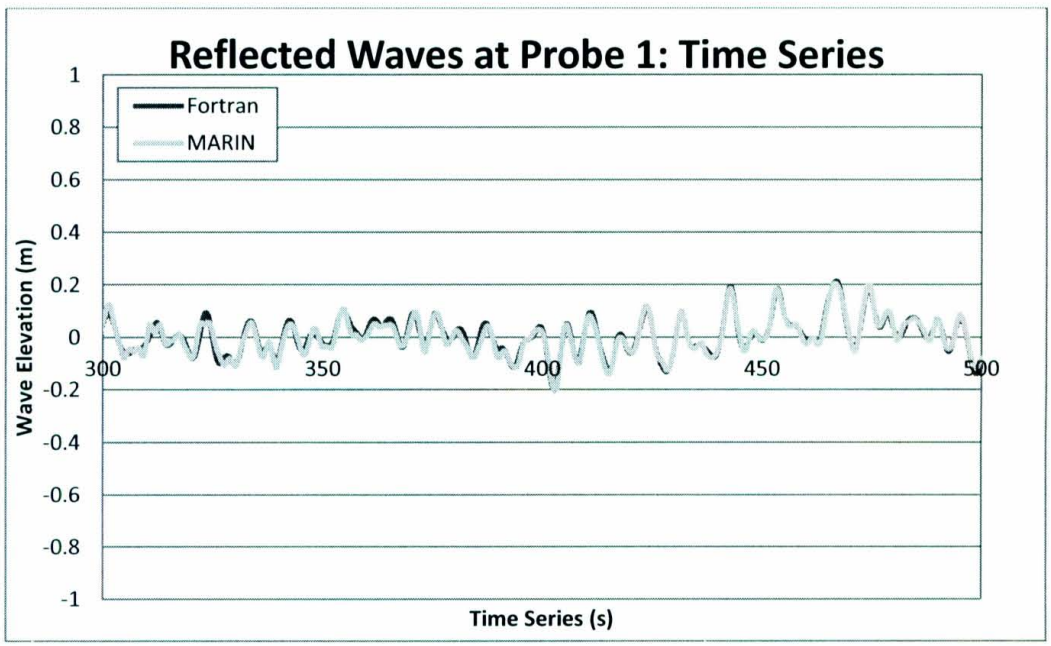

Figure 5-4 – Current Method versus MARIN: Reflected Wave, Time Series, Probe 1 (300-500s)

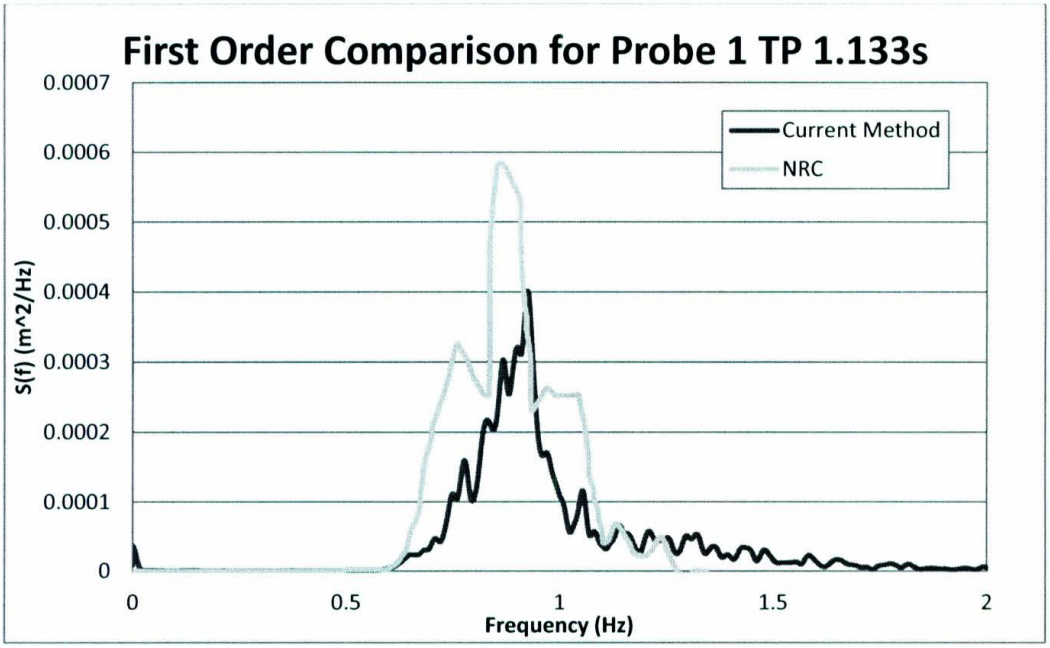

Figure 5-5 – Current Method versus NRC: FO Measured Wave, Frequency Series, Probe 1

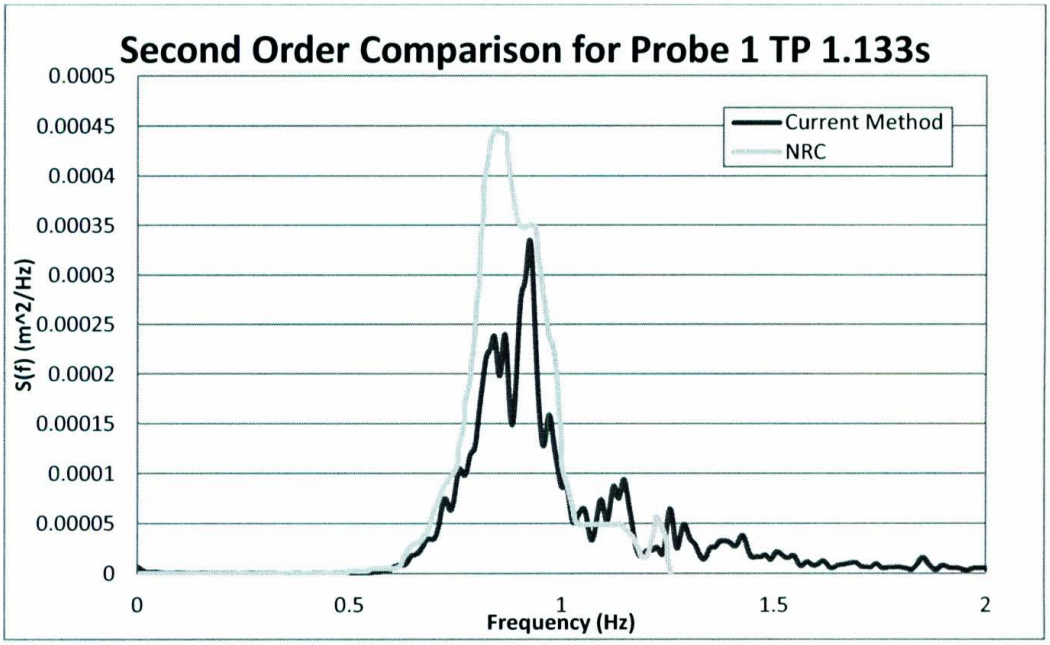

Figure 5-6 – Current Method versus NRC: SO Measured Wave, Frequency Series, Probe 1

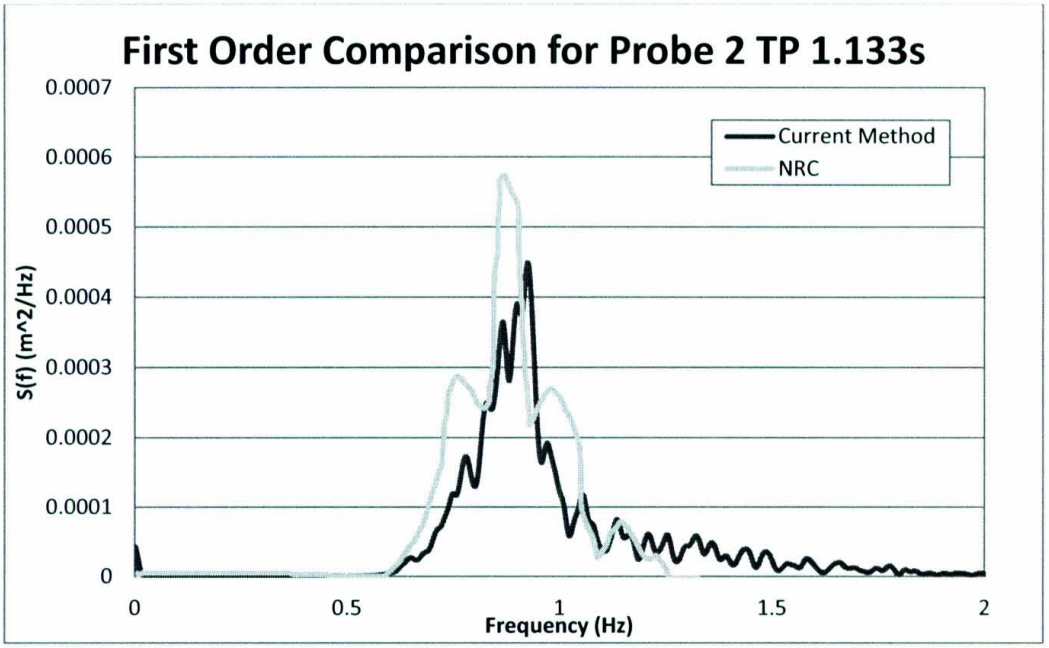

Figure 5-7 – Current Method versus NRC: FO Measured Wave, Frequency Series, Probe 2

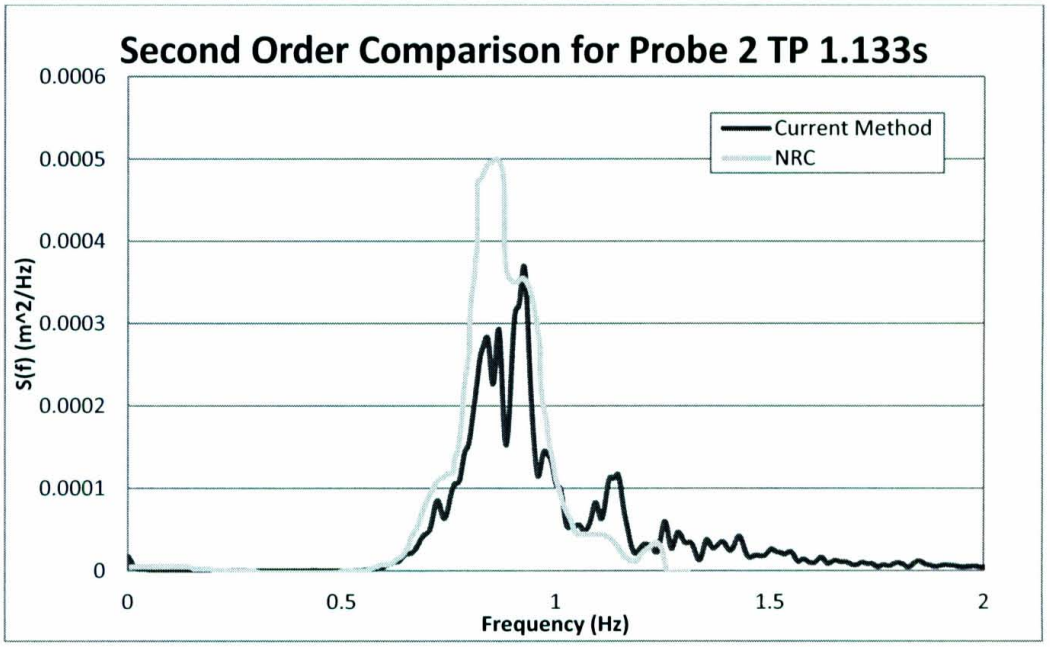

Figure 5-8 – Current Method versus NRC: SO Measured Wave, Frequency Series, Probe 2

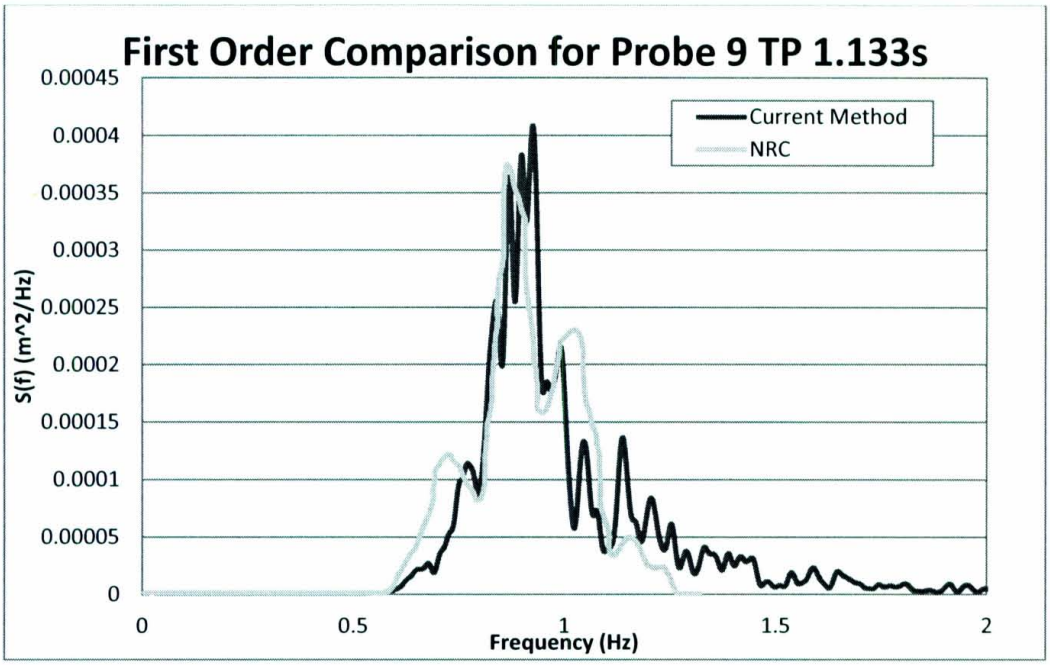

Figure 5-9 – Current Method versus NRC: FO Measured Wave, Frequency Series, Probe 9

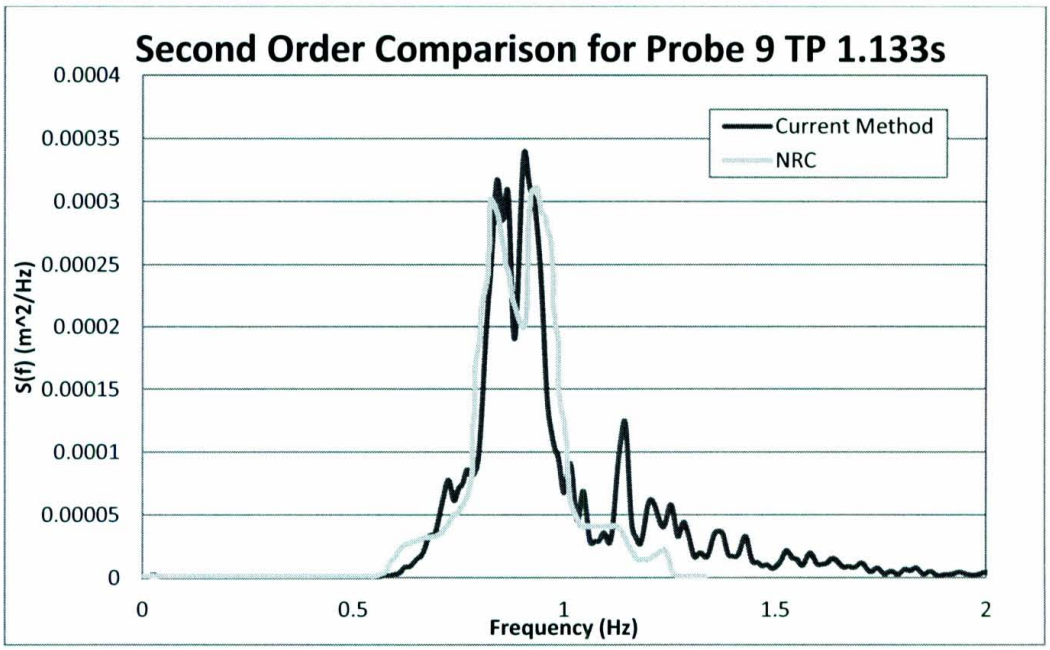

Figure 5-10 – Current Method versus NRC: SO Measured Wave, Frequency Series, Probe 9

5.2. OEB Results

Shallow water wave generation was completed at the NRC OEB for wave heights of 4 and 6 cm and for peak periods of 1.133, 1.705, and 2.145s at model scale. A scale of 50 was used to relate the data between model and full scale data. The results are shown for wave probes 1,2,3,8,9 since they follow the trajectory down the middle of the tank, as shown by Figure 3-3, so their wave heights should be proportionate to each other and separated by different wave phases due to their distance apart. The program was used to run both model scale and full scale cases to verify functionality in either case. Table 5.1 shows the data used to run both cases.

Table 5.1 –Parameters of Model Scale and Full Scale

Parameter	Model Scale	Full Scale
Depth (m)	0.4	20
Significant Height –H_s (m)	0.06	3
Peak Period – T_p: Case 1 (s)	1.133	8.012
Peak Period –T_p:Case 2 (s)	1.705	12.056
Peak Period – T_p: Case 3 (s)	2.145	15.167

The wave splitting code was applied to the OEB wave elevations and the following results were obtained. Figure 5-11 through Figure 5-20 show results for T_p-Case 3 in the time domain, for 0-1000s and 300-500s. Figure 5-21 through Figure 5-30 show results the frequency domain, for 0-1.4rad/s and 0-0.3rad/s which is the low frequency component frequency. Cases 1 and 2 are shown in Appendix B. The incident waves show good

agreement with the original measured waves in terms of amplitude and phase. The following figures display the results of the model scale only and the full scale data is shown in Appendix C.

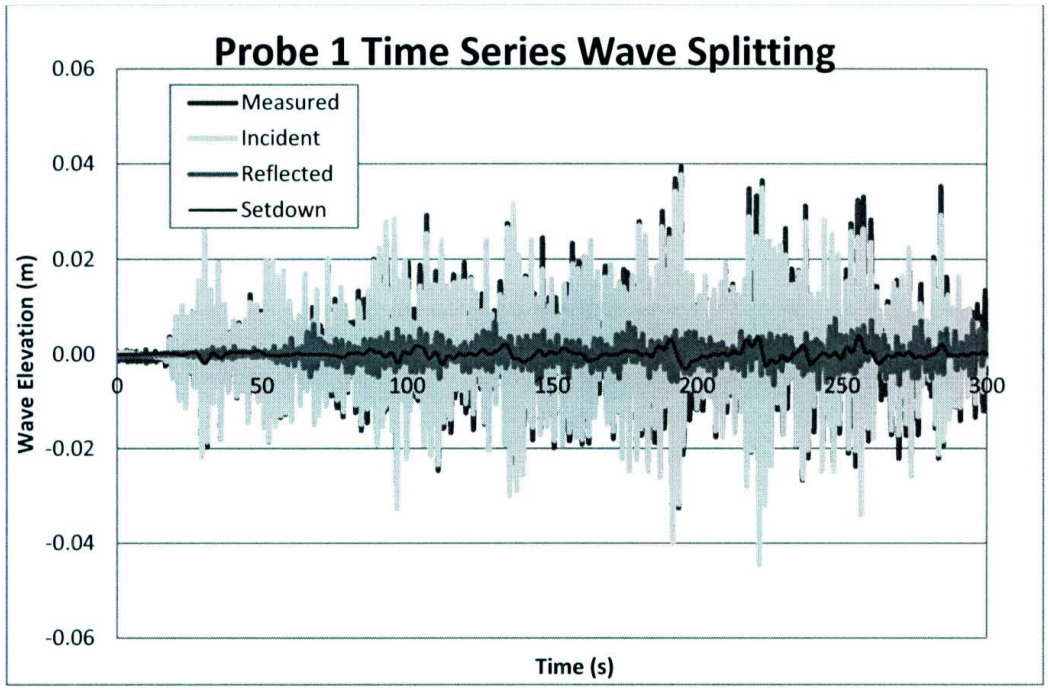

Figure 5-11 – Time Series Wave Splitting, Probe 1

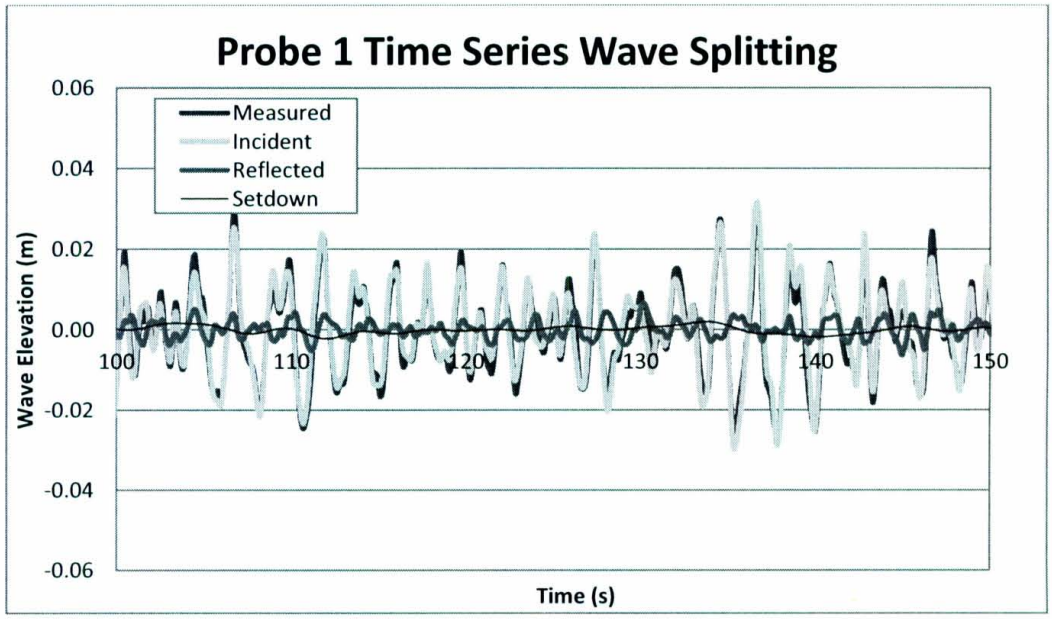

Figure 5-12 - Time Series Wave Splitting, Probe 1 (100-150s)

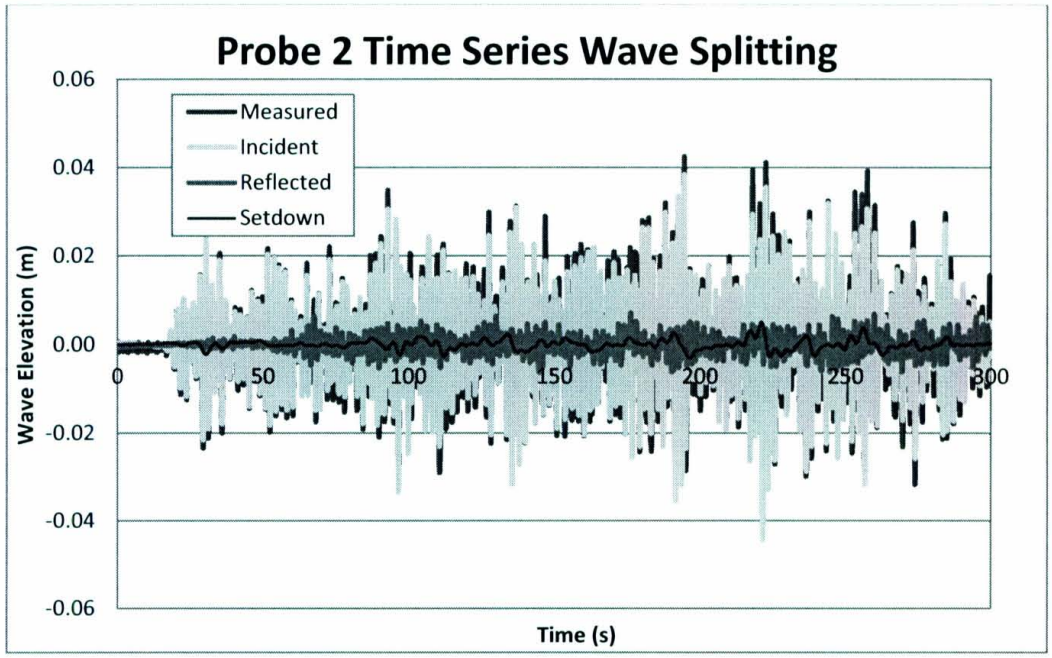

Figure 5-13 - Time Series Wave Splitting, Probe 2

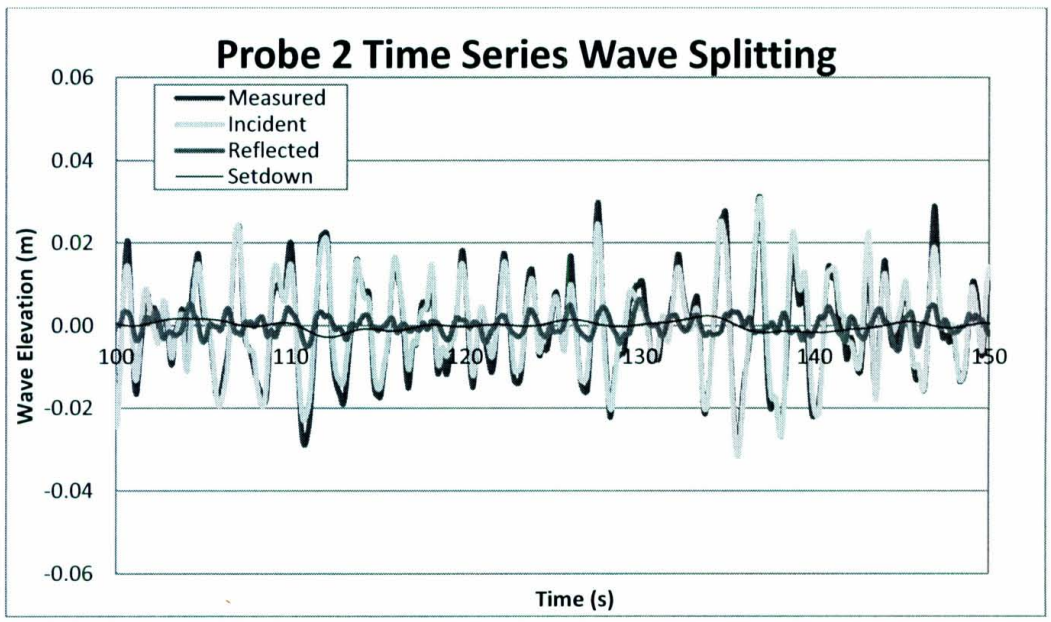

Figure 5-14 - Time Series Wave Splitting, Probe 2 (100-150s)

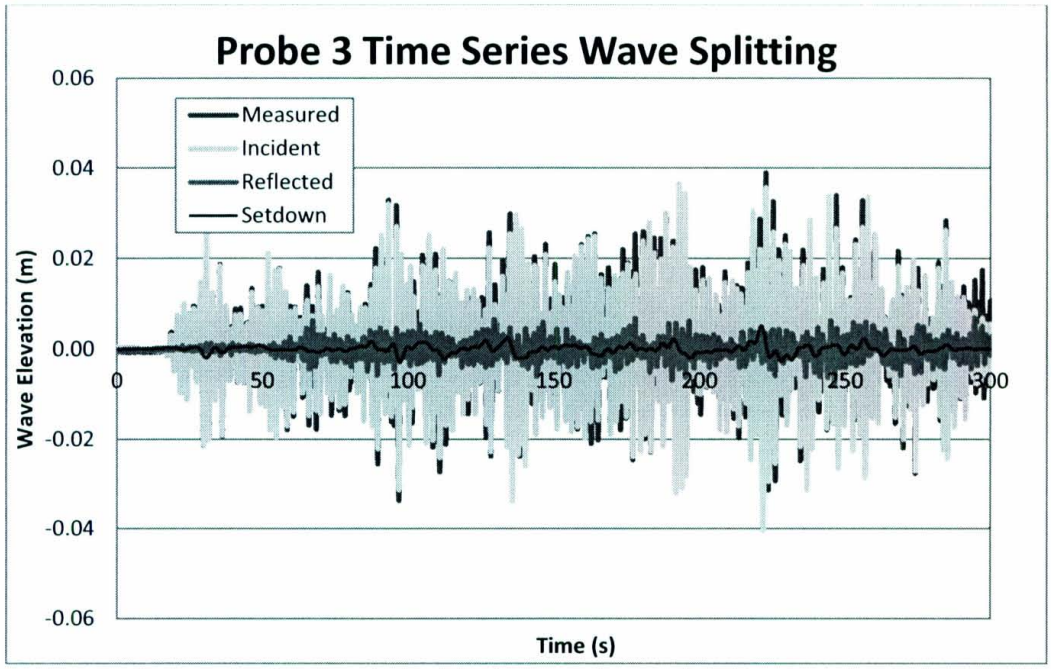

Figure 5-15 - Time Series Wave Splitting, Probe 3

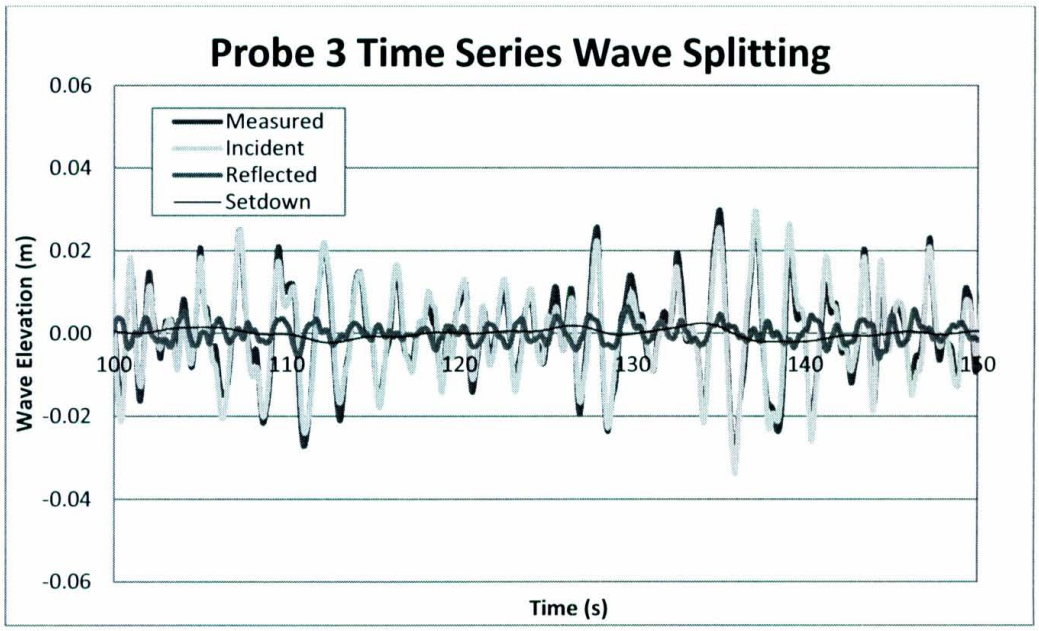

Figure 5-16 - Time Series Wave Splitting, Probe 3 (100-150s)

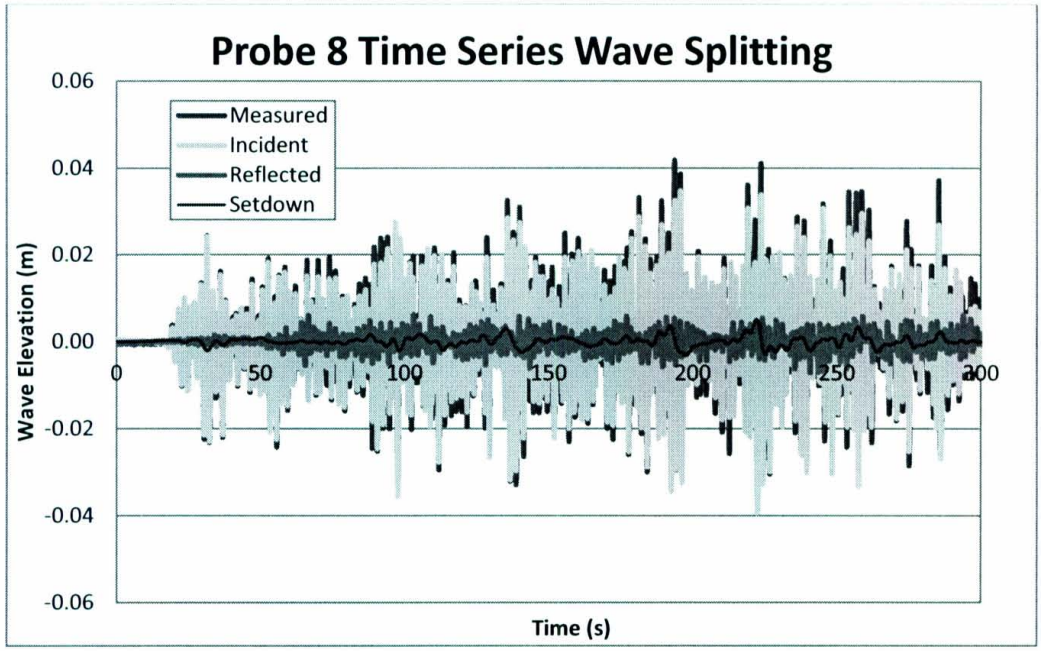

Figure 5-17 - Time Series Wave Splitting, Probe 8

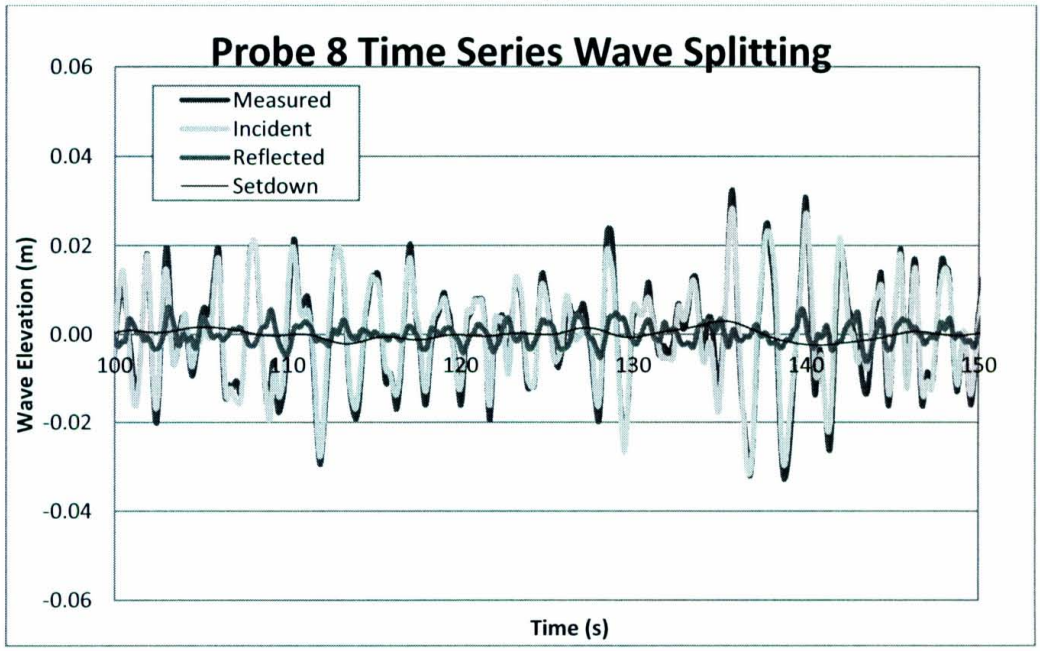

Figure 5-18 - Time Series Wave Splitting, Probe 8 (100-150s)

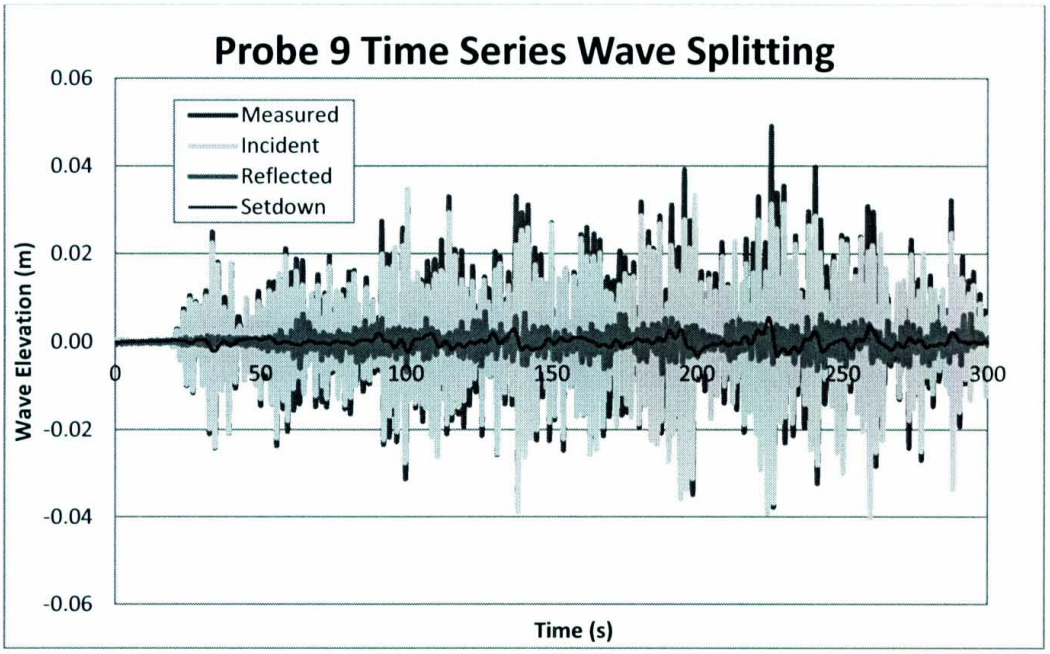

Figure 5-19 - Time Series Wave Splitting, Probe 9

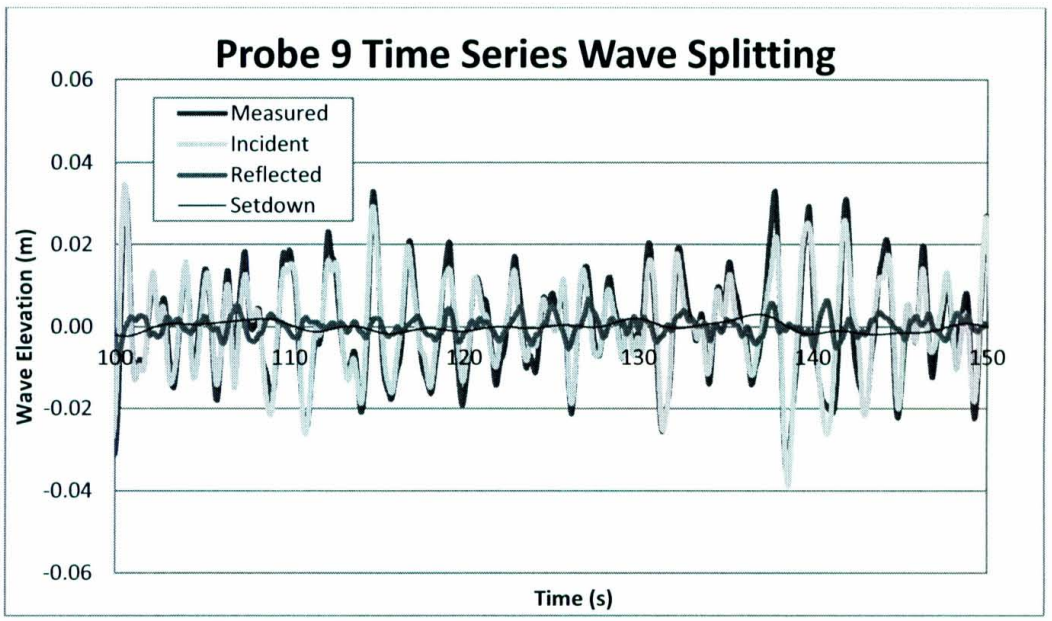

Figure 5-20 - Time Series Wave Splitting, Probe 9 (100-150s)

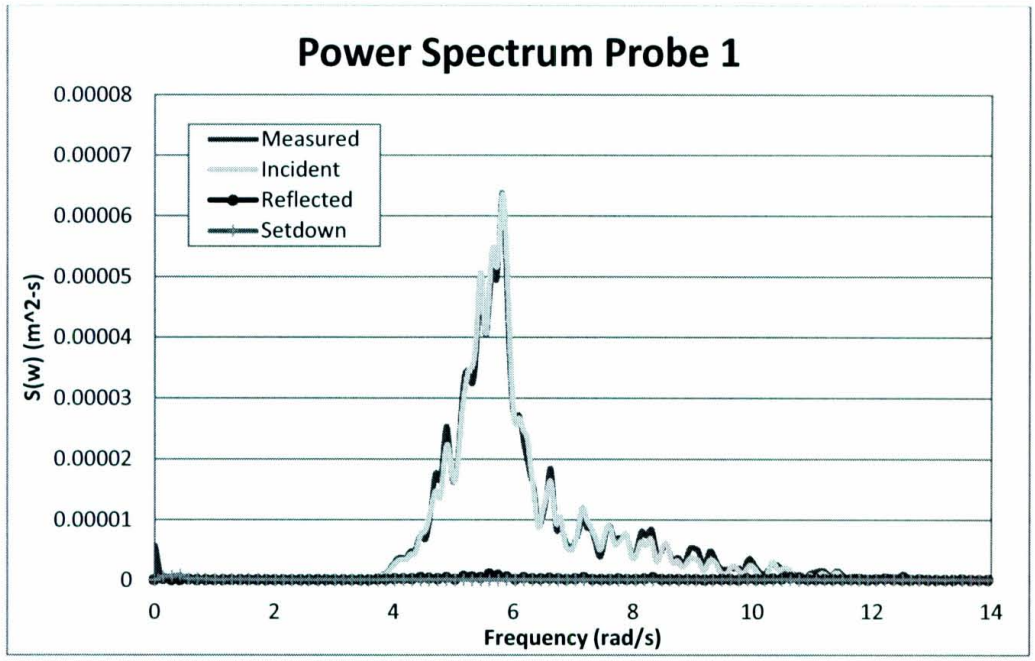

Figure 5-21 – Frequency Domain Wave Splitting, Probe 1

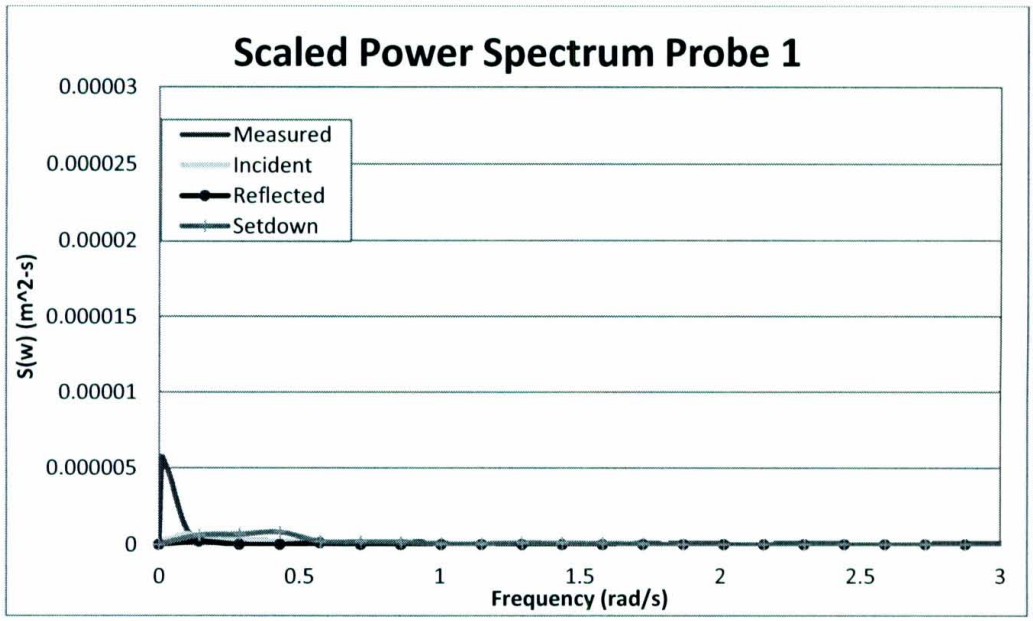

Figure 5-22 – Low Frequency Domain Wave Splitting, Probe 1

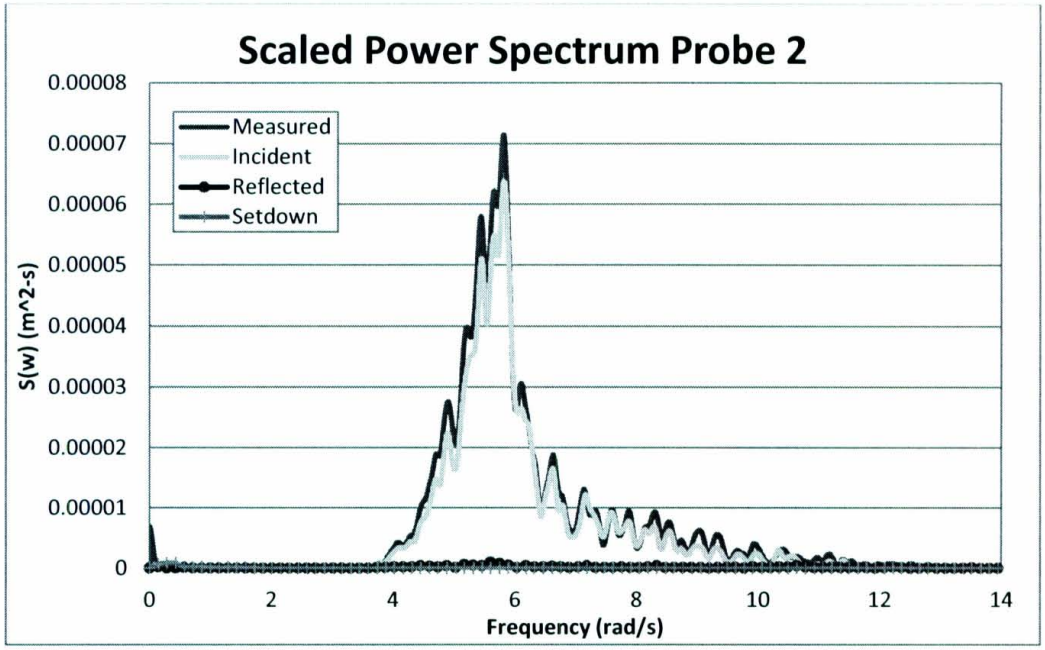

Figure 5-23 - Frequency Domain Wave Splitting, Probe 2

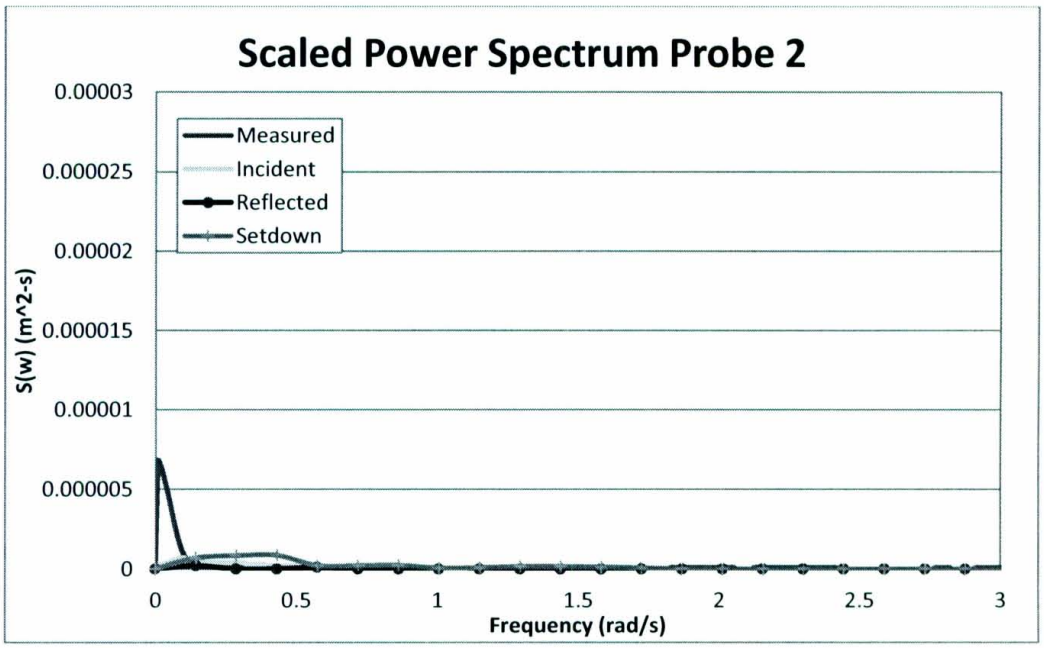

Figure 5-24 – Low Frequency Domain Wave Splitting, Probe 2

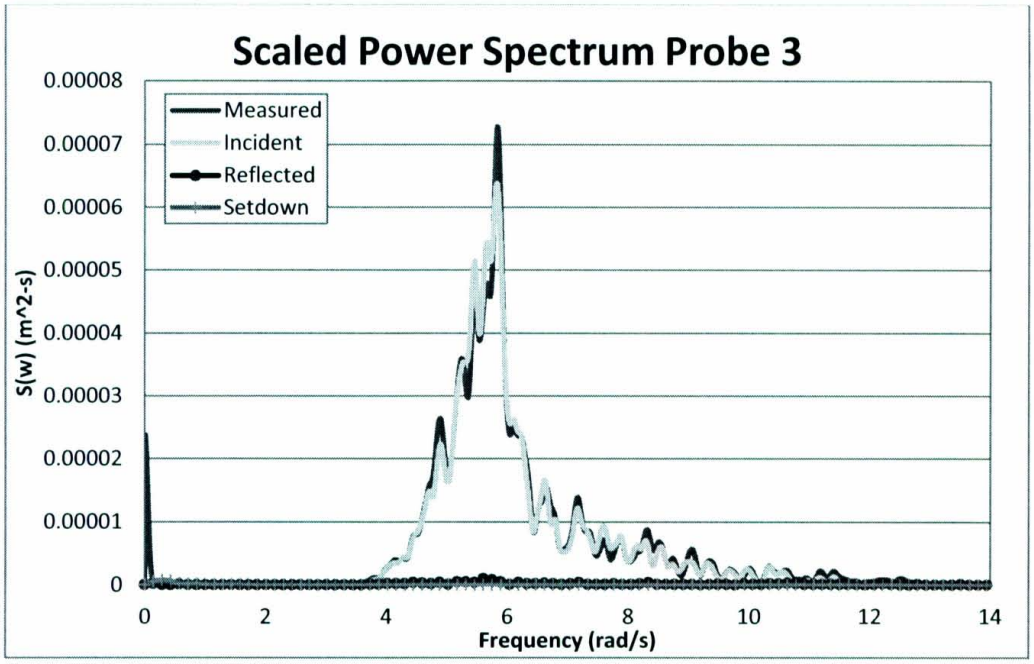

Figure 5-25 - Frequency Domain Wave Splitting, Probe 3

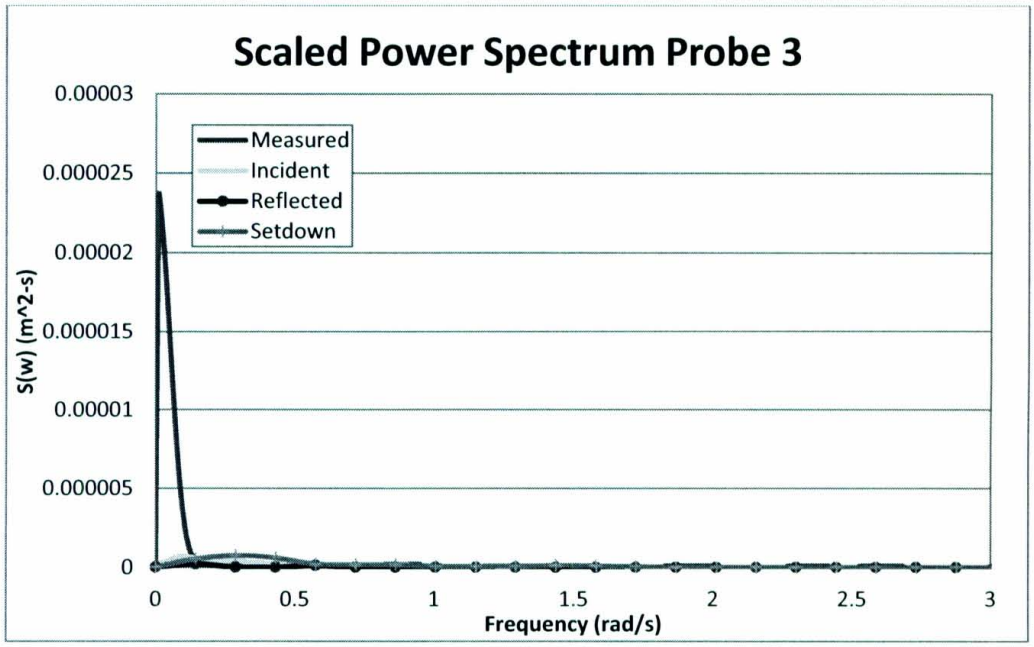

Figure 5-26 – Low Frequency Domain Wave Splitting, Probe 3

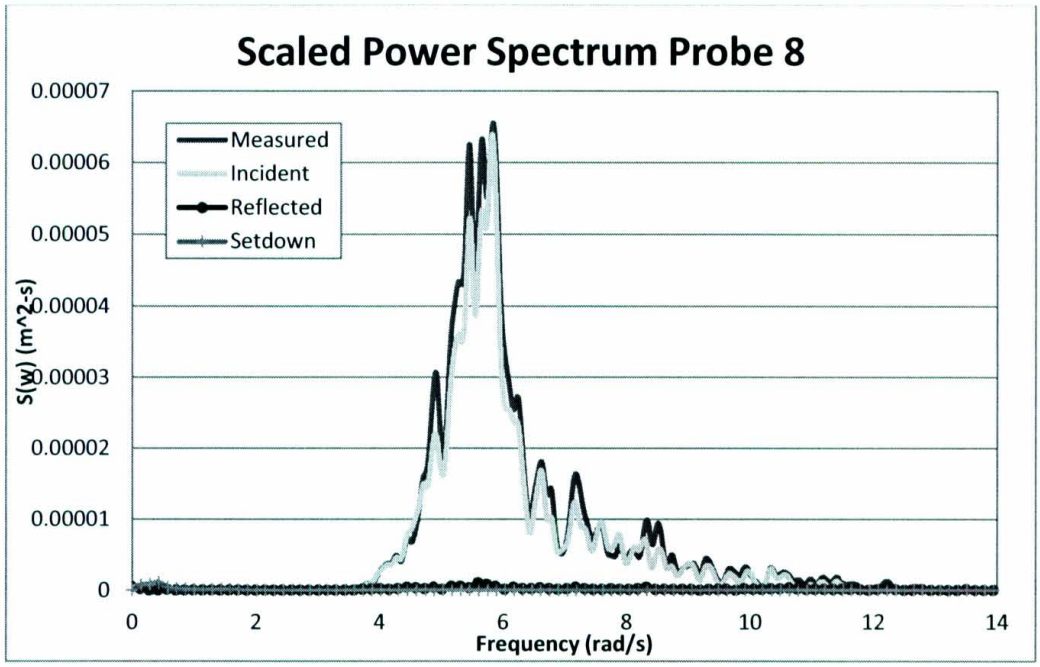

Figure 5-27 - Frequency Domain Wave Splitting, Probe 8

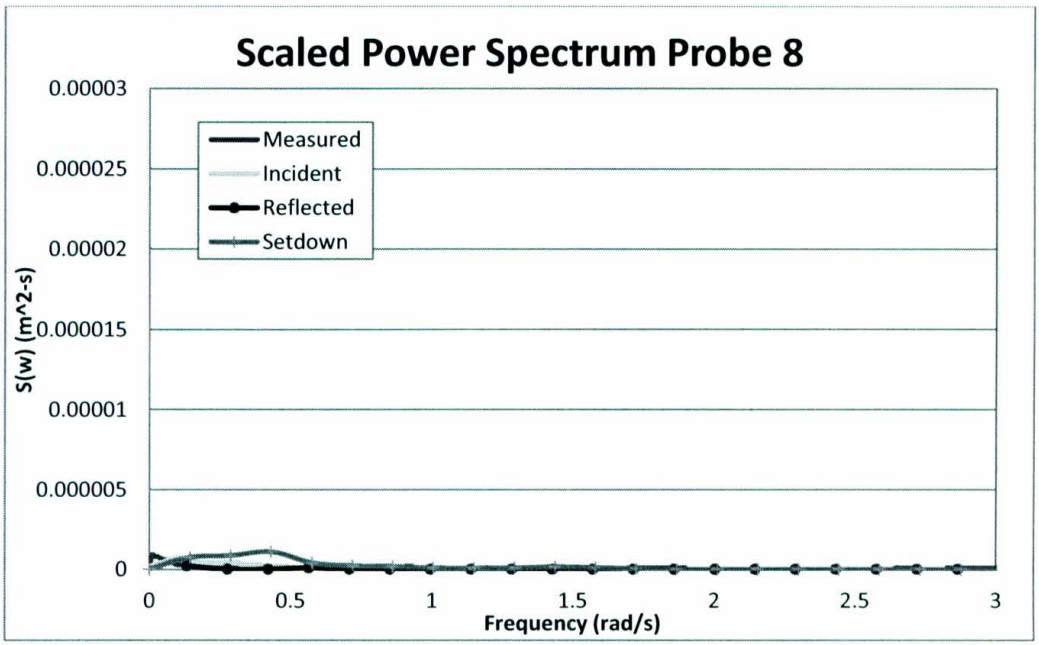

Figure 5-28 – Low Frequency Domain Wave Splitting, Probe 8

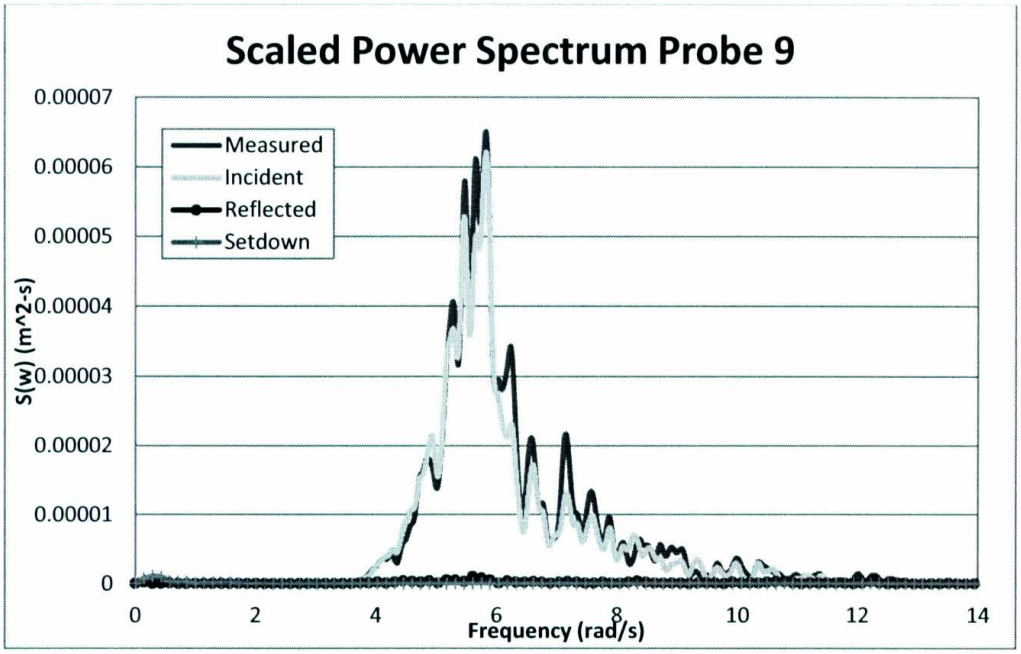

Figure 5-29 - Frequency Domain Wave Splitting, Probe 9

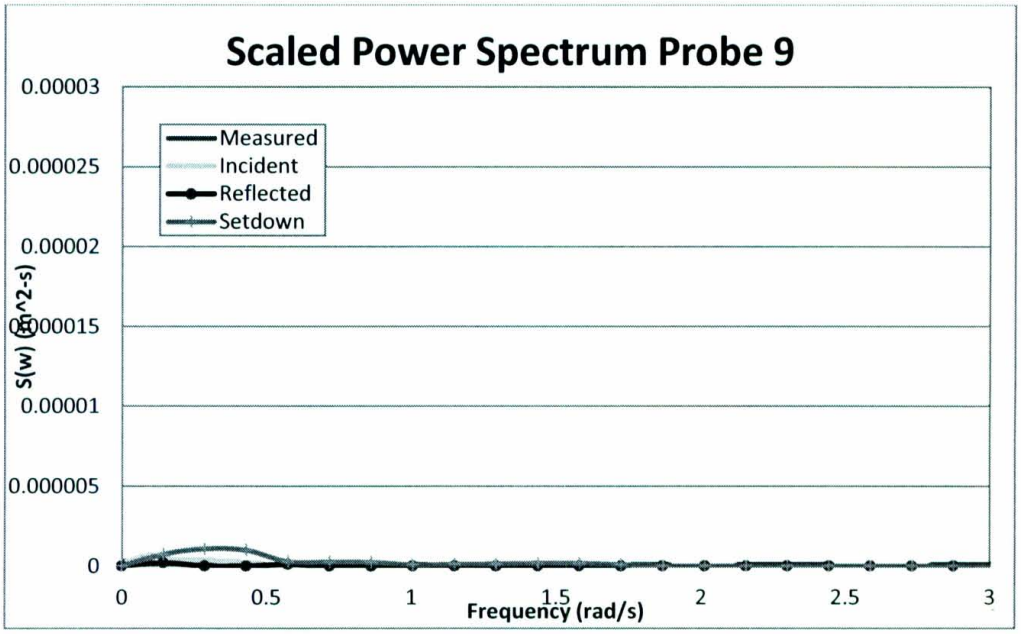

Figure 5-30 – Low Frequency Domain Wave Splitting, Probe 9

5.3. First Order Versus Second Order Wave Generation

The following results show a comparison between the first order generation and the second order generation waves for the same peak period, displayed in Figure 5-31 through Figure 5-46. In general there is little difference between the first order and second order components; Case 1 shows the least difference and Case 3 exhibits the most significant difference.

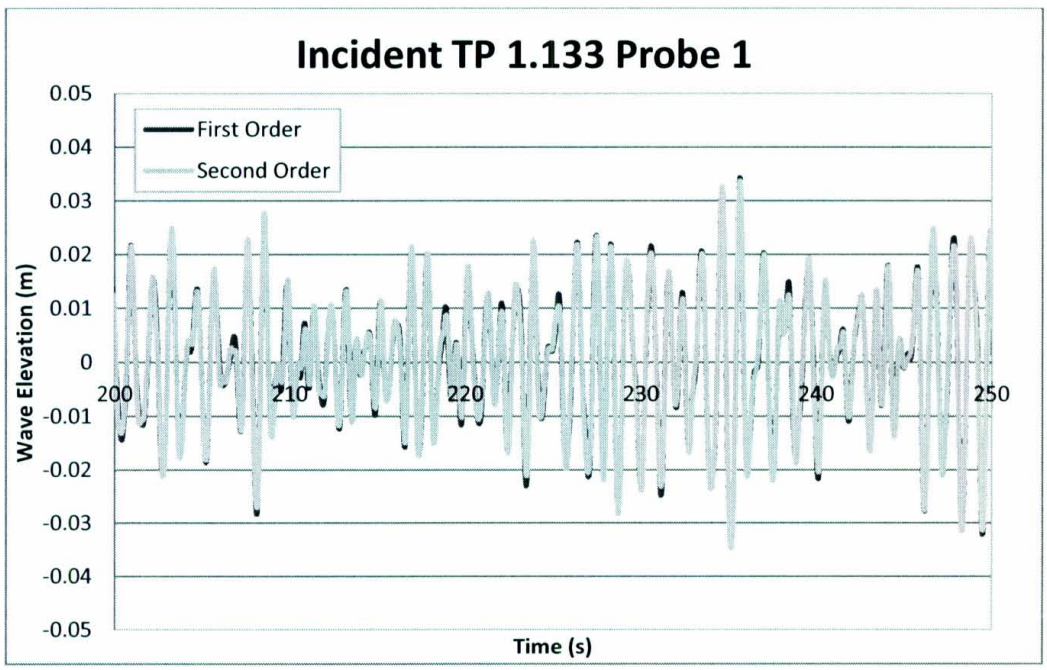

Figure 5-31 – FO versus SO: Time series, Incident Wave, Probe 1, Case 1

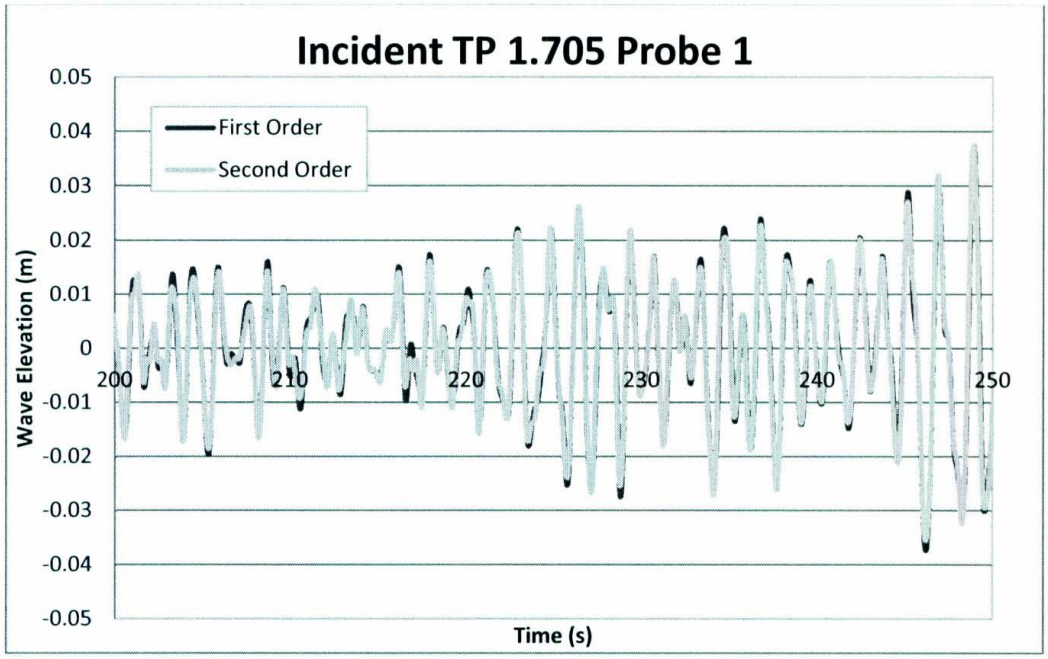

Figure 5-32 - FO versus SO: Time series, Incident Wave, Probe 1, Case 2

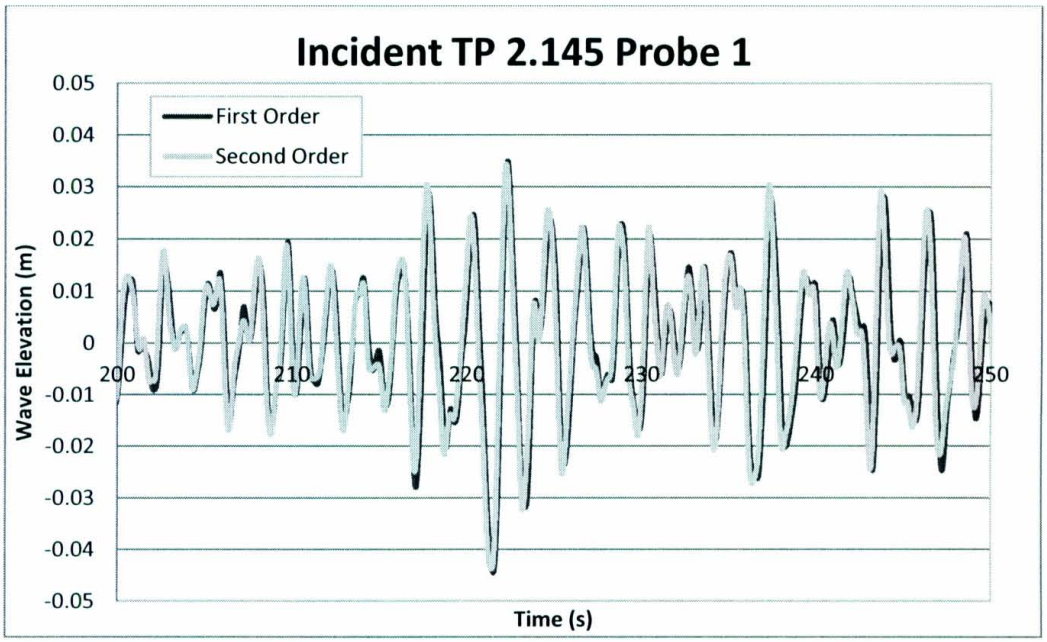

Figure 5-33 - FO versus SO: Time series, Incident Wave, Probe 1, Case 3

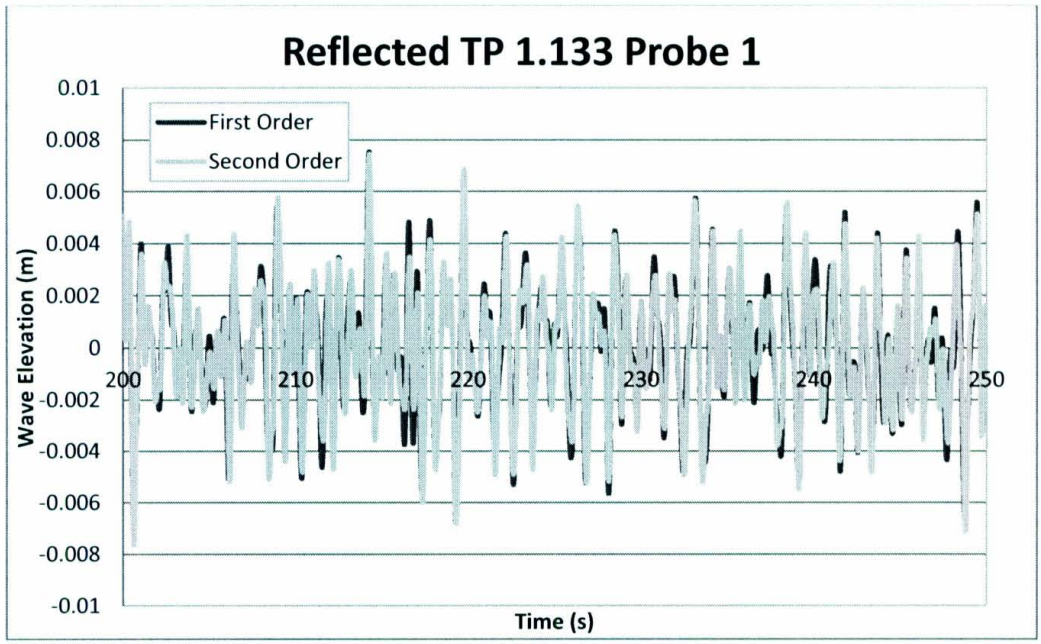

Figure 5-34 - FO versus SO: Time series, Reflected Wave, Probe 1, Case 1

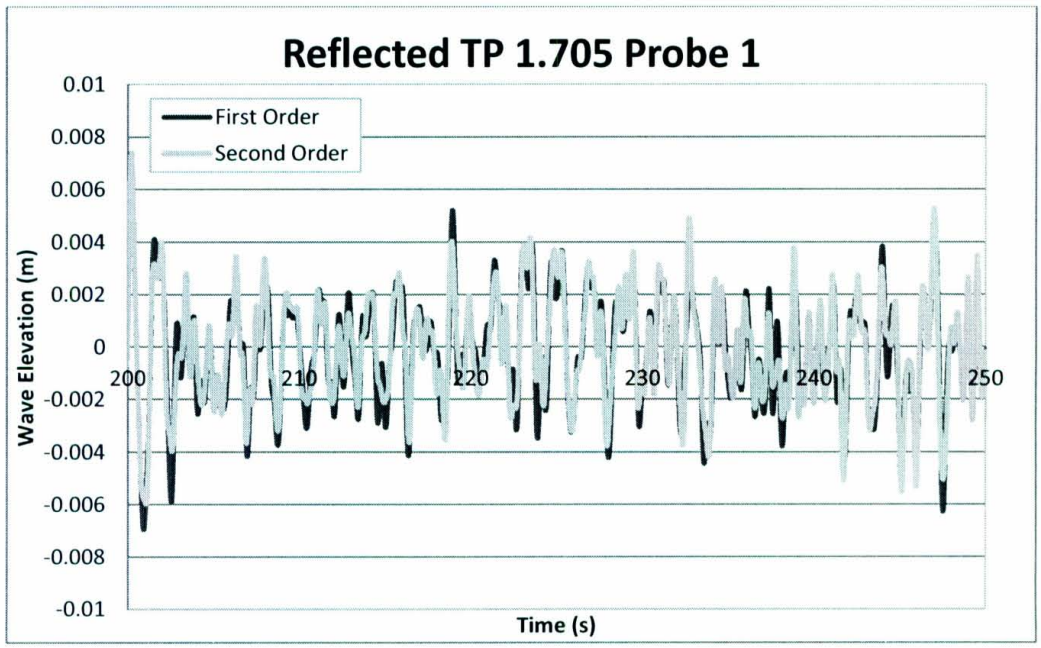

Figure 5-35 - FO versus SO: Time series, Reflected Wave, Probe 1, Case 2

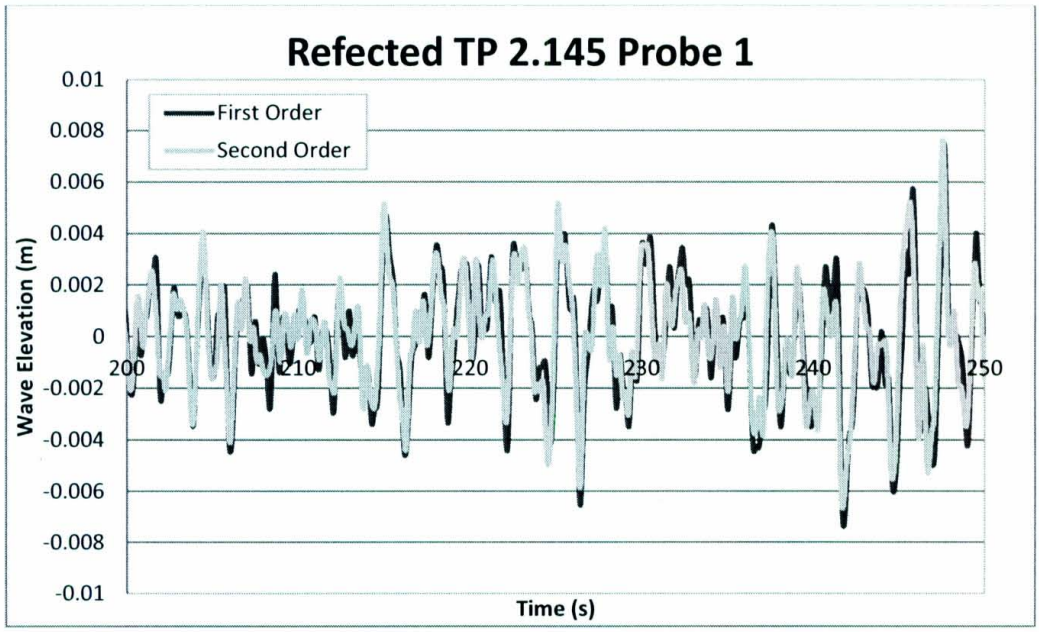

Figure 5-36 - FO versus SO: Time series, Reflected Wave, Probe 1, Case 3

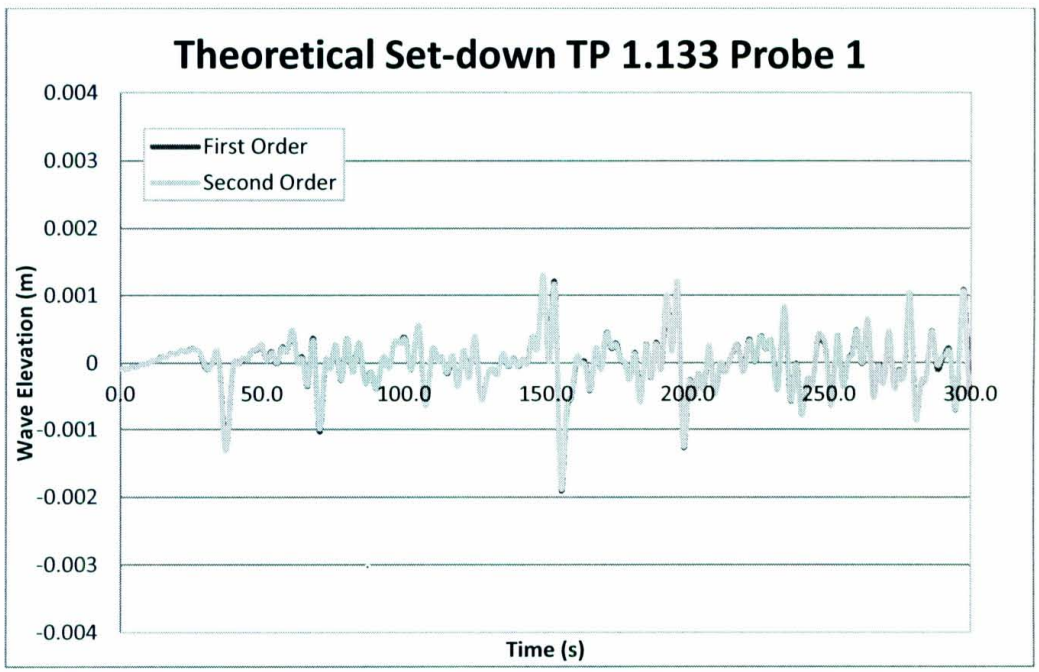

Figure 5-37 - FO versus SO: Time series, Theoretical Set-down, Probe 1, Case 1

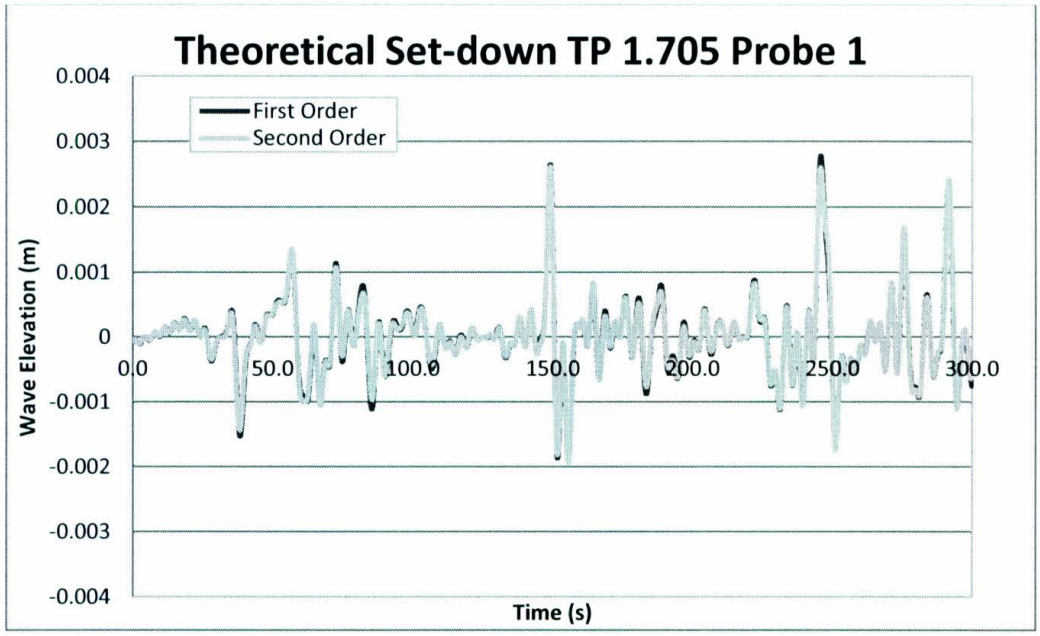

Figure 5-38 - FO versus SO: Time series, Theoretical Set-down, Probe 1, Case 2

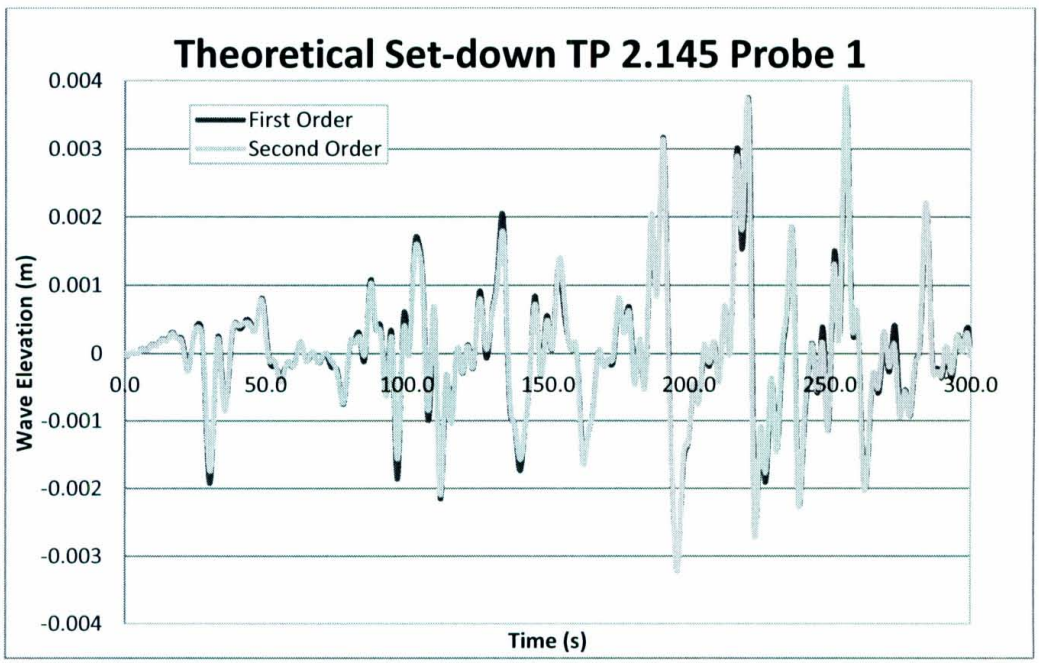

Figure 5-39 - FO versus SO: Time series, Theoretical Set-down, Probe 1, Case 3

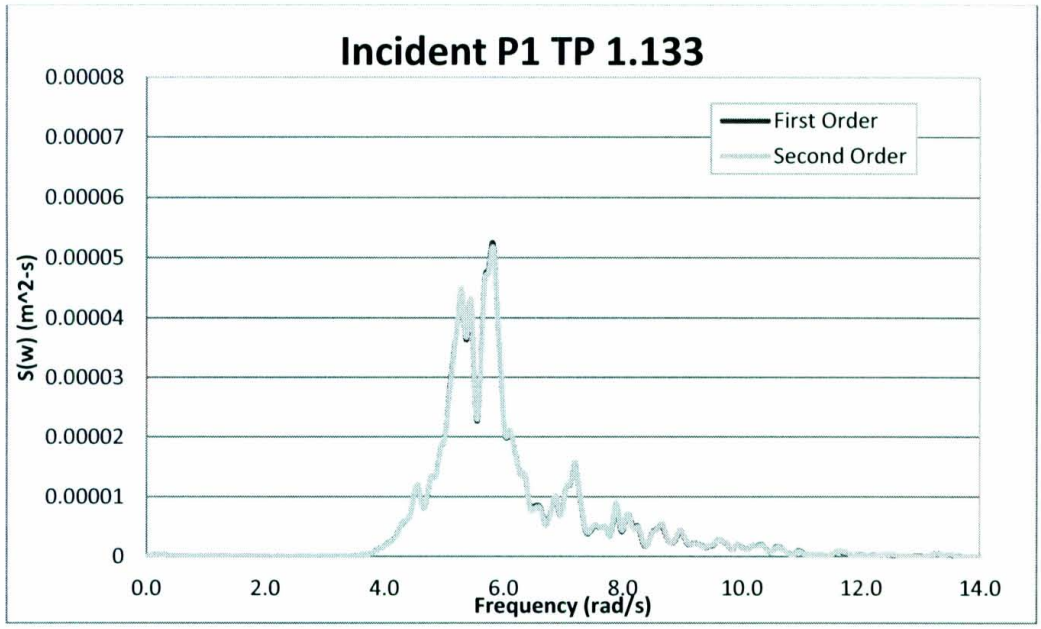

Figure 5-40 - FO versus SO: Frequency Domain, Incident Wave, Probe 1, Case 1

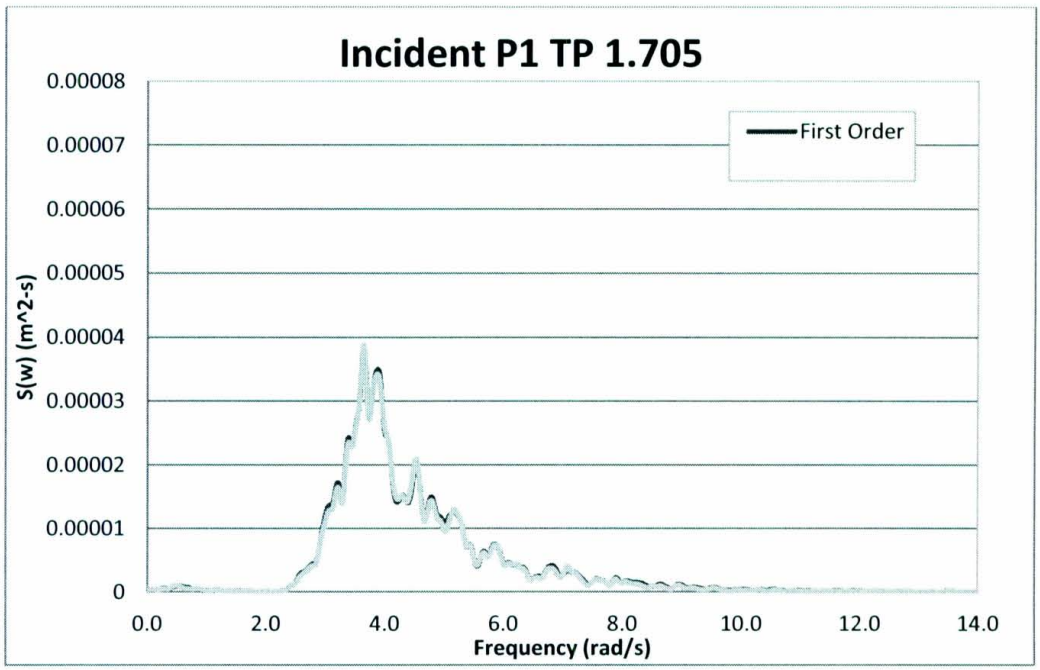

Figure 5-41 - FO versus SO: Frequency Domain, Incident Wave, Probe 1, Case 2

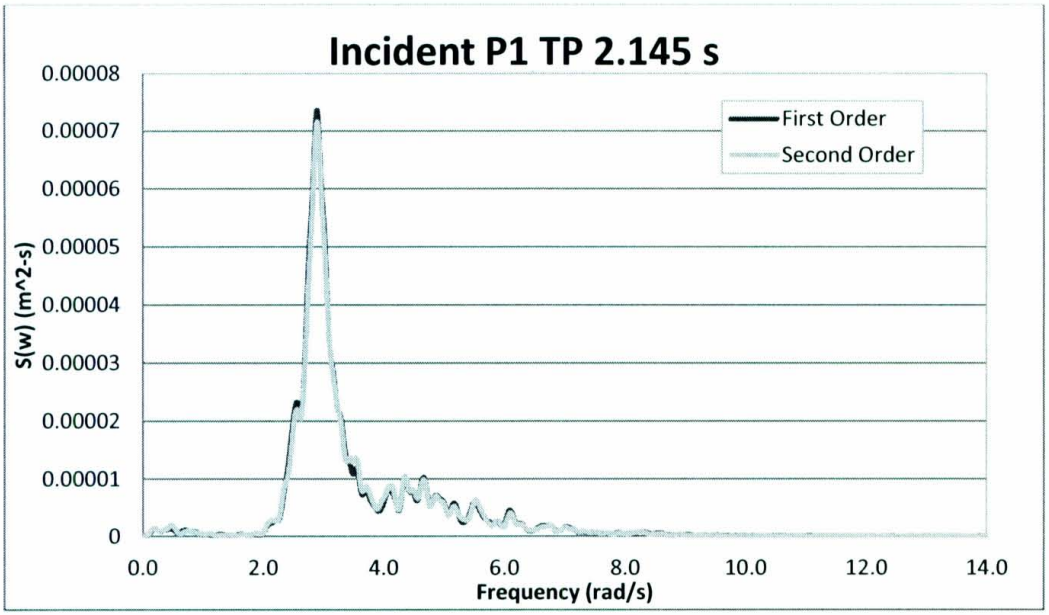

Figure 5-42 - FO versus SO: Frequency Domain, Incident Wave, Probe 1, Case 3

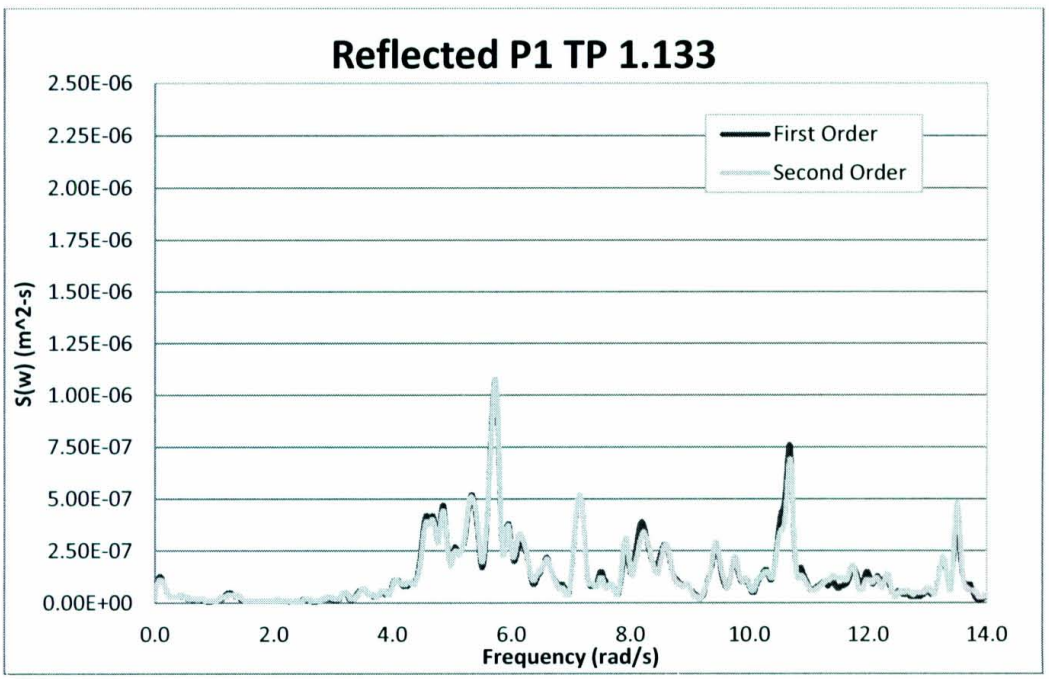

Figure 5-43 - FO versus SO: Frequency Domain, Reflected Wave, Probe 1, Case 1

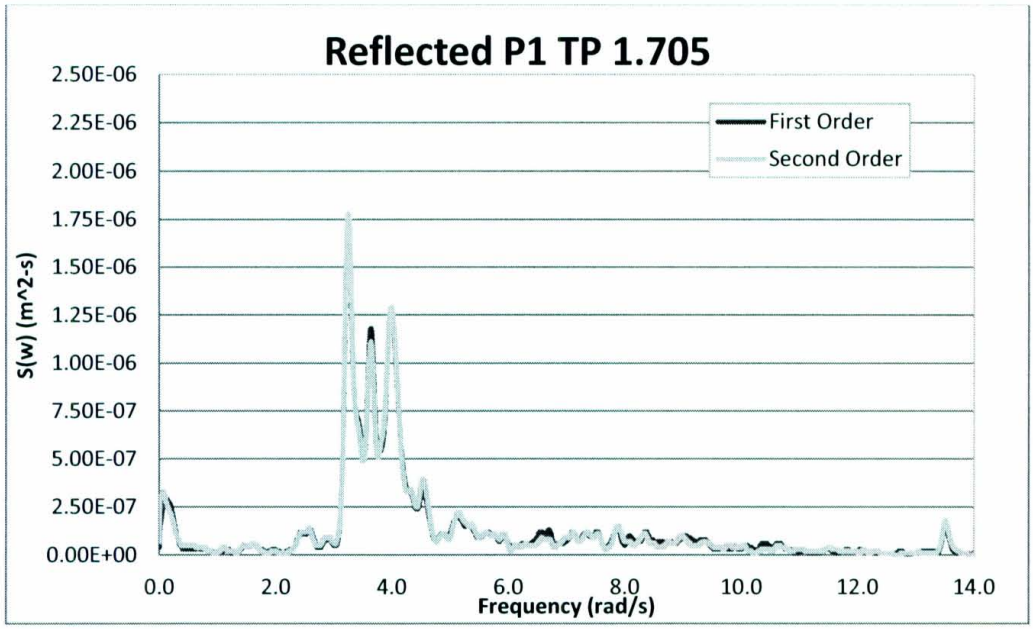

Figure 5-44 - FO versus SO: Frequency Domain, Reflected Wave, Probe 1, Case 2

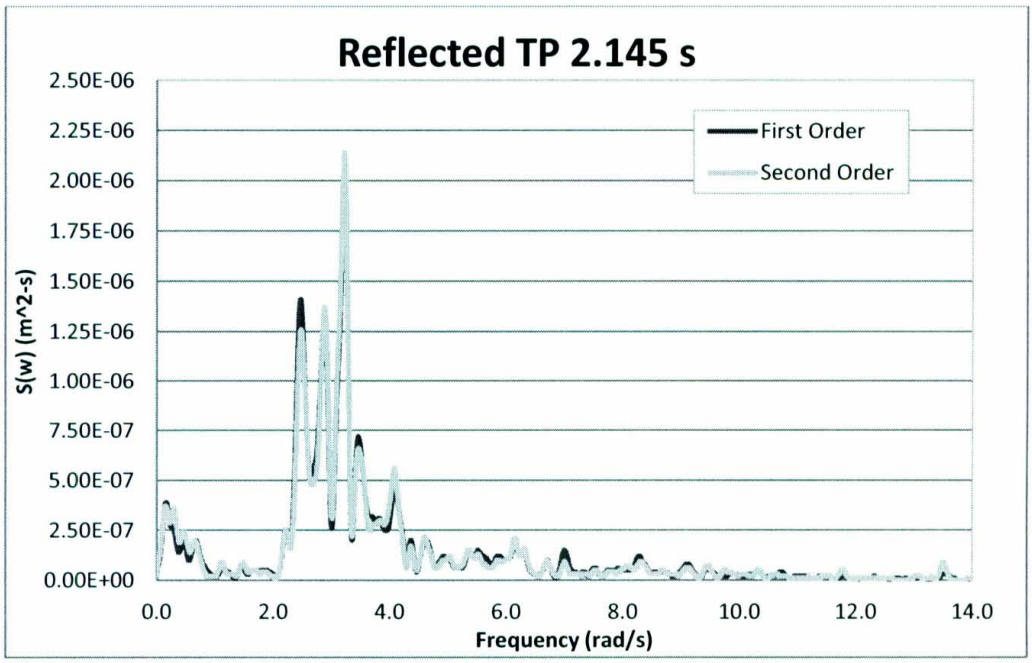

Figure 5-45 - FO versus SO: Frequency Domain, Reflected Wave, Probe 1, Case 3

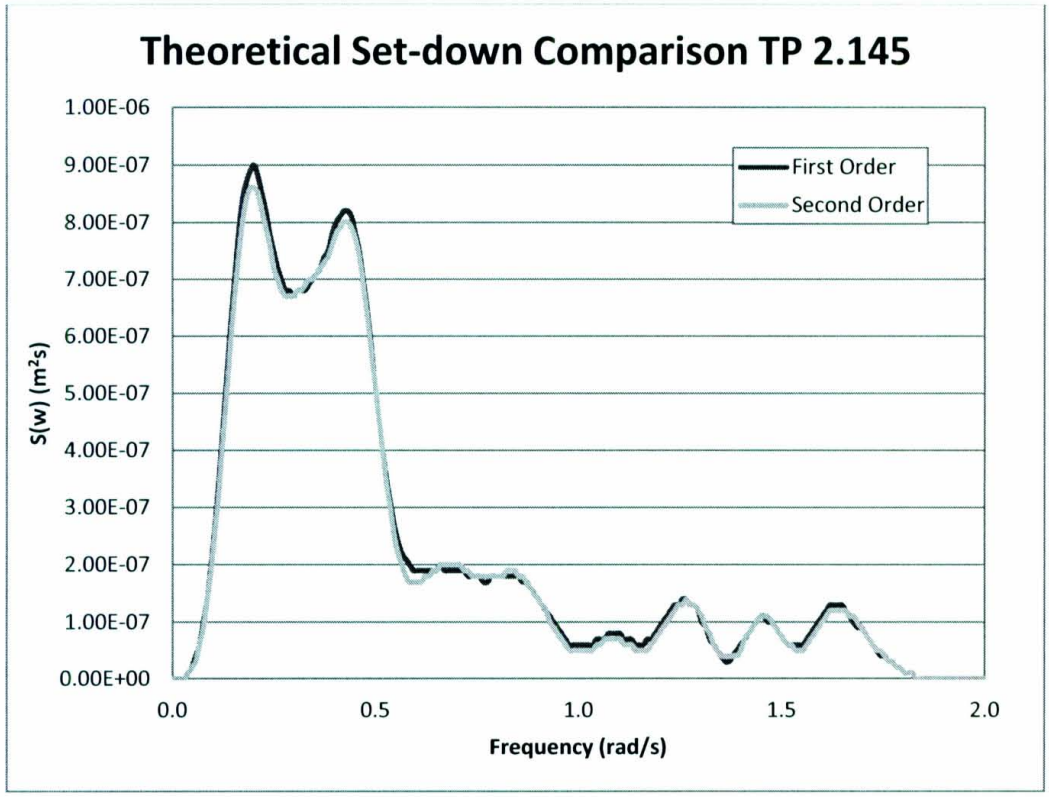

Figure 5-46 - FO versus SO: Frequency Domain, Set-down Wave, Probe 1, Case 3

5.4. Discussion

As expected, the spectrum for the set-down wave is the largest of the three cases as shown in Figure 5-47. This verifies the theory of an increasing set-down component with longer waves. Second order wave set-down is shown only since the difference between first and second order results vary only slightly.

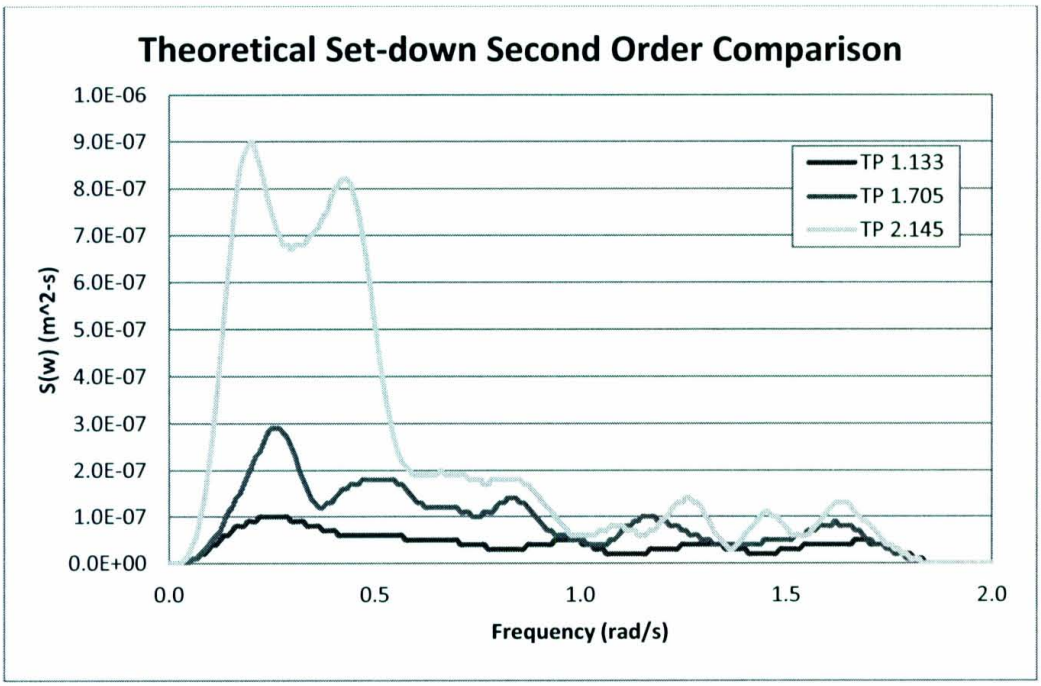

Figure 5-47 - Second Order Theoretical Set-down Wave Peak Period Comparison

Figure 5-48 through Figure 5-53 show the comparison of the spectra of the measured wave versus that of the theoretical set-down component for Probe 1 and 2. The measured wave has a spike in energy at the lowest frequency which is assumed to be an environmental factor of the model tank testing. For future work this should be reduced or removed in order to display more accurate readings. The second order generation measured waves have

more energy associated to it than the first order generation waves do as is expected to show added low frequency components. By inspection of Figure 5-48 through Figure 5-53 it appears as though the first case shows the best agreement with the measured data and the third case is the least agreeable case. The zeroth spectral moment was calculated, as shown by Equation [2.53], and the percent difference calculation results between probe 1 and 2 are shown in Table 5.2. The equation for the percent difference is shown by Equation [5.1].

$$Percent\ Difference = \frac{|Measured\ Value - Theoretical\ Value|}{|Theoretical\ Value|} \times 100\% \qquad \textbf{[5.1]}$$

Table 5.2 –Percent Difference between Measured and Theoretical Set-down Wave

Parameter	Probe 1	Probe 2
Case 1: First Order	53.39%	39.65%
Case 1: Second Order	52.46%	41.76%
Case 2: First Order	67.59%	62.86%
Case 2: Second Order	68.24%	63.42%
Case 3:First Order	58.91%	54.49%
Case 3: Second Order	64.22%	60.97%

Table 5.2 illustrates that though the third case looks like the worst case, Case 2 actually has the largest percent difference between the measured and the incident wave. This is due to

the fluctuation of the spectra in Case 3, which although the measured data has some large peaks it also oscillates around the spectra of the theoretical set-down more so than Case 2.

As stated in the previous section, the results show little variance from second order and first order wave generation. This could be caused by the estimating spectral density function which may underestimate the spectral density energy. It might be improved upon by changing the resolution of the results.

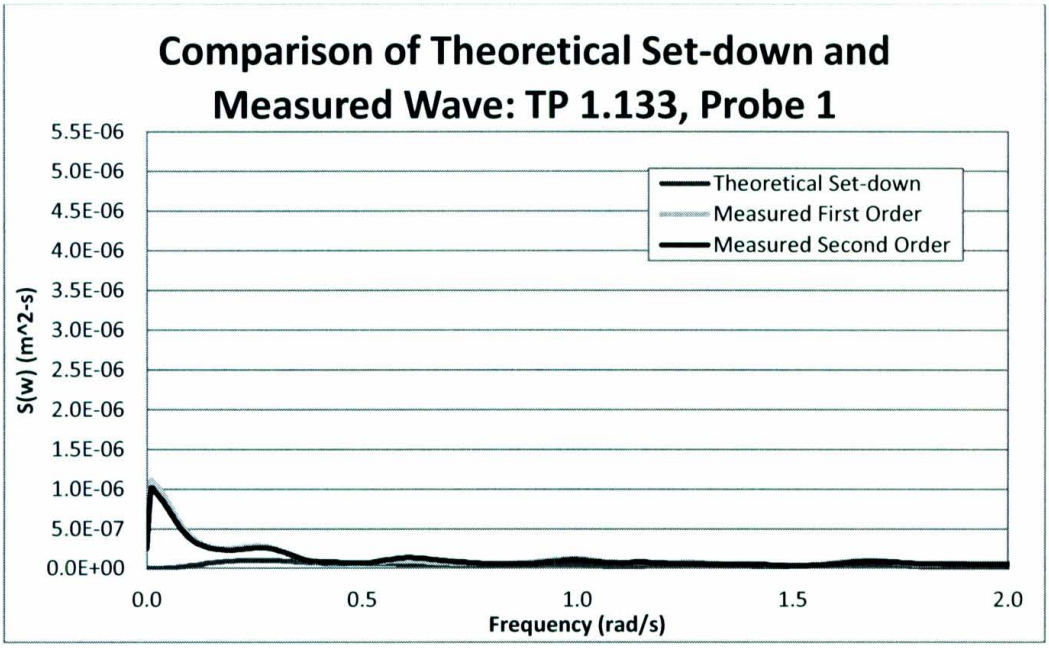

Figure 5-48 – Measured versus Theoretical Set-down Wave: Case 1, Probe 1

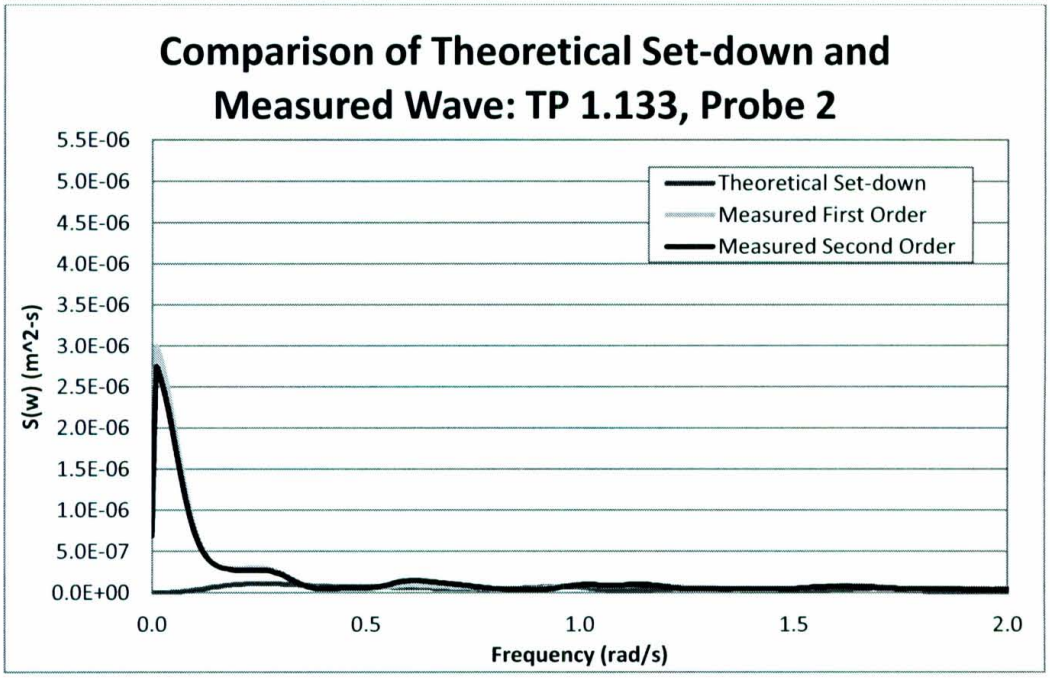

Figure 5-49– Measured versus Theoretical Set-down Wave: Case 1, Probe 2

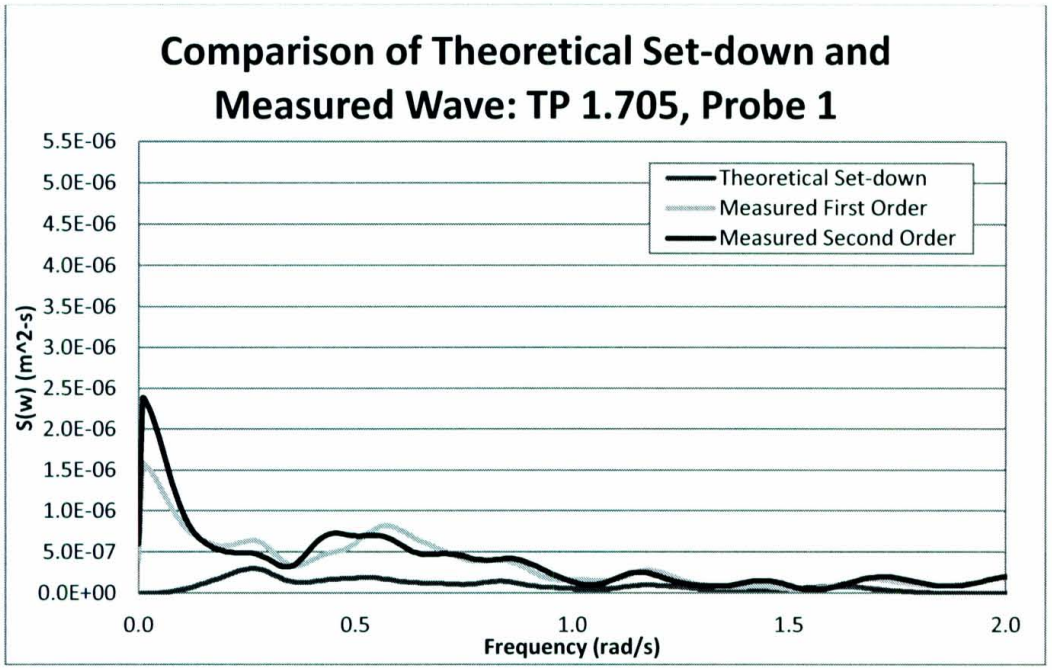

Figure 5-50 – Measured versus Theoretical Set-down Wave: Case 2, Probe 1

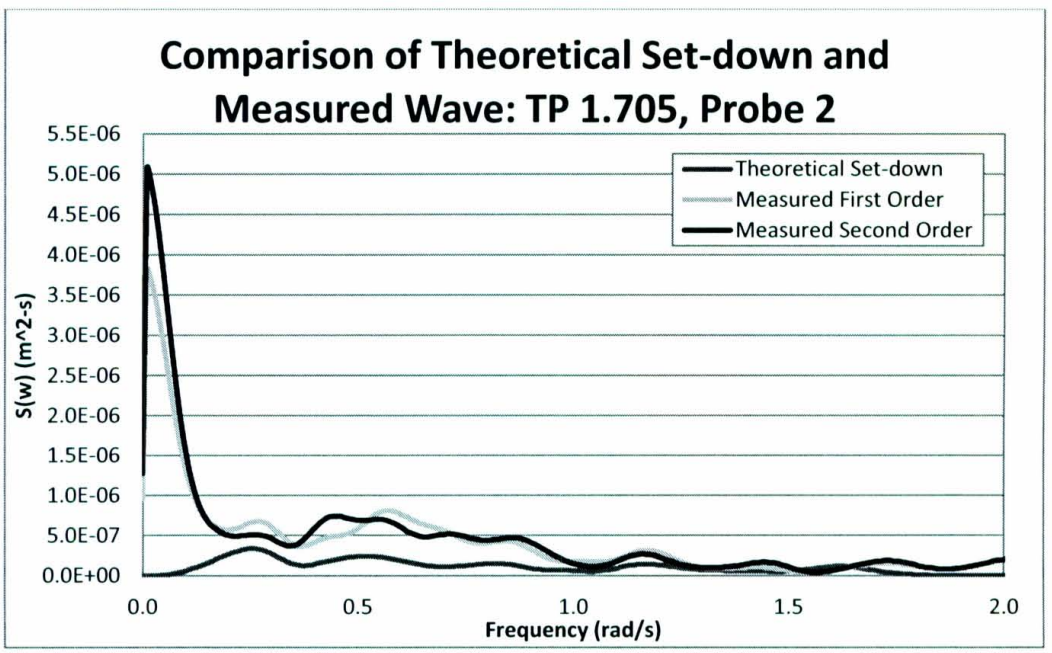

Figure 5-51– Measured versus Theoretical Set-down Wave: Case 2, Probe 2

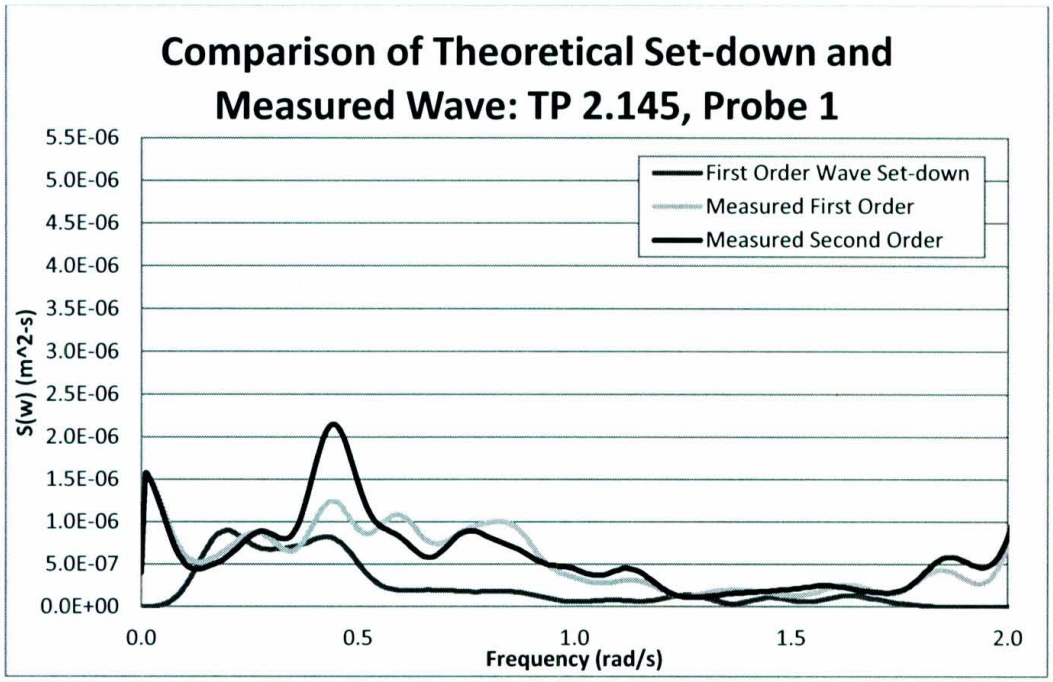

Figure 5-52 – Measured versus Theoretical Set-down Wave: Case 3, Probe 1

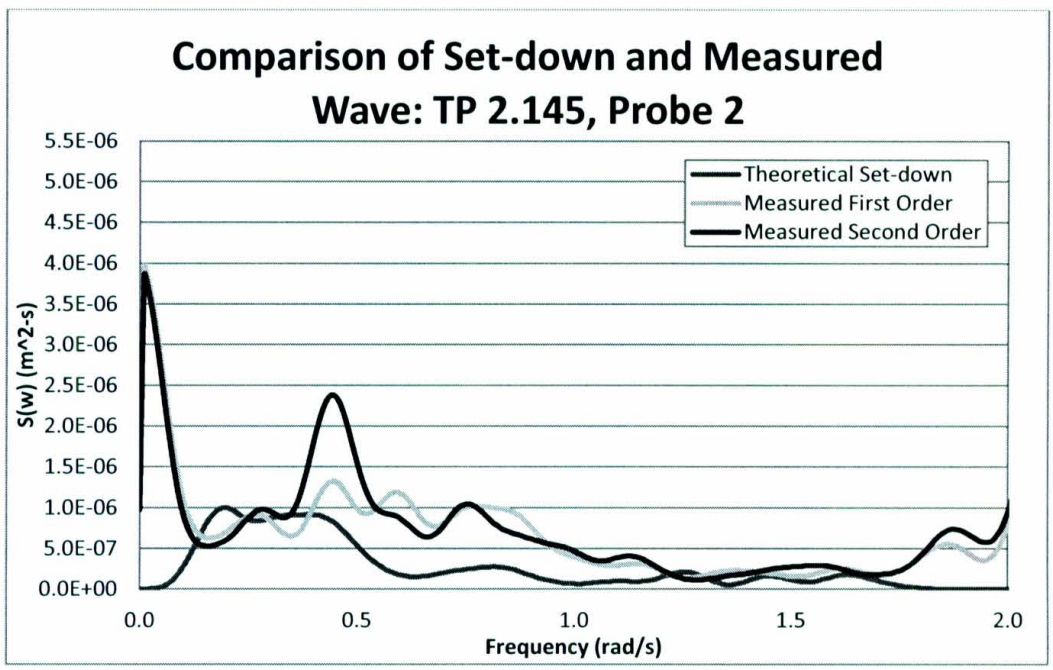

Figure 5-53 – Measured versus Theoretical Set-down Wave: Case 3, Probe 2

6. CONCLUSION AND RECOMMENDATIONS

A program was developed using FORTRAN language to identify the different components that make up a measured wave in a model tank. Since unrealistic waves are created in a model tank environment for first order wave generation, the process of identifying each wave in the tank allowed the unwanted waves to be removed from the analysis, ultimately to reduce the error in ship-wave interaction analysis. A set of wave generation data, which varied in peak period, was analyzed to show the different waves that make up the measured wave in a tank. The data consisted of both first order and second order wave generation. The results were validated against reported MARIN and NRC results. The time series and power spectral density plots were shown for both the first order and second order wave generation data.

The first order and second order wave comparison showed little variance to one another which may be attributed to an over-estimation in the spectral density estimation function. The theoretical set-down exhibited an increase with respect to the increase in wave period, which was expected. The comparison between the theoretical set-down wave and the measured wave gave varied results in terms of aligning in the low frequency region on the spectral plots. The shortest wave case displayed the most agreeable results and the second longest wave gave the least agreeable results as shown in Table 5.2. The comparison between measured and theoretical set-down could be improved by increasing the resolution of the spectral density function.

Future work recommendations include validating the model using the third and fourth wave decomposition which is built into the program. Improvements are required to more accurately create the theoretical set-down wave in the low frequency region so that it better aligns with the measured wave. The results of the wave splitting data can be further investigated with respect to ship-wave interaction to analyze the effects of removing unwanted waves as well as identifying previously hidden waves on the vessel. In reference to Figure 2-5, which shows the steps for using the wave splitting program, steps 1-5 have been completed with this research. It is recommended that steps 6 and 7 be completed for the next stage of this research. Step 6 and 7 can be done for example using commercial software such as WAMIT, wave analysis software developed at MIT.

REFERENCES

Beauchamp, K.G. & Yuen C.K. (1973). *Digital Methods for Signal Analysis*. London: George Allen & Unwin.

©BORES Signal Processing (2009). Introduction to DSP – basiscs – alisasing. Retrieved from http://www.bores.com/courses/intro/basics/1_alias.htm.

Bowen, A. J., D. L. Inman, and V. P. Simmons (1968), Wave 'Set-Down' and Set-Up, *J. Geophys. Res.*, 73(8), 2569–2577.

Chapira, S.C. (2008). *Applied Numerical Methods with MATLAB for Engineers and Scientists* (2nd ed.) McGraw-Hill.

Hansen, O.N.-E., Sand, S.E., Lundgren H., Sorensen, T., & Graveson, H. (1980). Correct Reproduction of Group-Induced Long Waves. *Proc. of 17th Conf. on Coastal Engr.* Sydney, Australia.

Huijsmans. R.H.M. (2002). Second Order Wave Elevation in Irregular Short Crested Seas. ARD Project 2002. Report No. 17712-1-RD. MARIN: The Netherlands.

Longuet-Higgins, M. S. and Stewart, R. W. (1964) Radiation stress in water waves, a physical discussion with application, *Deep-Sea Res. Vol 11* (pp 529-562). Pergamon Press Ltd.: Great Britain.

Mansard, E.P.D & Funke, E.R. (1980). The Measurement of Incident and Reflected Spectra Using a Least Squre Method. *Proc. 17th Int. Conf. Coastal Eng., ASCE* (pp. 154–172) New York,

Mansard, E.P.D (1991). On the Experimental Verification of Non-Linear Waves. *Proc. of the 3rd Intl. Conf. on Coastal and Port Engng. in Dev. Countries, Kenya.*

Naciri, M. & Buchner, B. & Bunnik T. & Huijmans, R. & Andrews, J. (2004). Low Frequency Motions of LNG Carriers Moored in Shallow Water. Proc. of OMAE 2004 Conf., Vancouver, Canada.

National Instruments (2009). The Fundamentals of FFT-Based Signal Analysis and Measurement in LABVIEW and LABWINDOW/CVI.

Press, W.H. & Teukolsky, S.A. & Vetterling, W.T. & Flannery, B.P. (1992). *Numerical Recipes in FORTRAN: The Art of Scientific Computing*. Cambridge: University of Cambridge.

Sand, S.E. (1982). Long Wave Problems in Laboratory Models. *Proc. of the ASCE, J. of Waterway, Port, coast. And Ocn. Div.* 198 (WW4), 492-503.

Sand, S.E. & Mansard, E.P.D. (1986). Reproduction of Higher Harmonics in Iregular Waves. *Ocean Engng. Vol 13*, No. 1. (pp. 57-88). Great Britain: Elsevier Science Ltd.

Schäffer, H.A. (1994). Second-Order Wavemaker Theory for Irregular Waves. *Ocean Engng. Vol. 23,* No. 1. (pp. 47-88). Great Britain: Elsevier Science Ltd.

Sclavounos, P. D. *Linearization of Free-Surface Conditions.* 2.24 Ocean Wave Interaction with Ships and Offshore Energy Systems (13.022), Spring 2002. (Massachusetts Institute of Technology: MIT OpenCourseWare), http://ocw.mit.edu. License: Creative Commons BY-NC-SA

Stransberg, C. T. (2006). Laboratory Wave Modelling for Floating Structures in Shallow Water. *OMAE 2006. 25th Int. Conf. on OMAE.* June 4-5, 2006. Hamburg, Germany.

Van Dijk, R.R.T. (2007). Hawai JIP, Description of Wave Seperation Methodology: Guideline for Wave Splitting Tool. Report 19436-2-PO. April 2007.

Voogt, A. & Bunnik, T. & Huijmans, R. (2005). Validation of an Analytical Method to Calculate Wave Set-down on Current. *Proc. OMAE 2005. 24th Int. Conf. on OMAE.* June 12-17, 2005. Halkidiki, Greece.

Wave Spectra. In *FormSys Software Help Guide.* Retrieved from http://www.formsys.com/extras/FDS/webhelp/seakeeper/wave_spectra1.htm

Wavemaker. Description of Facilities for a Shallow Water Basin on *Hydralab Research Website.* Retrieved from http://www.hydralab.eu/facilities_view.asp?id=7

Welsh, P.D. (1967). The Use of Fast Fourier Transform for the Estimation of Power Spectra: A Method Based on Time Averaging Over Short, Modified Periodograms. *IEEE Transaction Audio and Electroacoustics, vol. AU-15,* pp. 70-73.

Zaman, M.H. & Peng. H. & Baddour, E. & McKay, S. (2011). Spurious Waves During Generation of Multi-Chromatic Waves in The Wave Tank In Shallow Water. *Proceedings of the ASME 2011 30th International Conference on Ocean, Offshore and Arctic Engineering*. June 19 - June 24, 2011. Rotterdam: The Netherlands.

APPENDIX A – COSINE DECOMPOSITON

Cosine Decomposition

The total wave equation was proven to be:

$$A\cos(\omega_j t) + B\sin(\omega_j t) = \zeta_{if}\cos(\omega_j t - k_j x_n + \varepsilon_{if}) + \zeta_{rf}\cos(\omega_j t + K_j x_n + \varepsilon_{rf}) + \zeta_{ib}\cos(\omega_j t - \Delta k_j x_n + \varepsilon_{ib})$$

The following trigonometry identities are used in order to decompose the cosine terms into individual sine and cosine terms to simplify solving for the unknowns.

$$\cos x + i\sin x = e^{ix}$$

$$e^A e^B e^C = e^{(A+B+C)}$$

$$\cos(-B) = \cos B$$

$$\sin(-B) = -\sin B$$

In order to split up the three terms in the cosine expressions from the total elevation equation, we will simplify the cosine equation to:

$$\cos(A + B + C)$$

and

$$\cos(A - B + C)$$

Starting with the first cosine expression, we substitute x=A+B+C into the trigonometric identities which gives:

$$\cos(A + B + C) + i\sin(A + B + C) = e^{i(A+B+C)}$$

Simplifying the right hand side of the equation and noting that i^2=-1, we get the following:

$$e^{i(A+B+C)} = e^{iA}e^{iB}e^{iC} = (\cos A + i\sin A)(\cos B + i\,\mathrm{sinB})(\cos C + i\sin C)$$

$$= (\cos A\cos B + i\cos A\sin B + i\sin A\cos B - \sin A\sin B)(\cos C$$

$$+ i\sin C)$$

$$= \cos A\cos B\,cosC + i\cos A\cos B\sin C + i\cos A\sin B\cos C$$

$$- \cos A\sin B\sin C + i\sin A\cos B\cos C - \sin A\cos B\sin C$$

$$- \sin A\sin B\cos C - i\sin A\sin B\sin C$$

The real and imaginary terms can be collected and can be matched up with the cosine and sine terms on the left hand side of the above equation as all the real terms will equal the cosine term and all the imaginary terms will equal the sine term. Therefore:

$$\cos(A + B + C)$$

$$= \cos A\cos B\cos C - \cos A\sin B\sin C - \sin A\cos B\sin C$$

$$- \sin A\sin B\cos C$$

$$\sin(A + B + C)$$

$$= \cos A\cos B\sin C + \cos A\sin B\cos C + \sin A\cos B\cos C$$

$$- \sin A\sin B\sin C$$

For the second expression of cosine, we substitute x=A-B+C into the trigonometric identities which gives:

$$\cos(A - B + C) + i\sin(A - B + C) = e^{i(A-B+C)}$$

Using the previously stated identities, we can make the following simplification:

$$e^{i(-B)} = \cos(-B) + i\sin(-B) = \cos B - i\sin B$$

Incorporating the previous equation into the equation above and again simplifying the right hand side of the equation gives:

$$e^{i(A-B+C)} = e^{iA}e^{i(-B)}e^{iC} = (\cos A + i\sin A)(\cos B - i\,\mathrm{sinB})(\cos C + i\sin C)$$

$$= (\cos A\cos B - i\cos A\sin B + i\sin A\cos B + \sin A\sin B)(\cos C$$

$$+ i\sin C)$$

$$= \cos A\cos B\,cosC + i\cos A\cos B\sin C - i\cos A\sin B\cos C$$

$$+ \cos A\sin B\sin C + i\sin A\cos B\cos C - \sin A\cos B\sin C$$

$$+ \sin A\sin B\cos C + i\sin A\sin B\sin C$$

Collecting the real terms to equate to the cosine term and the imaginary terms to get the sine terms we get:

$$\cos(A - B + C)$$

$$= \cos A\cos B\cos C + \cos A\sin B\sin C - \sin A\cos B\sin C$$

$$+ \sin A\sin B\cos C$$

$$\sin(A - B + C)$$

$$= \cos A\cos B\sin C - \cos A\sin B\cos C + \sin A\cos B\cos C$$

$$+ \sin A\sin B\sin C$$

Using the found addition/subtraction cosine expression in the total wave elevation equation, we get:

$$A\cos(\omega_j t) + B\sin(\omega_j t)$$

$$= \zeta_{if}[\cos(\omega_j t)\cos(k_j x_n)\cos(\varepsilon_{if}) + \cos(\omega_j t)\sin(k_j x_n)\sin(\varepsilon_{if})$$

$$- \sin(\omega_j t)\cos(k_j x_n)\sin(\varepsilon_{if}) + \sin(\omega_j t)\sin(k_j x_n)\cos(\varepsilon_{if})]$$

$$+ \zeta_{rf}[\cos(\omega_j t)\cos(K_j x_n)\cos(\varepsilon_{rf}) - \cos(\omega_j t)\sin(K_j x_n)\sin(\varepsilon_{rf})$$

$$- \sin(\omega_j t)\cos(K_j x_n)\sin(\varepsilon_{rf}) - \sin(\omega_j t)\sin(K_j x_n)\cos(\varepsilon_{rf})]$$

$$+ \zeta_{ib}[\cos(\omega_j t)\cos(\Delta k_j x_n)\cos(\varepsilon_{ib}) + \cos(\omega_j t)\sin(\Delta k_j x_n)\sin(\varepsilon_{ib})$$

$$- \sin(\omega_j t)\cos(\Delta k_j x_n)\sin(\varepsilon_{ib}) + \sin(\omega_j t)\sin(\Delta k_j x_n)\cos(\varepsilon_{ib})]$$

We can collect the sine and cosine terms in order to make two equations:

$$A\cos(\omega_j t) = \cos(\omega_j t)[\zeta_{if}[\cos(k_j x_n)\cos(\varepsilon_{if}) + \sin(k_j x_n)\sin(\varepsilon_{if})$$

$$+ \zeta_{rf}[\cos(K_j x_n)\cos(\varepsilon_{rf}) - \sin(K_j x_n)\sin(\varepsilon_{rf})]$$

$$+ \zeta_{ib}[\cos(\Delta k_j x_n)\cos(\varepsilon_{ib}) + \sin(\Delta k_j x_n)\sin(\varepsilon_{ib})]]$$

$$B\sin(\omega_j t) = \sin(\omega_j t)\,[\zeta_{if}[-\cos(k_j x_n)\sin(\varepsilon_{if}) + \sin(k_j x_n)\cos(\varepsilon_{if})]$$

$$+ \zeta_{rf}[-\cos(K_j x_n)\sin(\varepsilon_{rf}) - \sin(K_j x_n)\cos(\varepsilon_{rf})]$$

$$+ \zeta_{ib}[-\cos(\Delta k_j x_n)\sin(\varepsilon_{ib}) + \sin(\Delta k_j x_n)\cos(\varepsilon_{ib})]]$$

The $\cos(\omega_j t)$ and $\sin(\omega_j t)$ terms can be cancelled out of their respective equations and the equations are reduced to:

$$A = \zeta_{if}\cos(k_j x_n)\cos(\varepsilon_{if}) + \zeta_{if}\sin(k_j x_n)\sin(\varepsilon_{if}) + \zeta_{rf}\cos(K_j x_n)\cos(\varepsilon_{rf})$$

$$- \zeta_{rf}\sin(K_j x_n)\sin(\varepsilon_{rf}) + \zeta_{ib}\cos(\Delta k_j x_n)\cos(\varepsilon_{ib})$$

$$+ \zeta_{ib}\sin(\Delta k_j x_n)\cos(\varepsilon_{ib})$$

$$B = -\zeta_{if}\cos(k_j x_n)\sin(\varepsilon_{if}) + \zeta_{if}\sin(k_j x_n)\cos(\varepsilon_{if}) - \zeta_{rf}\cos(K_j x_n)\sin(\varepsilon_{rf}) - \zeta_{rf}\sin(K_j x_n)\cos(\varepsilon_{rf}) + \zeta_{ib}\cos(\Delta k_j x_n)\sin(\varepsilon_{ib}) - \zeta_{ib}\sin(\Delta k_j x_n)\cos(\varepsilon_{ib})$$

We can rewrite in matrix notation in include a known and unknown matrices, where y is denoted as the unknown matrix.

$$A = \begin{bmatrix}\cos(k_j x_n) & \sin(k_j x_n) & \cos(K_j x_n) & -\sin(K_j x_n) & \cos(\Delta k_j x_n) & \sin(\Delta k_j x_n)\end{bmatrix}\begin{bmatrix}\zeta_{if}\cos(\varepsilon_{if})\\ \zeta_{if}\sin(\varepsilon_{if})\\ \zeta_{rf}\cos(\varepsilon_{rf})\\ \zeta_{rf}\sin(\varepsilon_{rf})\\ \zeta_{ib}\cos(\varepsilon_{ib})\\ \zeta_{ib}\cos(\varepsilon_{ib})\end{bmatrix}$$

$$B = \begin{bmatrix}\sin(k_j x_n) & -\cos(k_j x_n) & -\sin(K_j x_n) & -\cos(K_j x_n) & \sin(\Delta k_j x_n) & -\cos(\Delta k_j x_n)\end{bmatrix}\begin{bmatrix}\zeta_{if}\cos(\varepsilon_{if})\\ \zeta_{if}\sin(\varepsilon_{if})\\ \zeta_{rf}\cos(\varepsilon_{rf})\\ \zeta_{rf}\sin(\varepsilon_{rf})\\ \zeta_{ib}\cos(\varepsilon_{ib})\\ \zeta_{ib}\cos(\varepsilon_{ib})\end{bmatrix}$$

$$A = \begin{bmatrix}\cos(k_j x_n) & \sin(k_j x_n) & \cos(K_j x_n) & -\sin(K_j x_n) & \cos(\Delta k_j x_n) & \sin(\Delta k_j x_n)\end{bmatrix} * y$$

$$B = \begin{bmatrix}\sin(k_j x_n) & -\cos(k_j x_n) & -\sin(K_j x_n) & -\cos(K_j x_n) & \sin(\Delta k_j x_n) & -\cos(\Delta k_j x_n)\end{bmatrix} * y$$

APPENDIX B – MODEL SCALE RESULTS

1.133 Model Scale

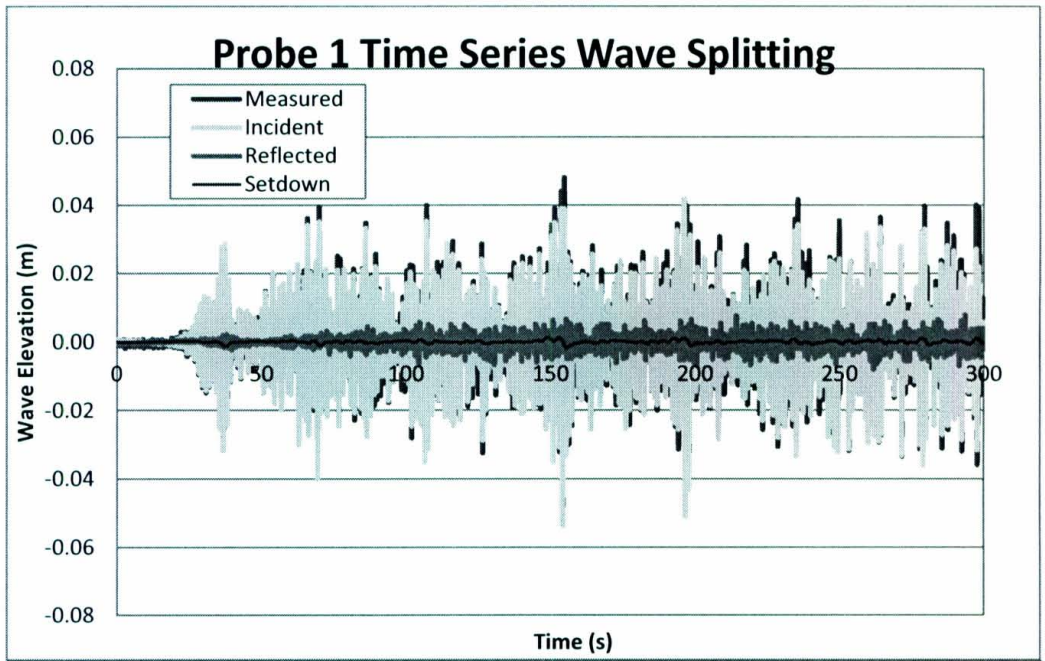

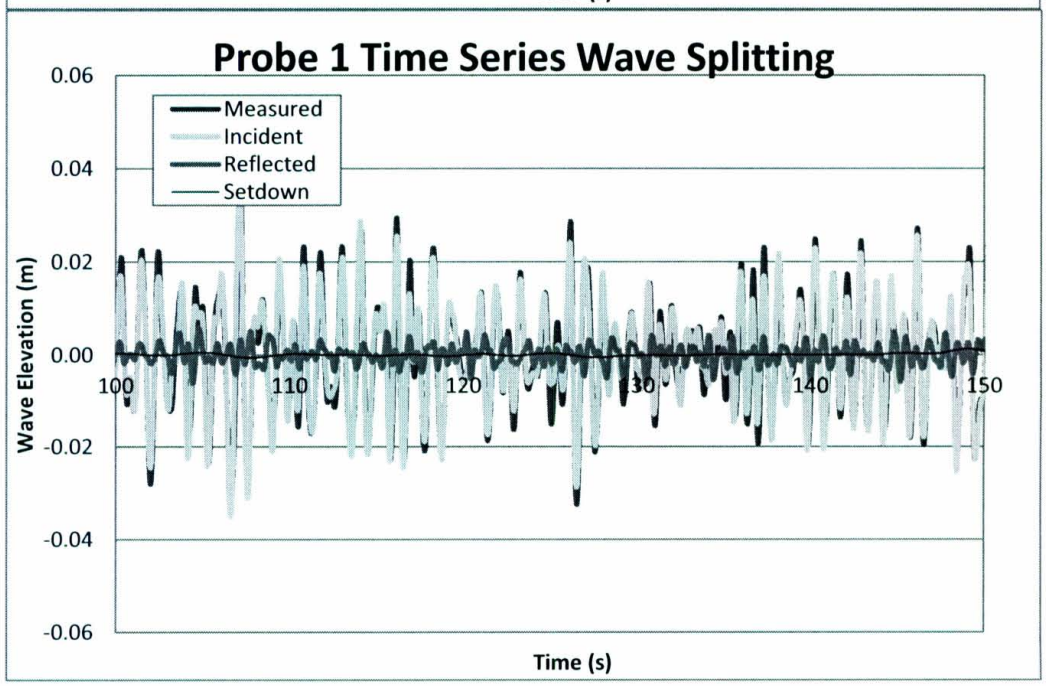

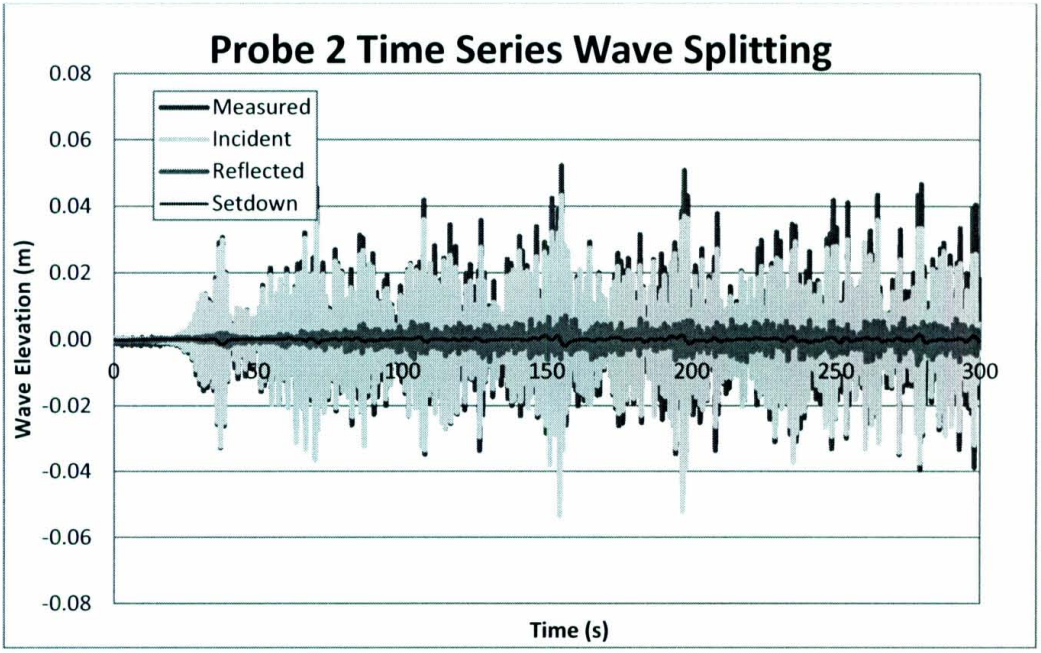
Probe 2 Time Series Wave Splitting
Measured
Incident
Reflected
Setdown
Wave Elevation (m)
0.08
0.06
0.04
0.02
0.00
-0.02
-0.04
-0.06
-0.08
0
50
100
150
200
250
300
Time (s)

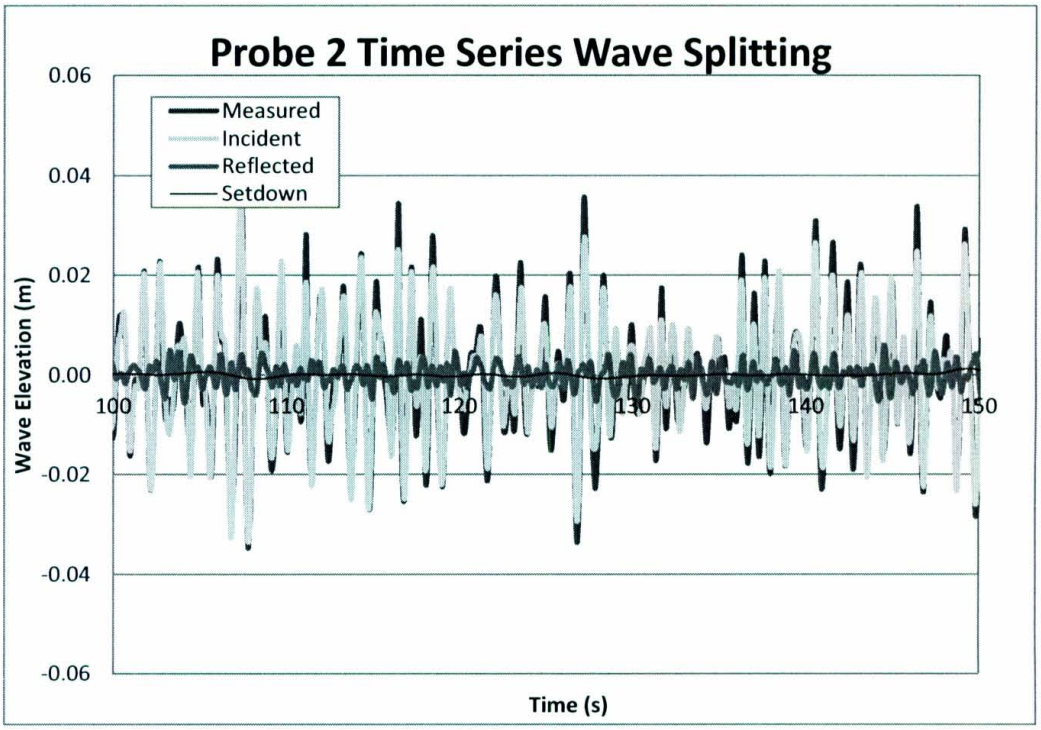
Probe 2 Time Series Wave Splitting
Measured
Incident
Reflected
Setdown
Wave Elevation (m)
0.06
0.04
0.02
0.00
-0.02
-0.04
-0.06
100
110
120
130
140
150
Time (s)

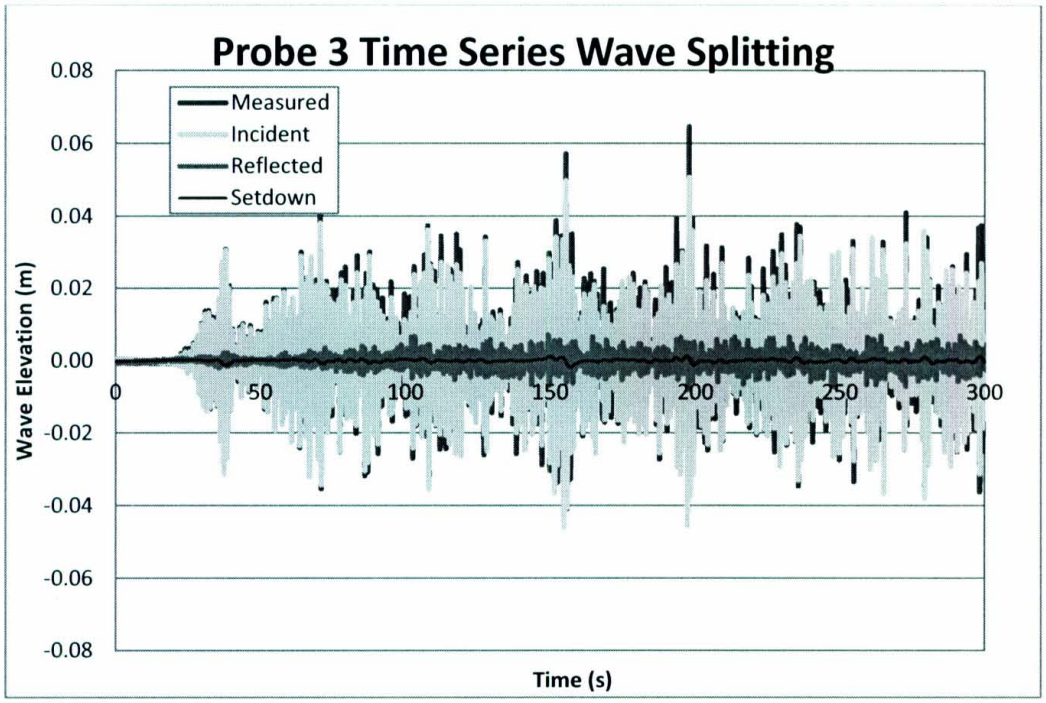
Probe 3 Time Series Wave Splitting
Measured
Incident
Reflected
Setdown
Wave Elevation (m)
0.08
0.06
0.04
0.02
0.00
-0.02
-0.04
-0.06
-0.08
0
50
100
150
200
250
300
Time (s)

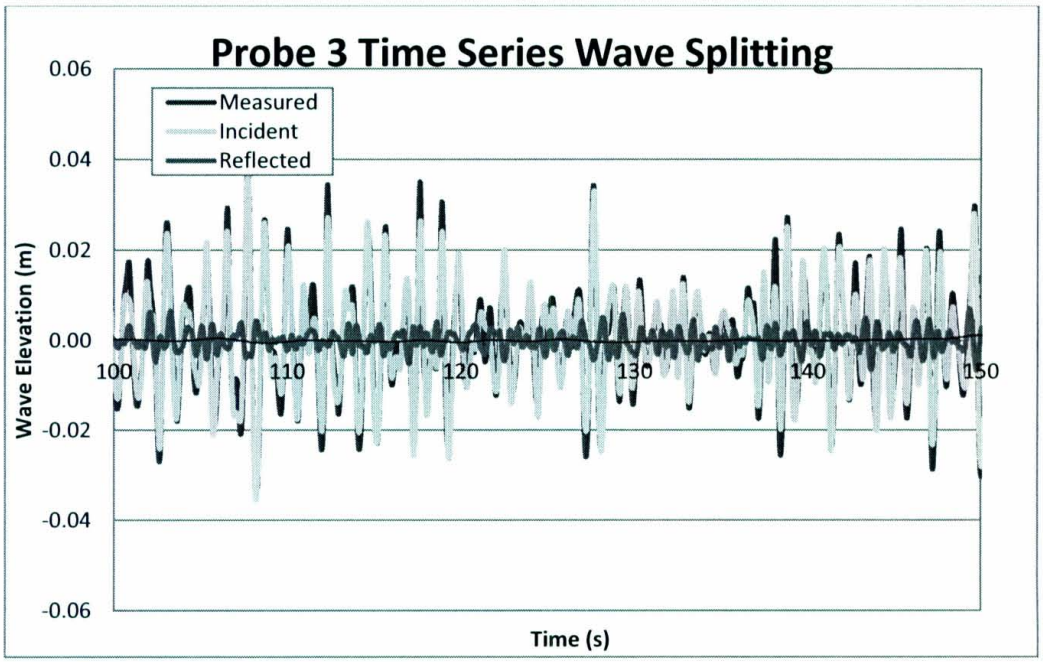
Probe 3 Time Series Wave Splitting
Measured
Incident
Reflected
Wave Elevation (m)
0.06
0.04
0.02
0.00
-0.02
-0.04
-0.06
100
110
120
130
140
150
Time (s)

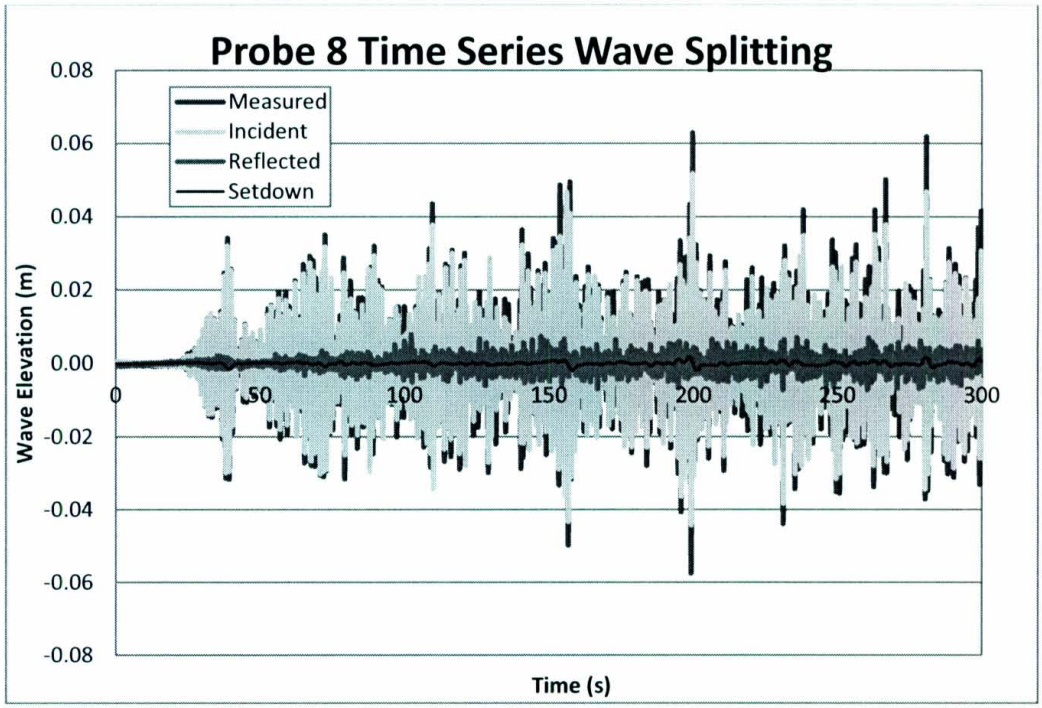
Probe 8 Time Series Wave Splitting
Measured
Incident
Reflected
Setdown
Wave Elevation (m)
0.08
0.06
0.04
0.02
0.00
-0.02
-0.04
-0.06
-0.08
0
50
100
150
200
250
300
Time (s)

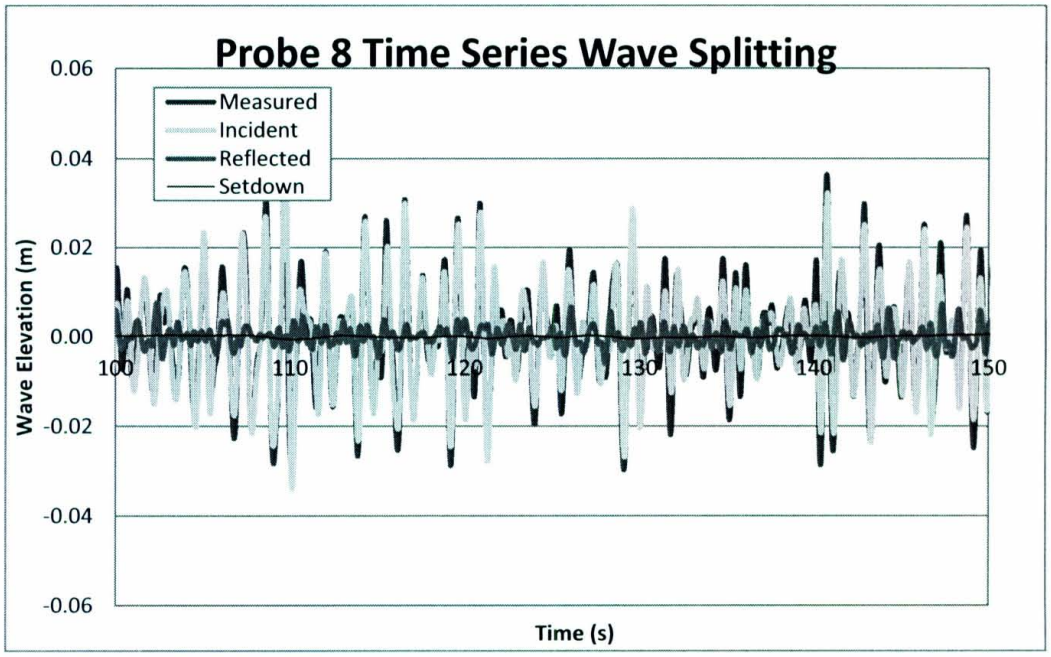
Probe 8 Time Series Wave Splitting
Measured
Incident
Reflected
Setdown
Wave Elevation (m)
0.06
0.04
0.02
0.00
-0.02
-0.04
-0.06
100
110
120
130
140
150
Time (s)

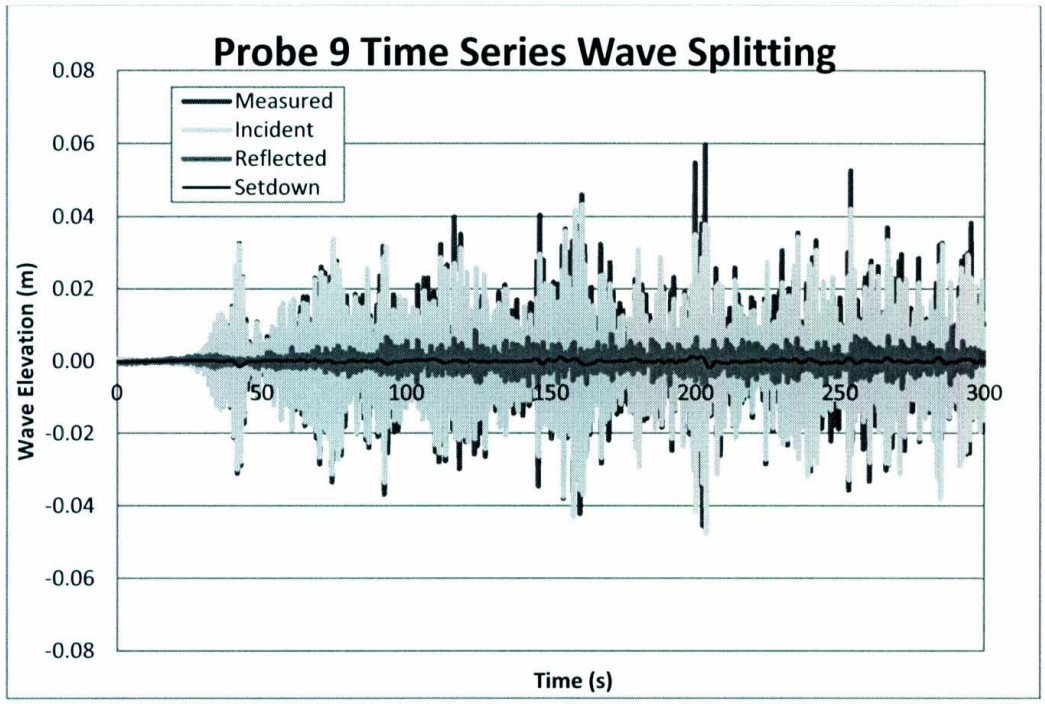
Probe 9 Time Series Wave Splitting
Measured
Incident
Reflected
Setdown
Wave Elevation (m)
0.08
0.06
0.04
0.02
0.00
-0.02
-0.04
-0.06
-0.08
0
50
100
150
200
250
300
Time (s)

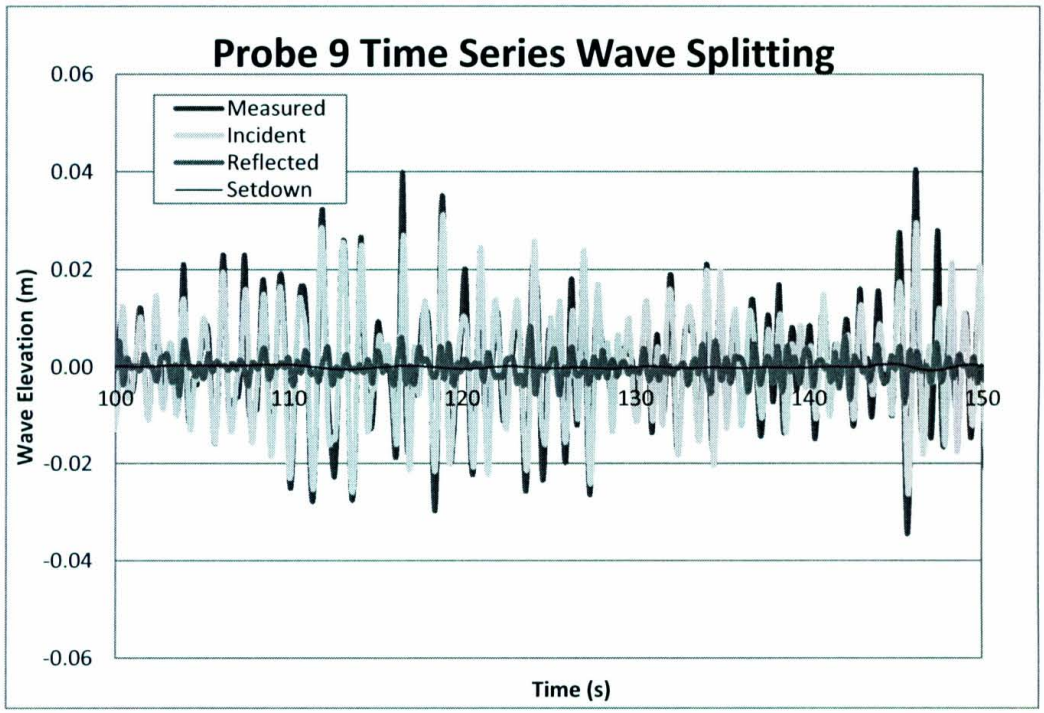
Probe 9 Time Series Wave Splitting
Measured
Incident
Reflected
Setdown
Wave Elevation (m)
0.06
0.04
0.02
0.00
-0.02
-0.04
-0.06
100
110
120
130
140
150
Time (s)

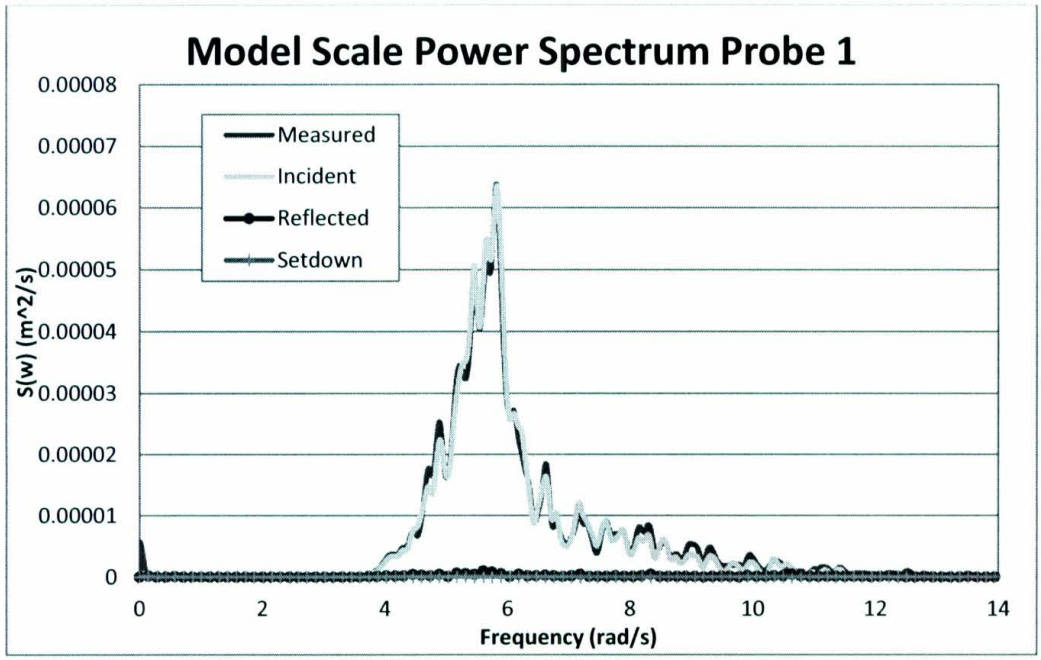
Model Scale Power Spectrum Probe 1
0.00008
0.00007
0.00006
0.00005
0.00004
0.00003
0.00002
0.00001
0
S(w) (m^2/s)
Measured
Incident
Reflected
Setdown
0
2
4
6
8
10
12
14
Frequency (rad/s)

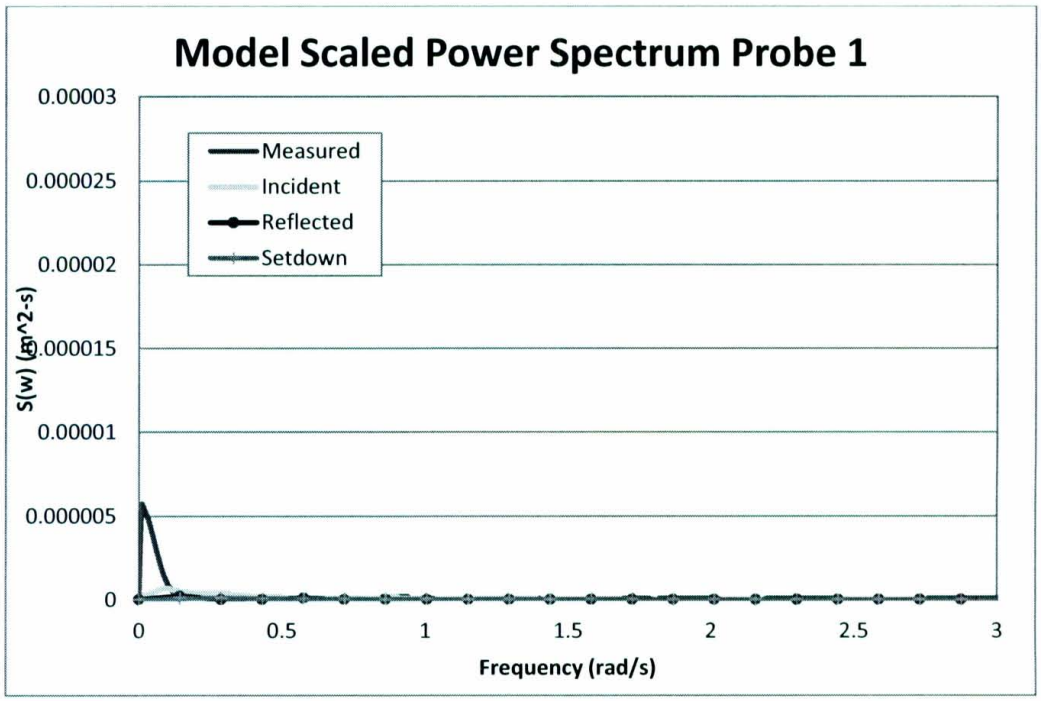
Model Scaled Power Spectrum Probe 1
0.00003
0.000025
0.00002
0.000015
0.00001
0.000005
0
S(w) (m^2-s)
Measured
Incident
Reflected
Setdown
0
0.5
1
1.5
2
2.5
3
Frequency (rad/s)

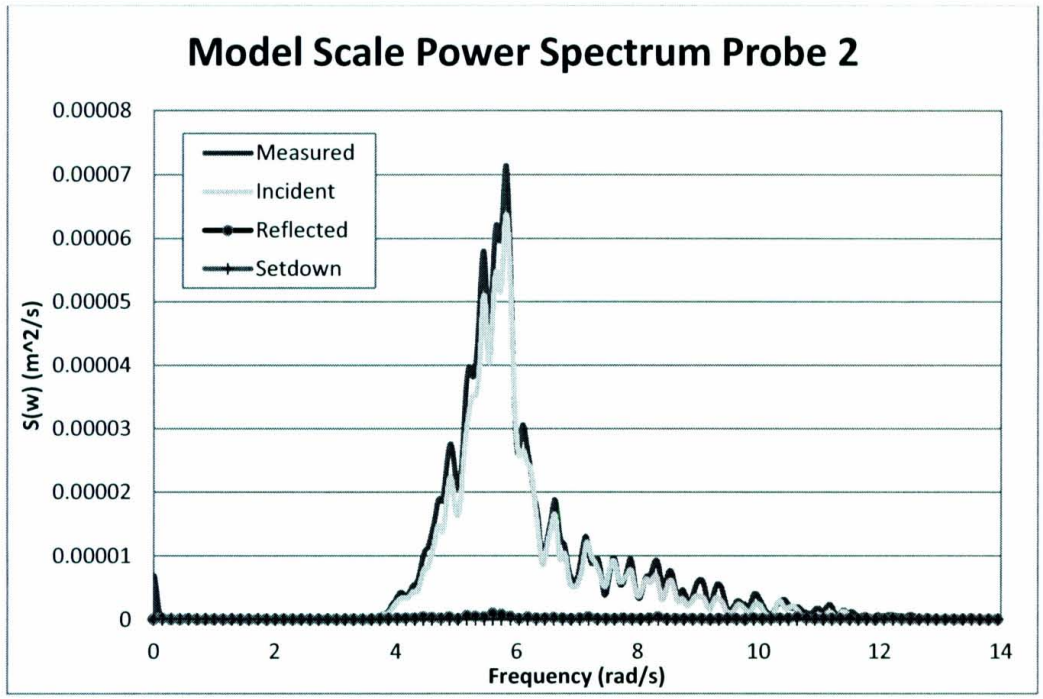
Model Scale Power Spectrum Probe 2
0.00008
0.00007
0.00006
0.00005
0.00004
0.00003
0.00002
0.00001
0
S(w) (m^2/s)
Measured
Incident
Reflected
Setdown
0
2
4
6
8
10
12
14
Frequency (rad/s)

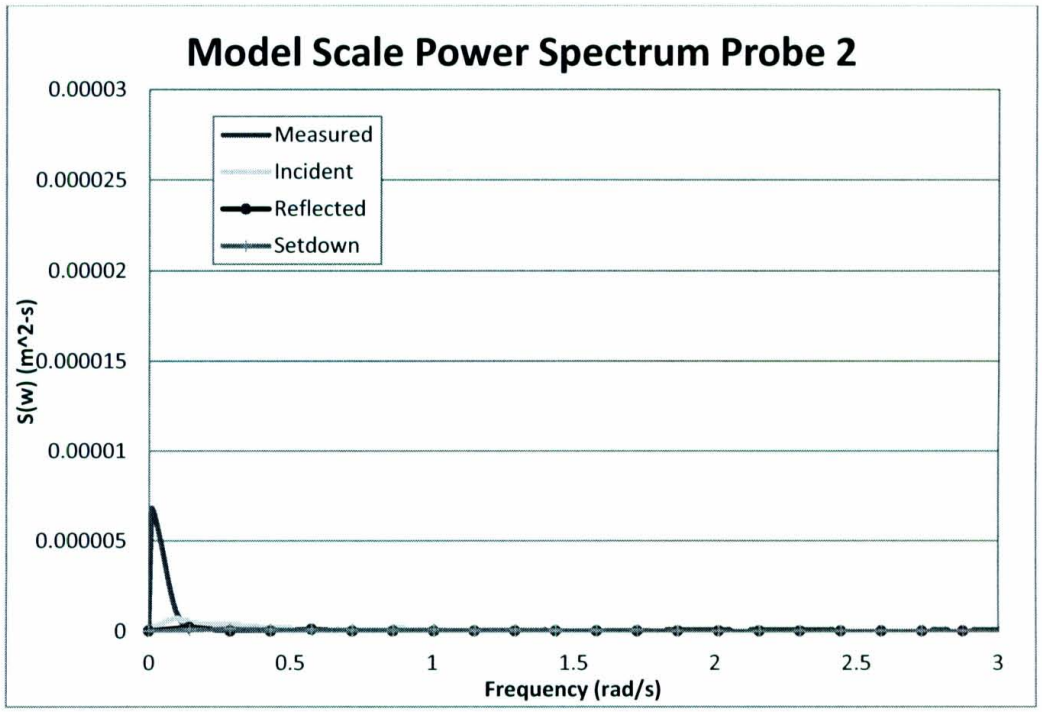
Model Scale Power Spectrum Probe 2
0.00003
0.000025
0.00002
0.000015
0.00001
0.000005
0
S(w) (m^2-s)
Measured
Incident
Reflected
Setdown
0
0.5
1
1.5
2
2.5
3
Frequency (rad/s)

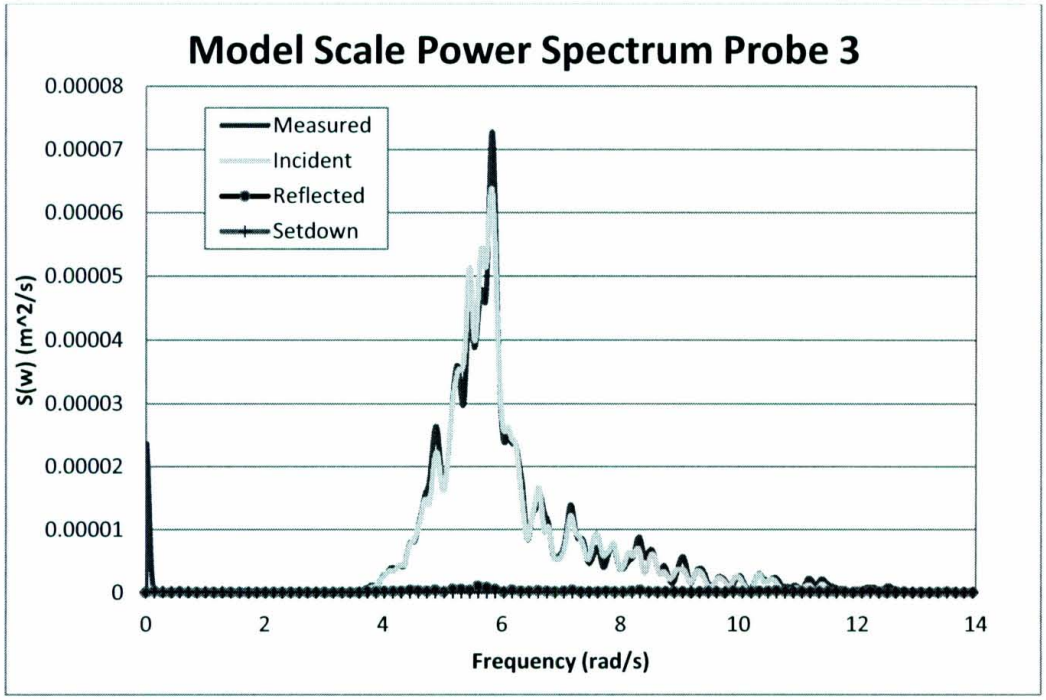
Model Scale Power Spectrum Probe 3
Measured
Incident
Reflected
Setdown
S(w) (m^2/s)
0.00008
0.00007
0.00006
0.00005
0.00004
0.00003
0.00002
0.00001
0
0
2
4
6
8
10
12
14
Frequency (rad/s)

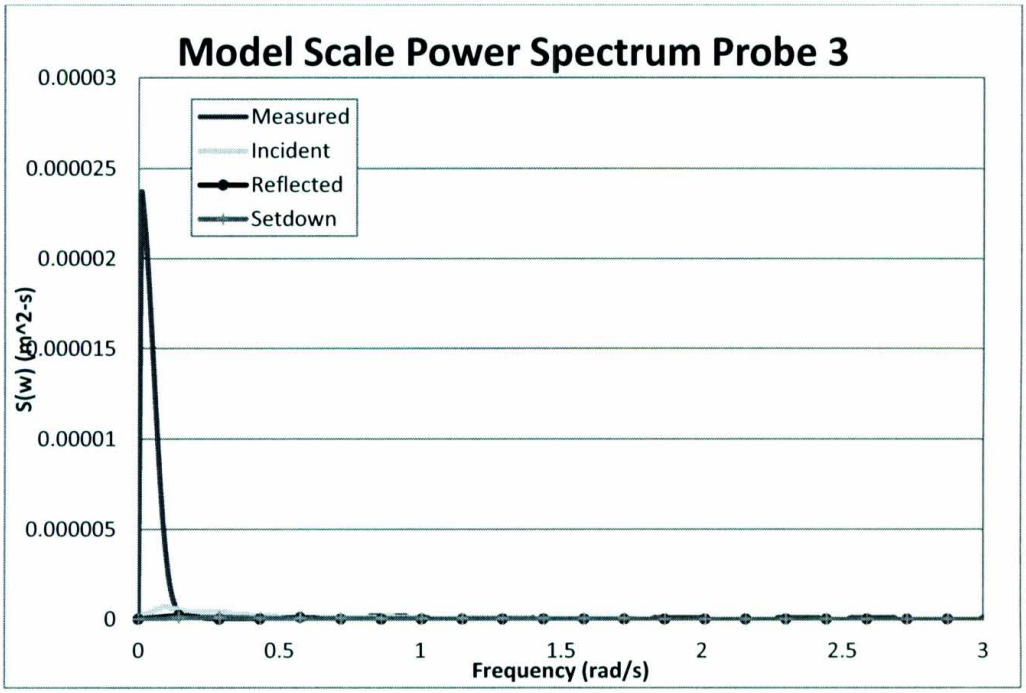
Model Scale Power Spectrum Probe 3
Measured
Incident
Reflected
Setdown
S(w) (m^2-s)
0.00003
0.000025
0.00002
0.000015
0.00001
0.000005
0
0
0.5
1
1.5
2
2.5
3
Frequency (rad/s)

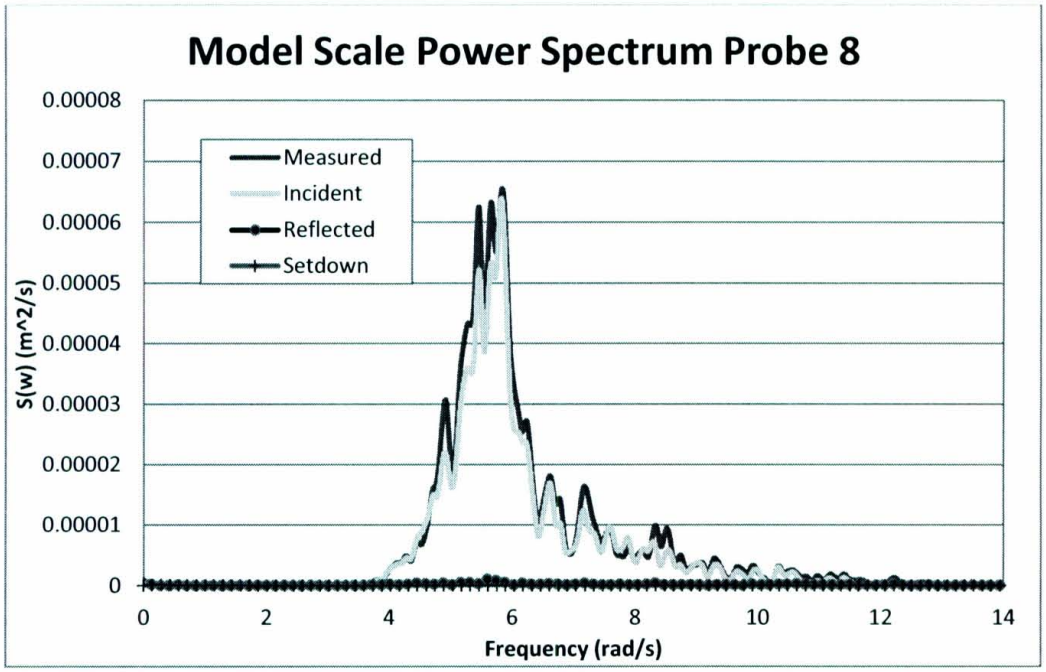
Model Scale Power Spectrum Probe 8
0.00008
0.00007
0.00006
0.00005
0.00004
0.00003
0.00002
0.00001
0
S(w) (m^2/s)
Measured
Incident
Reflected
Setdown
0
2
4
6
8
10
12
14
Frequency (rad/s)

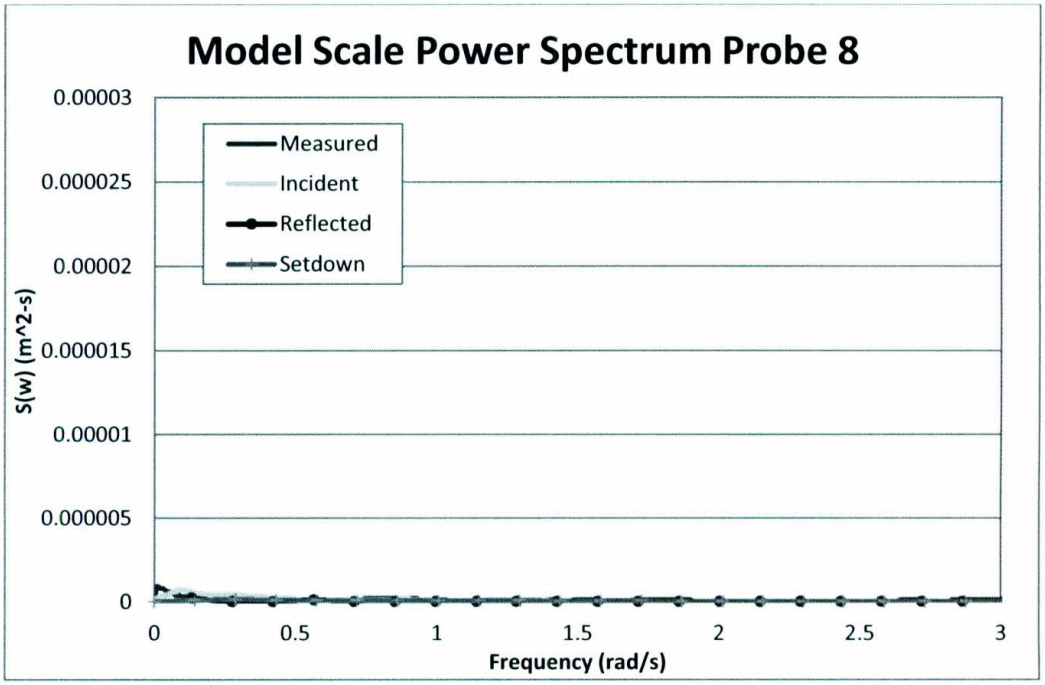
Model Scale Power Spectrum Probe 8
0.00003
0.000025
0.00002
0.000015
0.00001
0.000005
0
S(w) (m^2-s)
Measured
Incident
Reflected
Setdown
0
0.5
1
1.5
2
2.5
3
Frequency (rad/s)

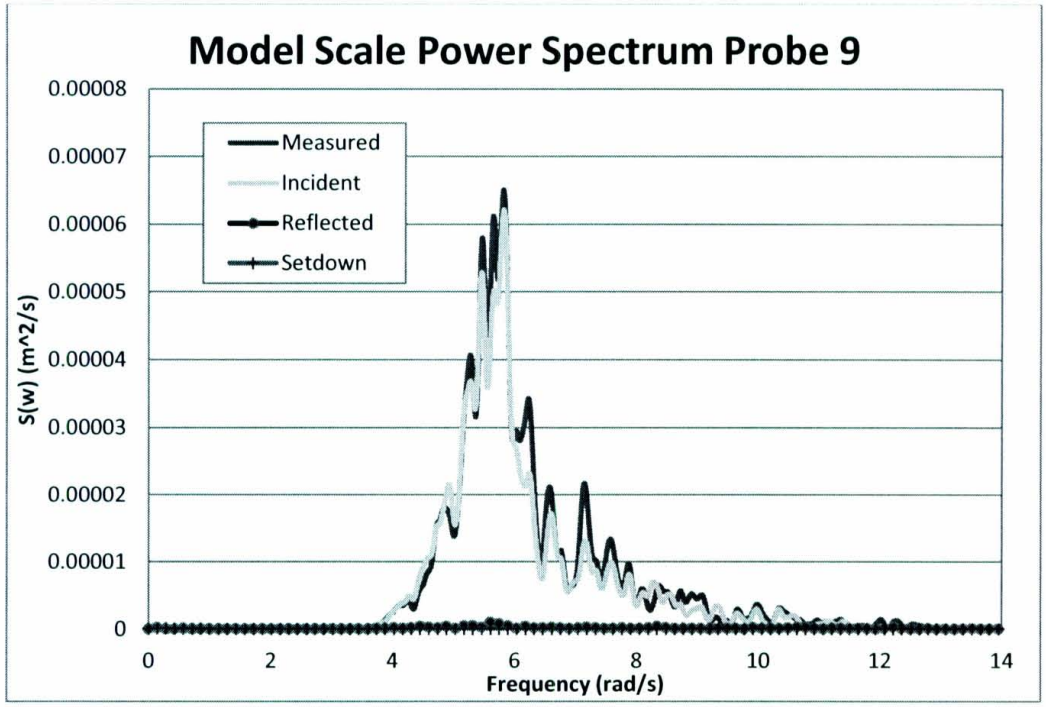
Model Scale Power Spectrum Probe 9
Measured
Incident
Reflected
Setdown
S(w) (m^2/s)
0.00008
0.00007
0.00006
0.00005
0.00004
0.00003
0.00002
0.00001
0
0
2
4
6
8
10
12
14
Frequency (rad/s)

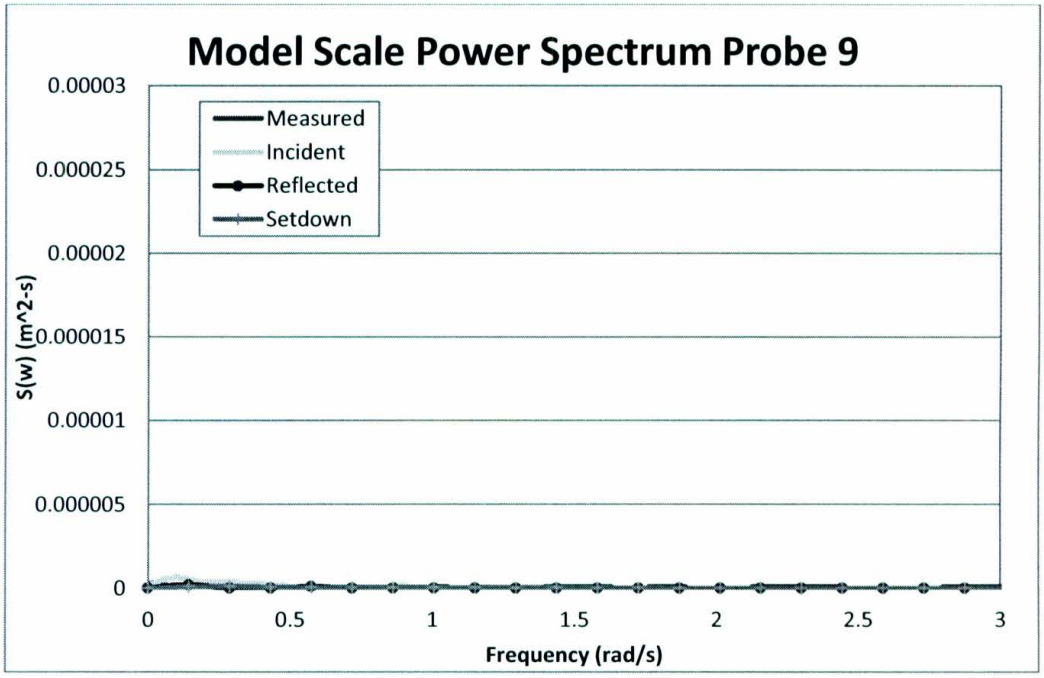
Model Scale Power Spectrum Probe 9
Measured
Incident
Reflected
Setdown
S(w) (m^2-s)
0.00003
0.000025
0.00002
0.000015
0.00001
0.000005
0
0
0.5
1
1.5
2
2.5
3
Frequency (rad/s)

1.705 Model Scale

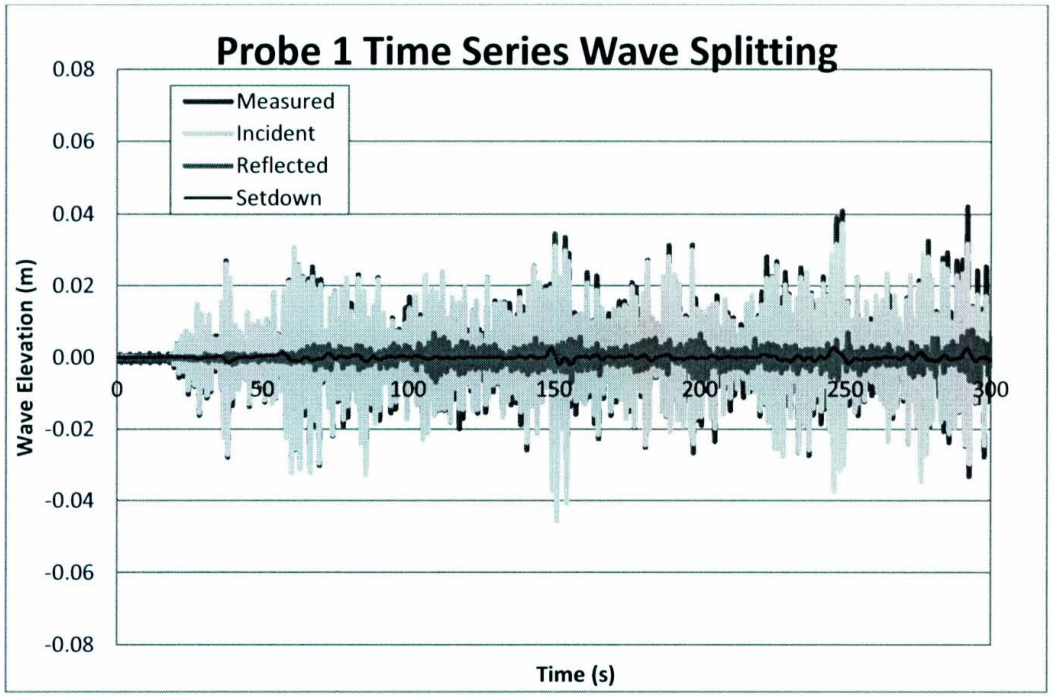

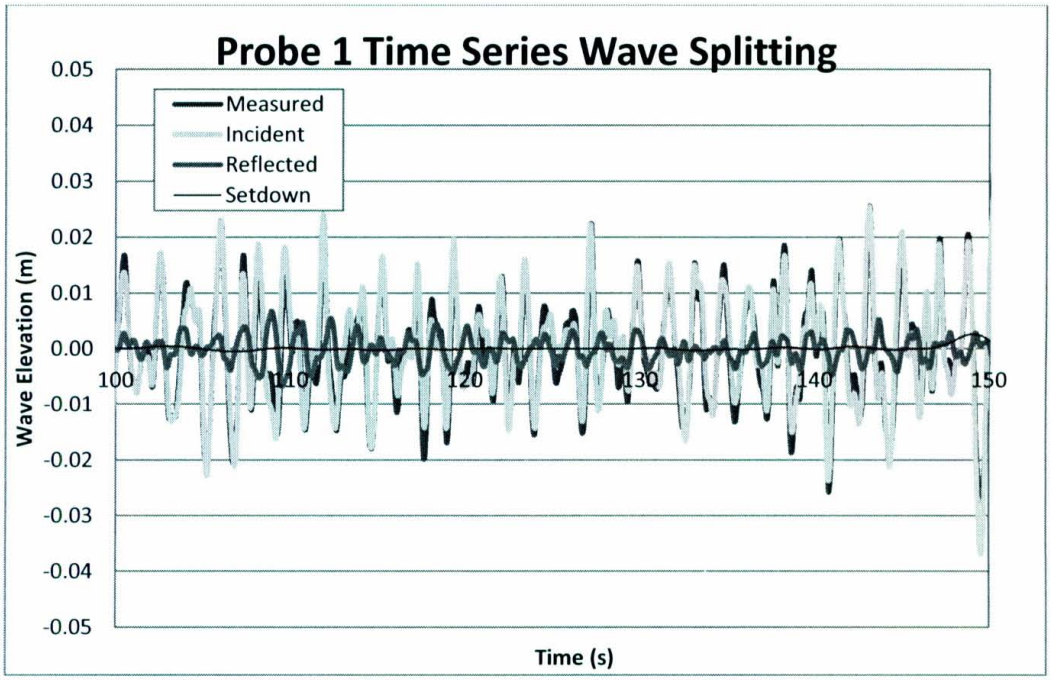

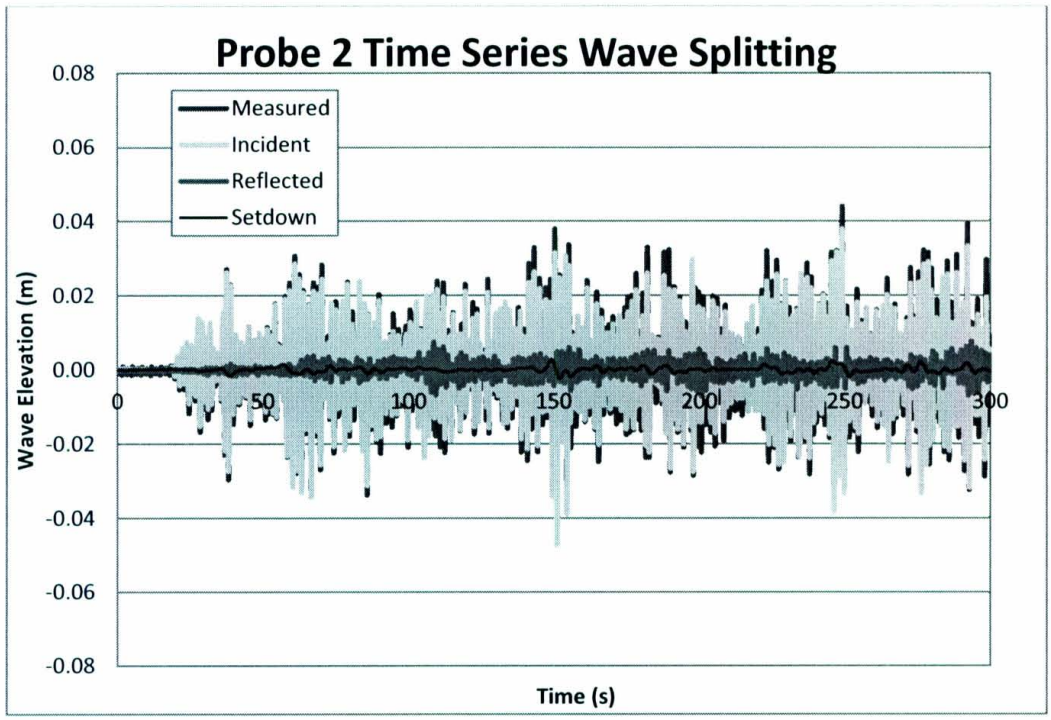
Probe 2 Time Series Wave Splitting
Measured
Incident
Reflected
Setdown
Wave Elevation (m)
0.08
0.06
0.04
0.02
0.00
-0.02
-0.04
-0.06
-0.08
0
50
100
150
200
250
300
Time (s)

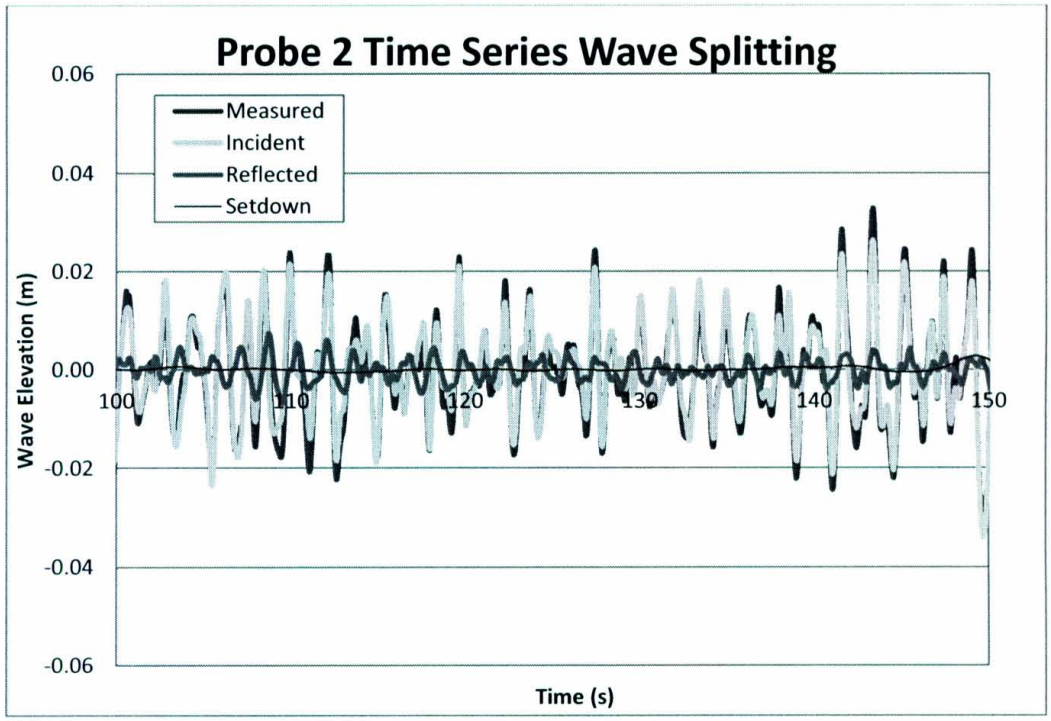
Probe 2 Time Series Wave Splitting
Measured
Incident
Reflected
Setdown
Wave Elevation (m)
0.06
0.04
0.02
0.00
-0.02
-0.04
-0.06
100
110
120
130
140
150
Time (s)

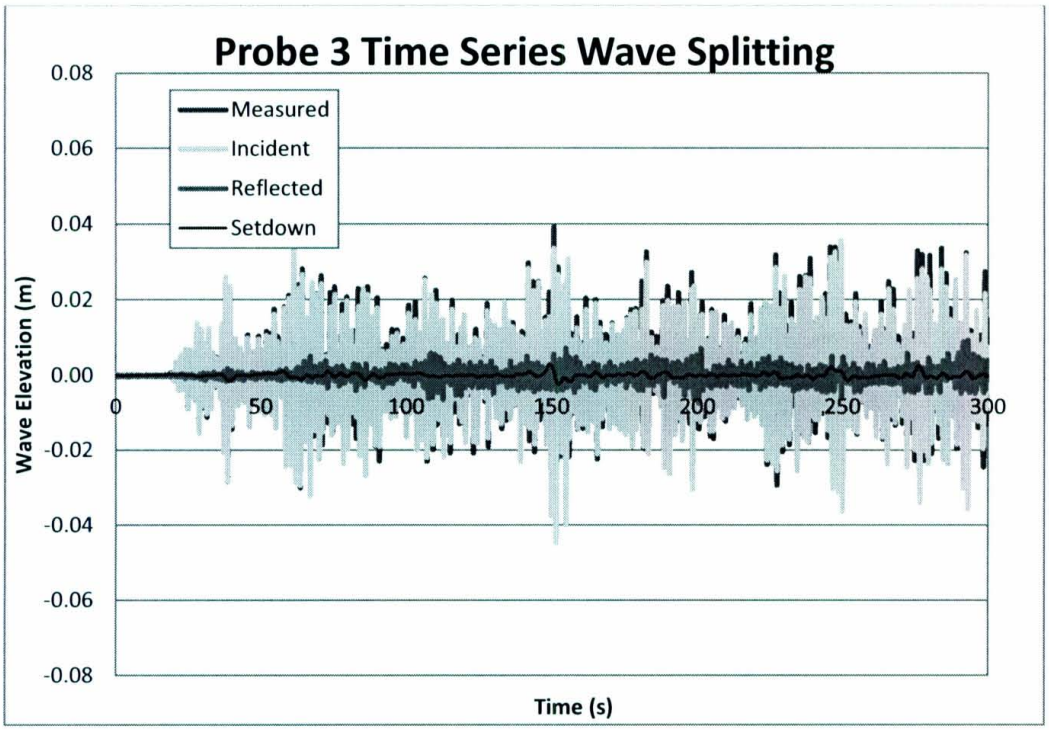
Probe 3 Time Series Wave Splitting
Measured
Incident
Reflected
Setdown
Wave Elevation (m)
0.08
0.06
0.04
0.02
0.00
-0.02
-0.04
-0.06
-0.08
0
50
100
150
200
250
300
Time (s)

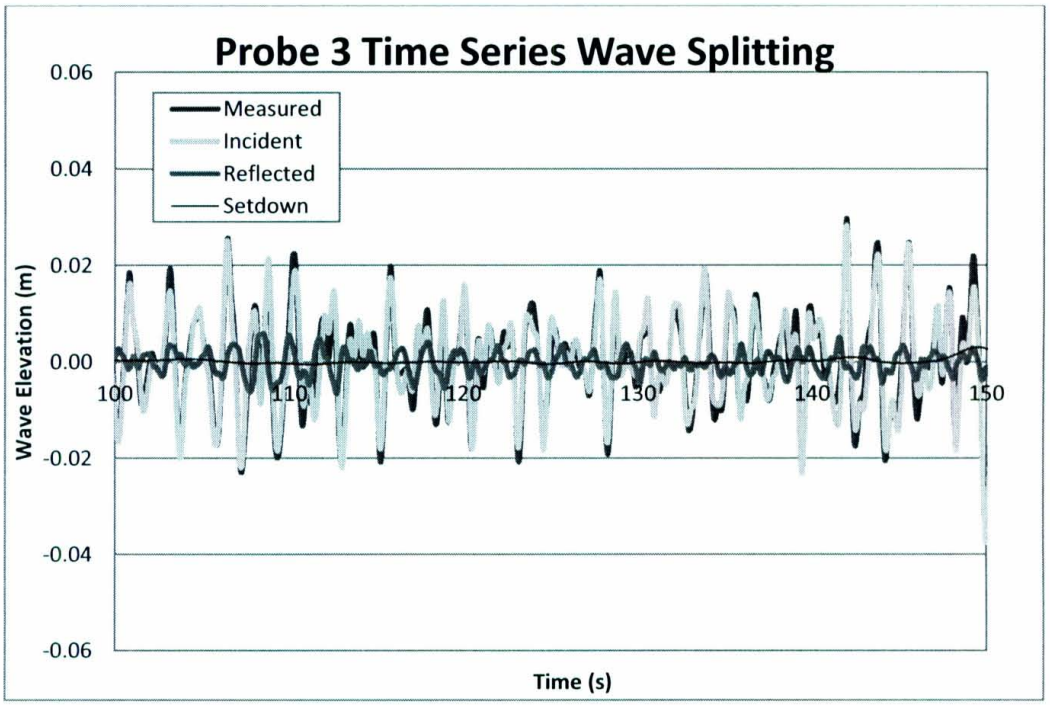
Probe 3 Time Series Wave Splitting
Measured
Incident
Reflected
Setdown
Wave Elevation (m)
0.06
0.04
0.02
0.00
-0.02
-0.04
-0.06
100
110
120
130
140
150
Time (s)

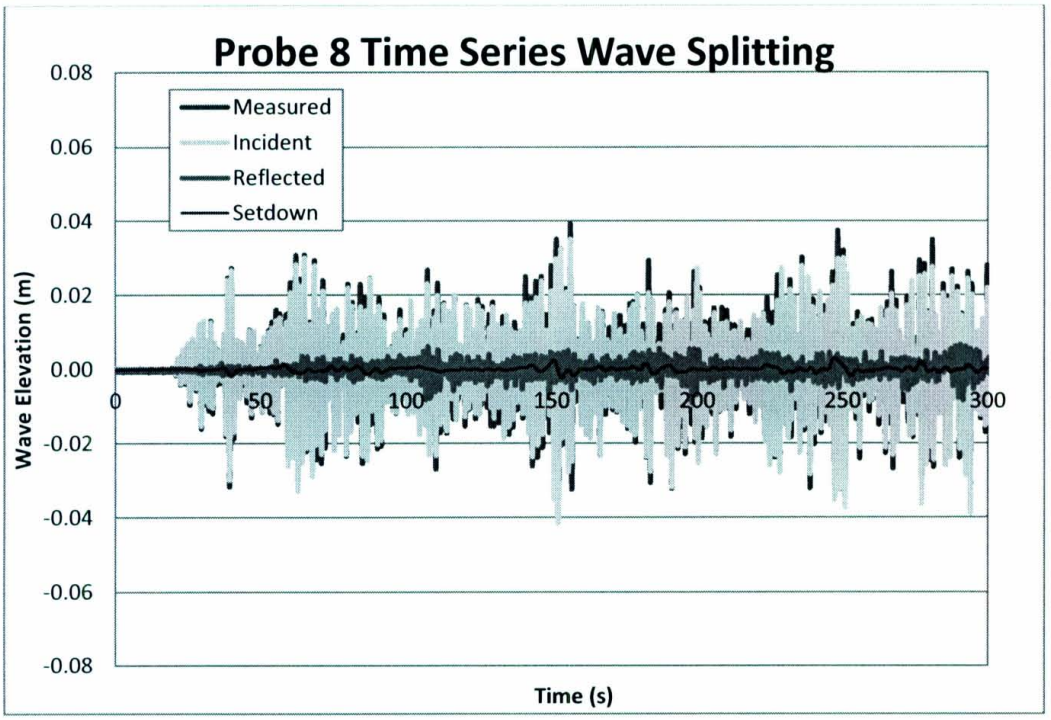
Probe 8 Time Series Wave Splitting
Measured
Incident
Reflected
Setdown
Wave Elevation (m)
0.08
0.06
0.04
0.02
0.00
-0.02
-0.04
-0.06
-0.08
0
50
100
150
200
250
300
Time (s)

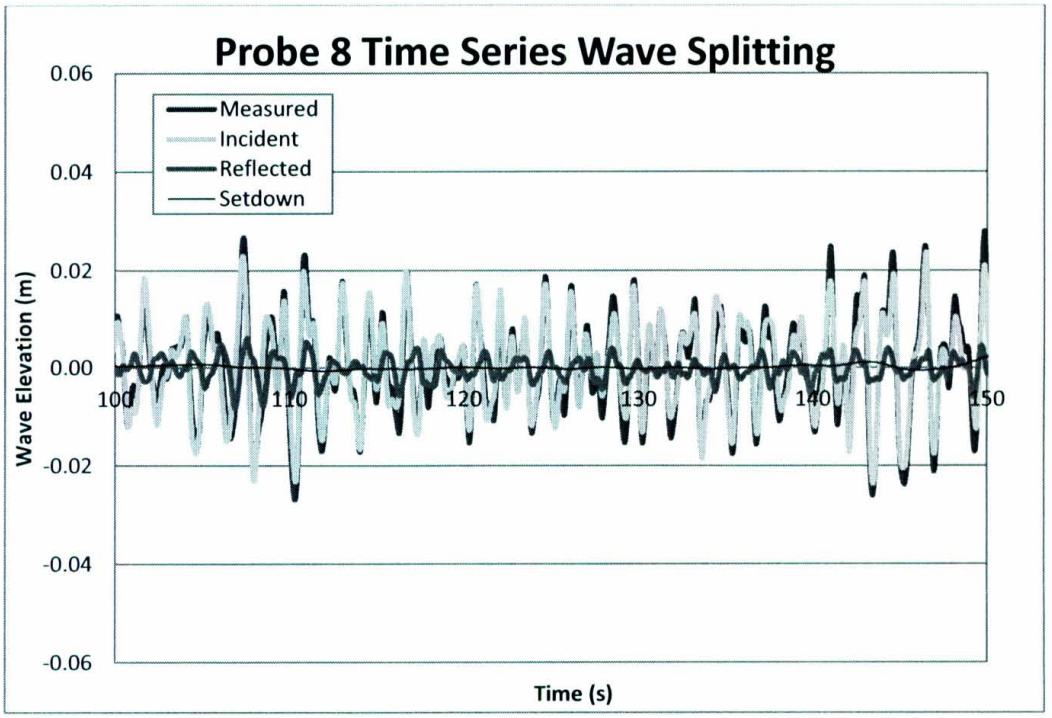
Probe 8 Time Series Wave Splitting
Measured
Incident
Reflected
Setdown
Wave Elevation (m)
0.06
0.04
0.02
0.00
-0.02
-0.04
-0.06
100
110
120
130
140
150
Time (s)

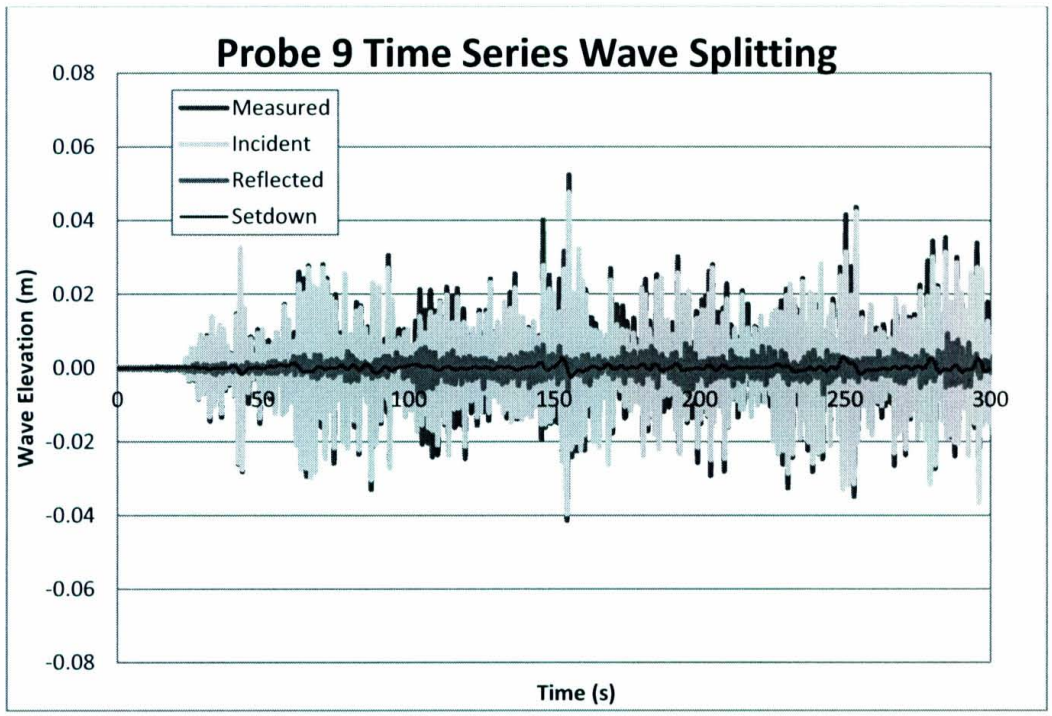
Probe 9 Time Series Wave Splitting
Measured
Incident
Reflected
Setdown
Wave Elevation (m)
0.08
0.06
0.04
0.02
0.00
-0.02
-0.04
-0.06
-0.08
0
50
100
150
200
250
300
Time (s)

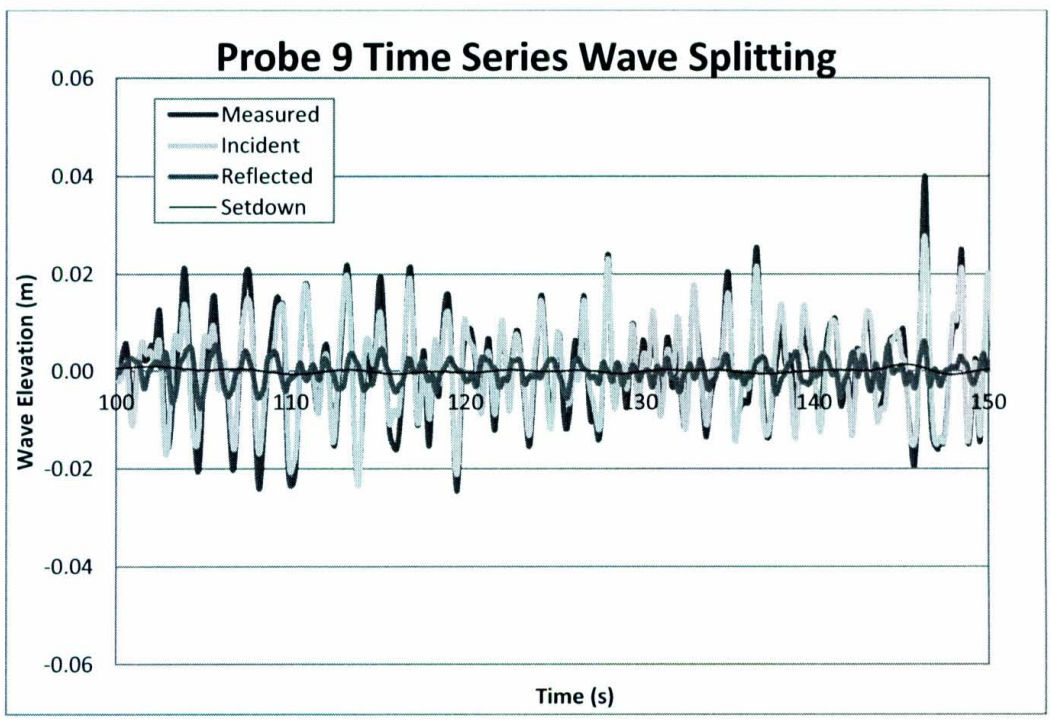
Probe 9 Time Series Wave Splitting
Measured
Incident
Reflected
Setdown
Wave Elevation (m)
0.06
0.04
0.02
0.00
-0.02
-0.04
-0.06
100
110
120
130
140
150
Time (s)

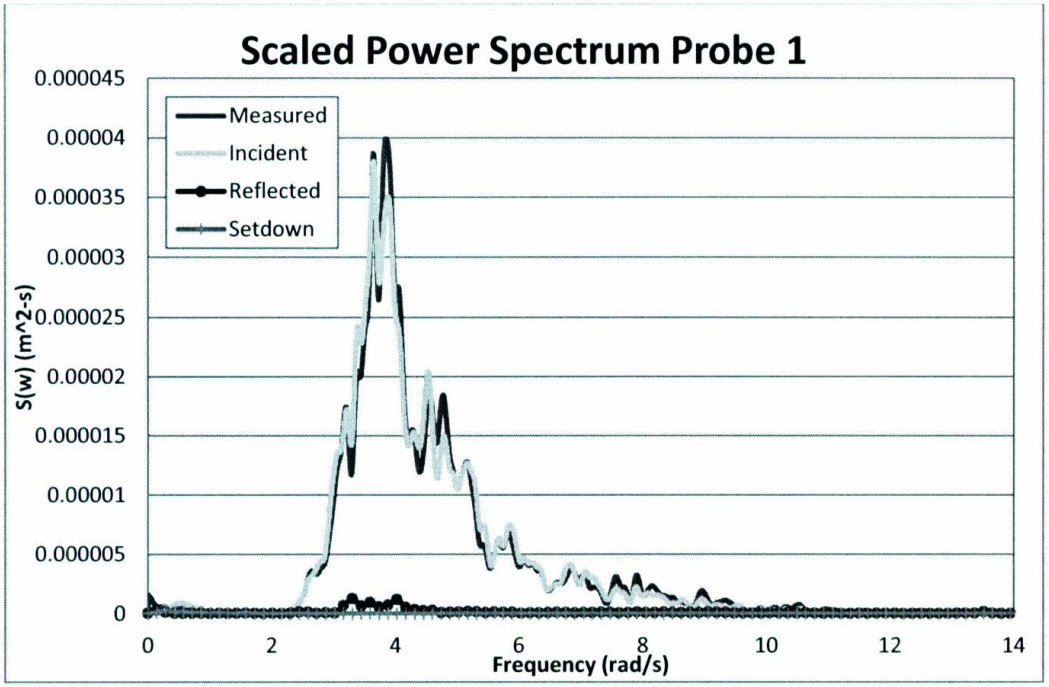
Scaled Power Spectrum Probe 1
Measured
Incident
Reflected
Setdown
S(w) (m^2-s)
0.000045
0.00004
0.000035
0.00003
0.000025
0.00002
0.000015
0.00001
0.000005
0
0
2
4
6
8
10
12
14
Frequency (rad/s)

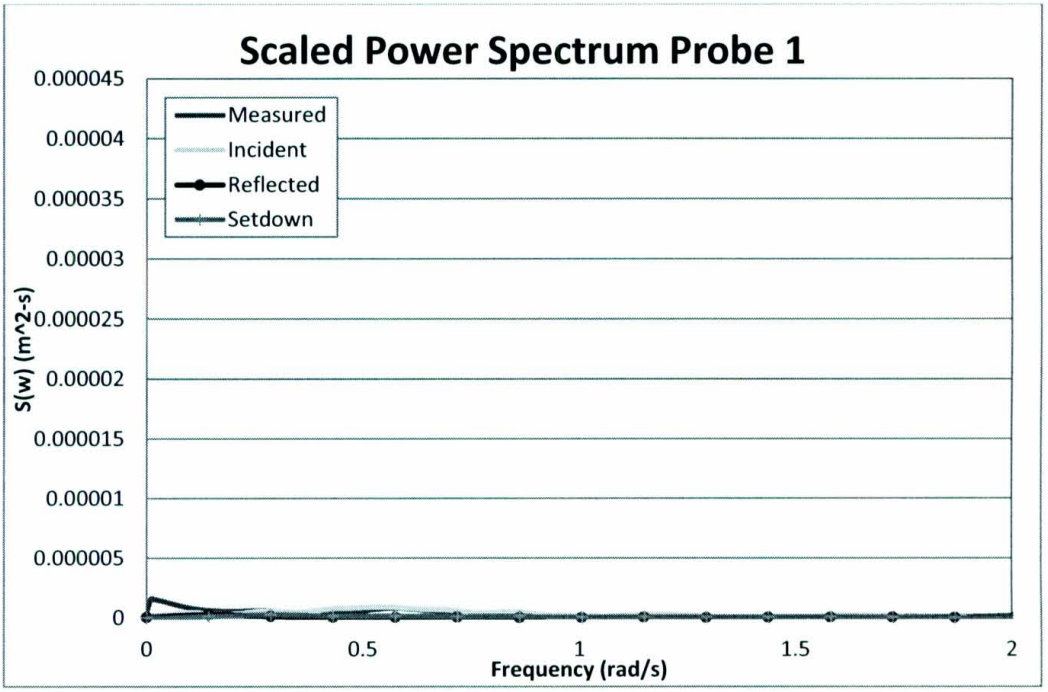
Scaled Power Spectrum Probe 1
Measured
Incident
Reflected
Setdown
S(w) (m^2-s)
0.000045
0.00004
0.000035
0.00003
0.000025
0.00002
0.000015
0.00001
0.000005
0
0
0.5
1
1.5
2
Frequency (rad/s)

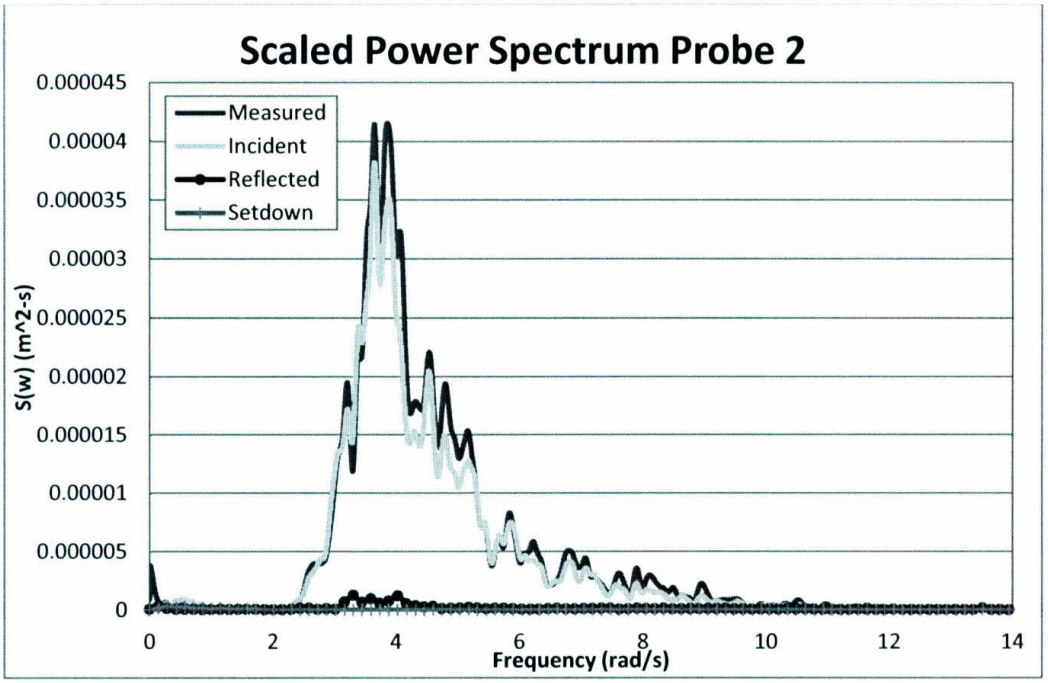
Scaled Power Spectrum Probe 2
Measured
Incident
Reflected
Setdown
S(w) (m^2-s)
0.000045
0.00004
0.000035
0.00003
0.000025
0.00002
0.000015
0.00001
0.000005
0
0
2
4
6
8
10
12
14
Frequency (rad/s)

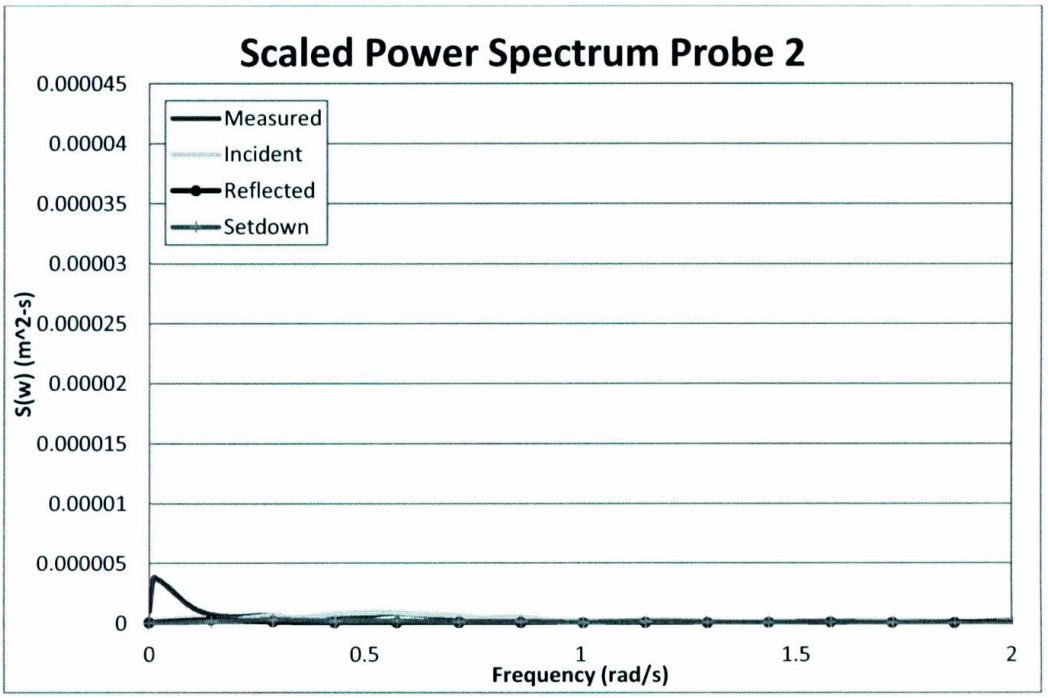
Scaled Power Spectrum Probe 2
Measured
Incident
Reflected
Setdown
S(w) (m^2-s)
0.000045
0.00004
0.000035
0.00003
0.000025
0.00002
0.000015
0.00001
0.000005
0
0
0.5
1
1.5
2
Frequency (rad/s)

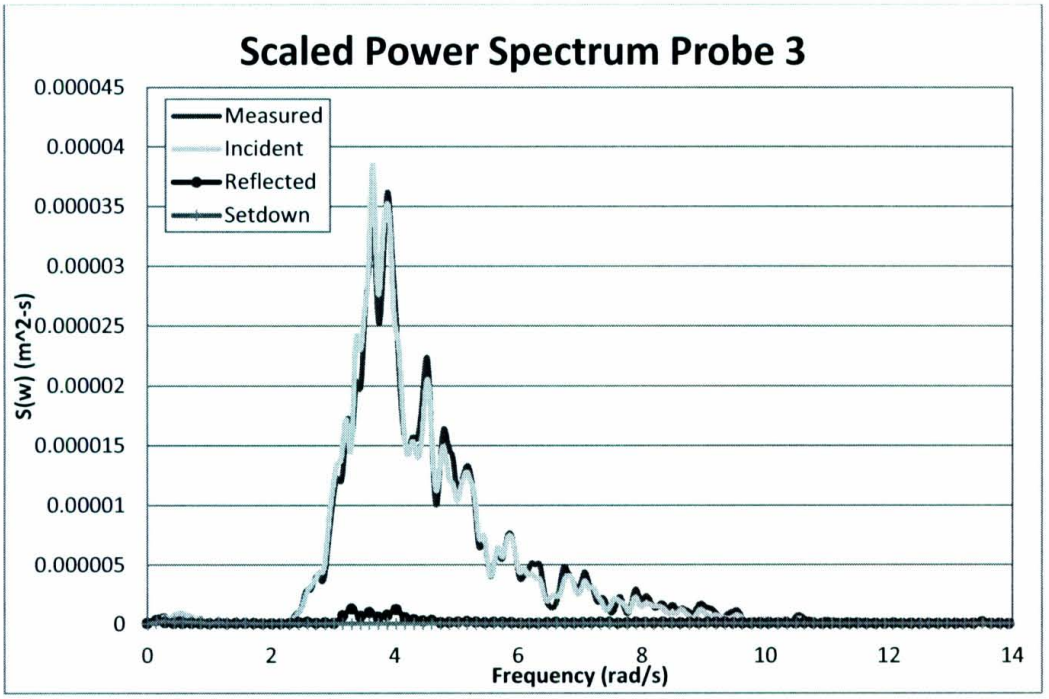
Scaled Power Spectrum Probe 3
Measured
Incident
Reflected
Setdown
S(w) (m^2-s)
0.000045
0.00004
0.000035
0.00003
0.000025
0.00002
0.000015
0.00001
0.000005
0
0
2
4
6
8
10
12
14
Frequency (rad/s)

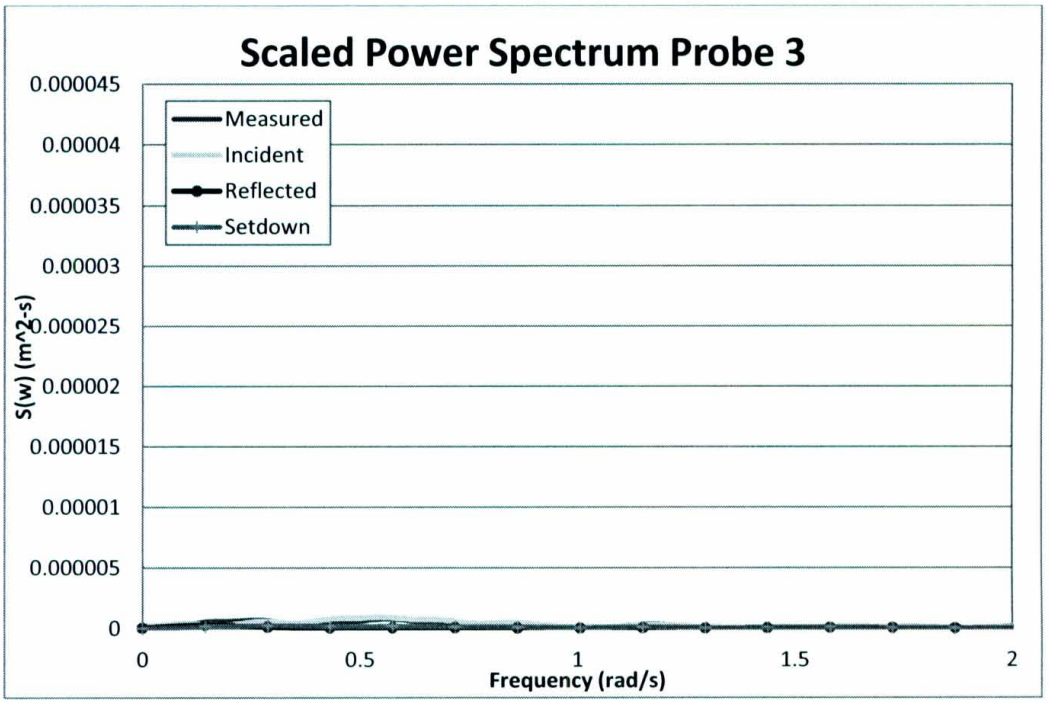
Scaled Power Spectrum Probe 3
Measured
Incident
Reflected
Setdown
S(w) (m^2-s)
0.000045
0.00004
0.000035
0.00003
0.000025
0.00002
0.000015
0.00001
0.000005
0
0
0.5
1
1.5
2
Frequency (rad/s)

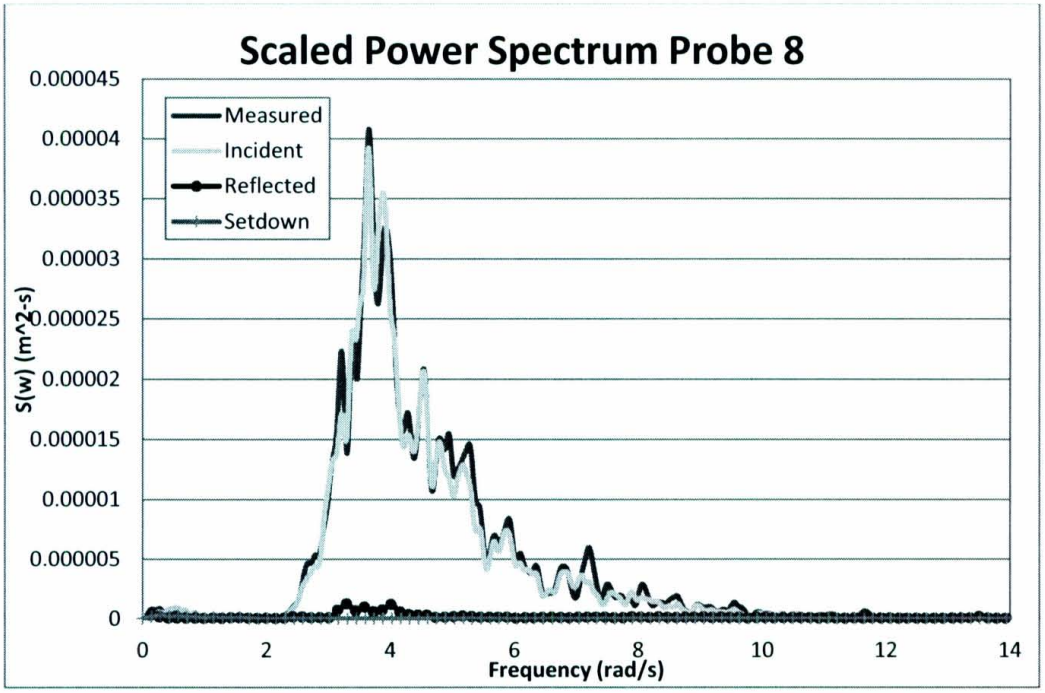
Scaled Power Spectrum Probe 8
Measured
Incident
Reflected
Setdown
S(w) (m^2-s)
0.000045
0.00004
0.000035
0.00003
0.000025
0.00002
0.000015
0.00001
0.000005
0
0
2
4
6
8
10
12
14
Frequency (rad/s)

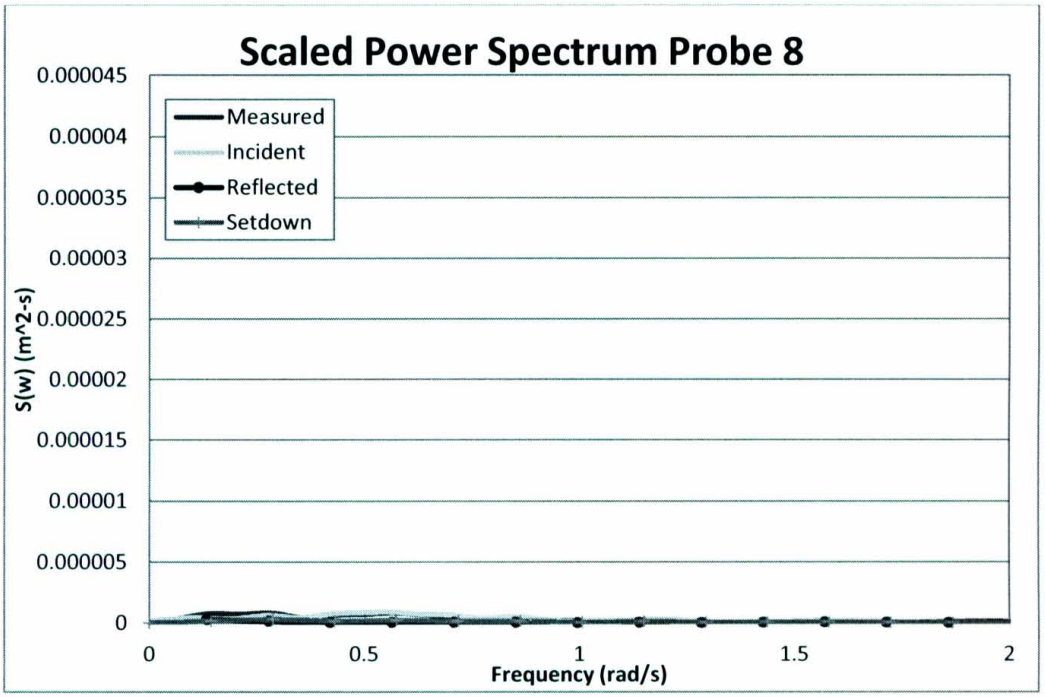
Scaled Power Spectrum Probe 8
Measured
Incident
Reflected
Setdown
S(w) (m^2-s)
0.000045
0.00004
0.000035
0.00003
0.000025
0.00002
0.000015
0.00001
0.000005
0
0
0.5
1
1.5
2
Frequency (rad/s)

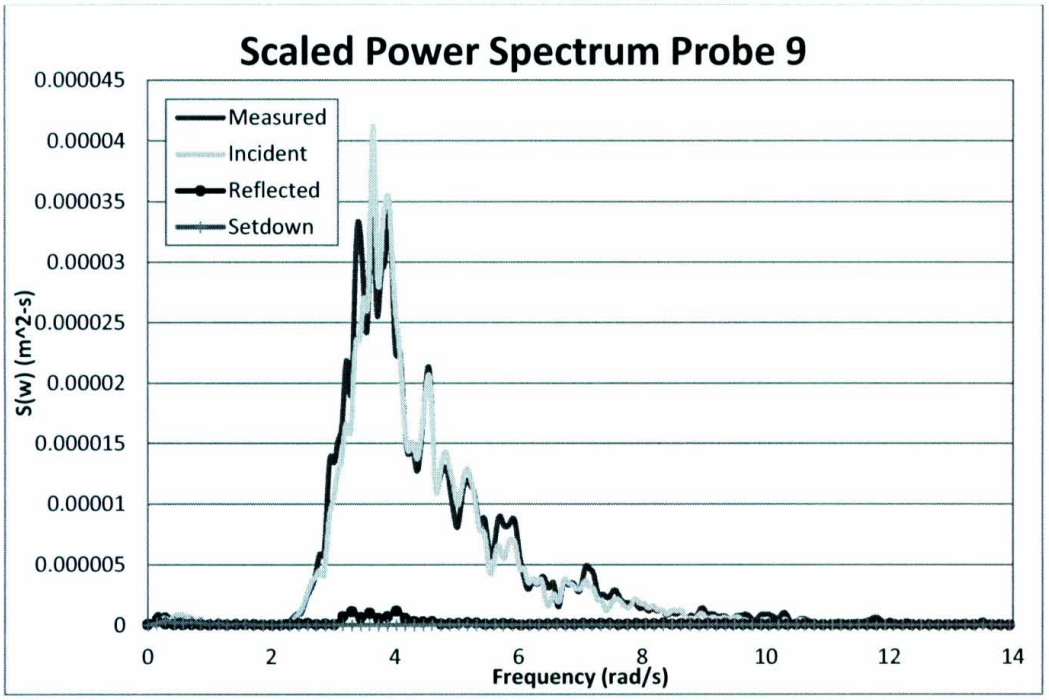
Scaled Power Spectrum Probe 9
Measured
Incident
Reflected
Setdown
S(w) (m^2-s)
0.000045
0.00004
0.000035
0.00003
0.000025
0.00002
0.000015
0.00001
0.000005
0
0
2
4
6
8
10
12
14
Frequency (rad/s)

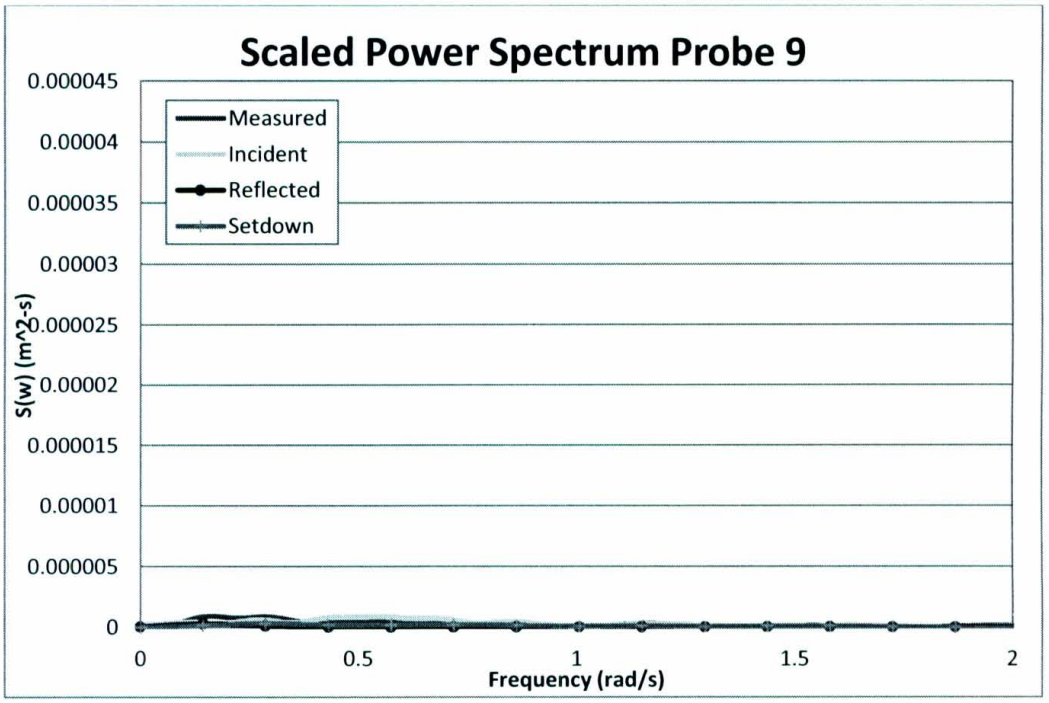
Scaled Power Spectrum Probe 9
Measured
Incident
Reflected
Setdown
S(w) (m^2-s)
0.000045
0.00004
0.000035
0.00003
0.000025
0.00002
0.000015
0.00001
0.000005
0
0
0.5
1
1.5
2
Frequency (rad/s)

APPENDIX C – FULL SCALE RESULTS

Full Scale

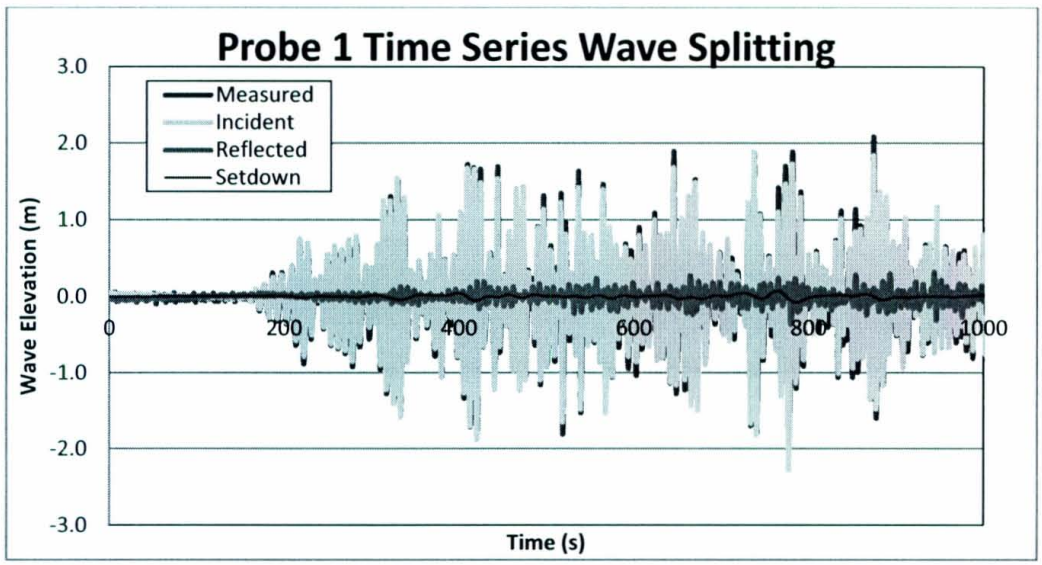

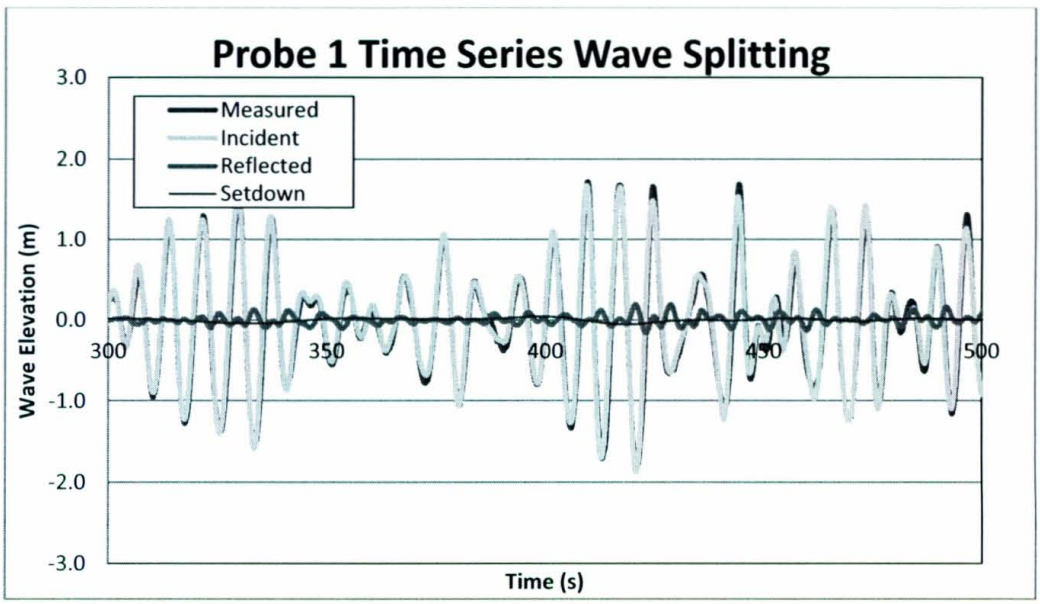

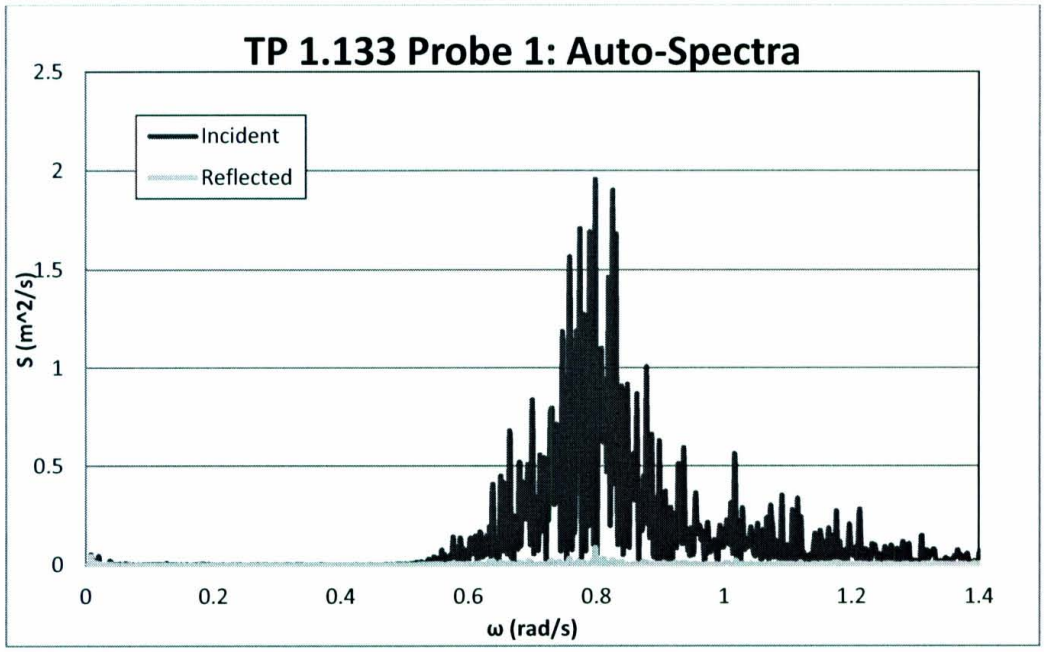
TP 1.133 Probe 1: Auto-Spectra
Incident
Reflected
S (m^2/s)
ω (rad/s)
0
0.5
1
1.5
2
2.5
0.2
0.4
0.6
0.8
1.2
1.4

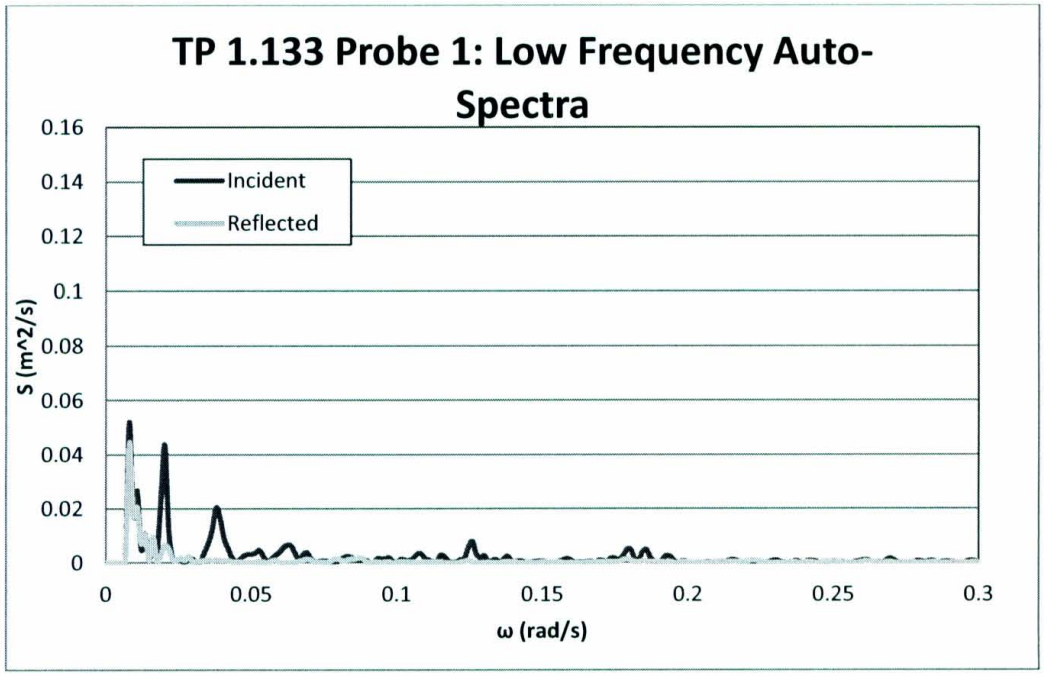
TP 1.133 Probe 1: Low Frequency Auto-Spectra
Incident
Reflected
S (m^2/s)
ω (rad/s)
0
0.02
0.04
0.06
0.08
0.1
0.12
0.14
0.16
0.05
0.15
0.2
0.25
0.3

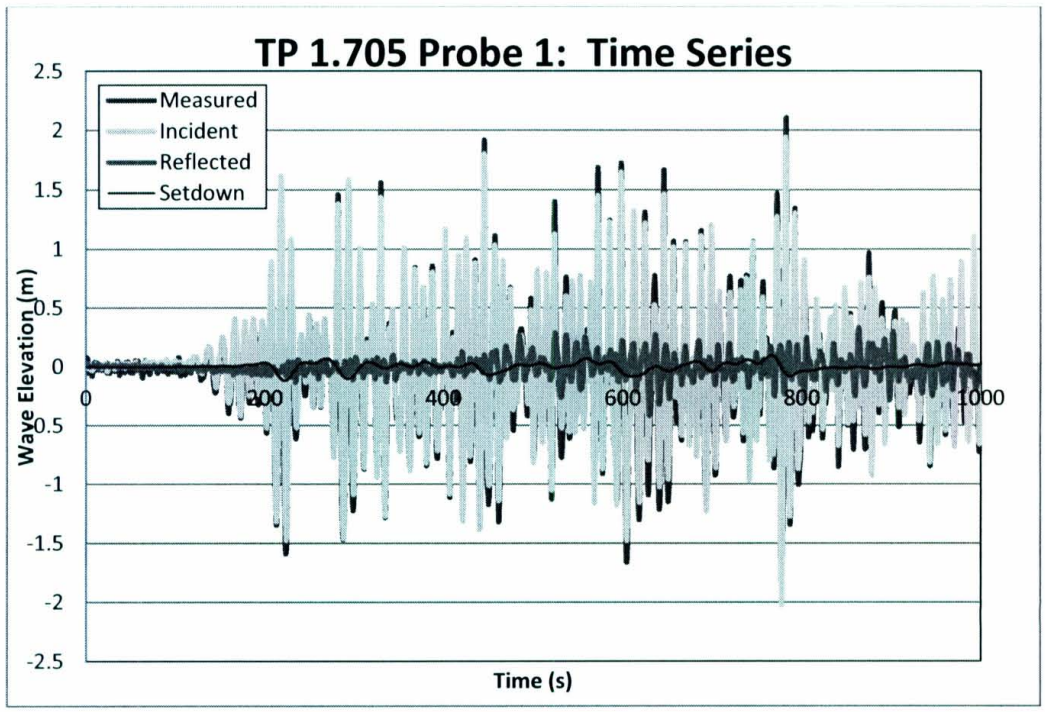
TP 1.705 Probe 1: Time Series
Measured
Incident
Reflected
Setdown
Wave Elevation (m)
Time (s)
2.5
2
1.5
1
0.5
0
-0.5
-1
-1.5
-2
-2.5
0
200
400
600
800
1000

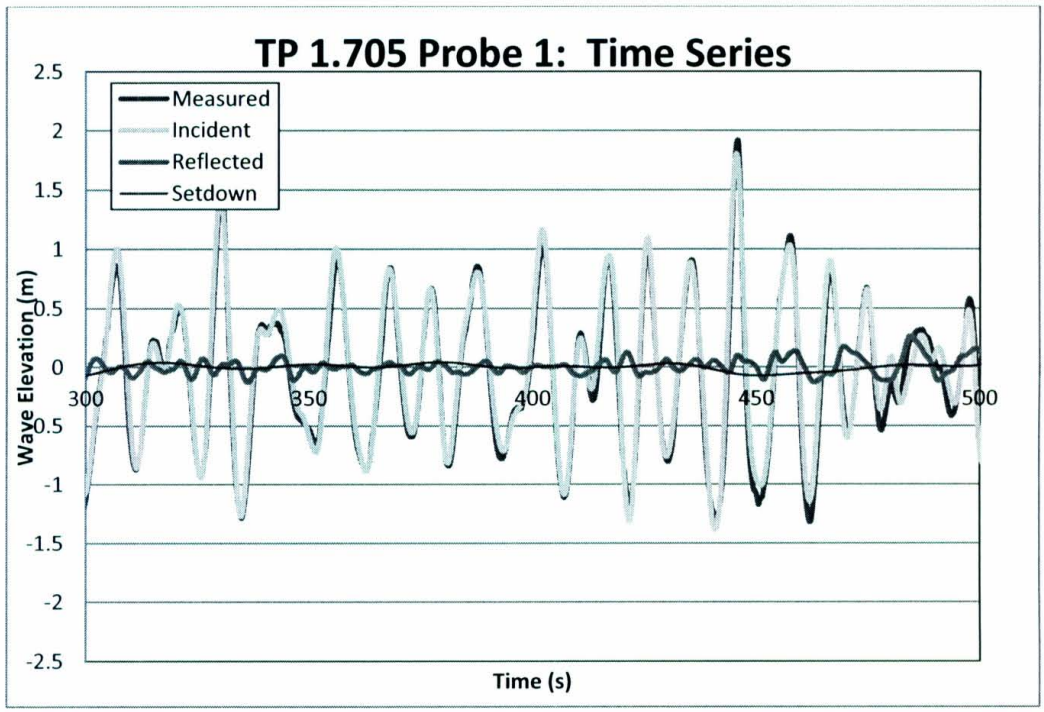
TP 1.705 Probe 1: Time Series
Measured
Incident
Reflected
Setdown
Wave Elevation (m)
Time (s)
2.5
2
1.5
1
0.5
0
-0.5
-1
-1.5
-2
-2.5
300
350
400
450
500

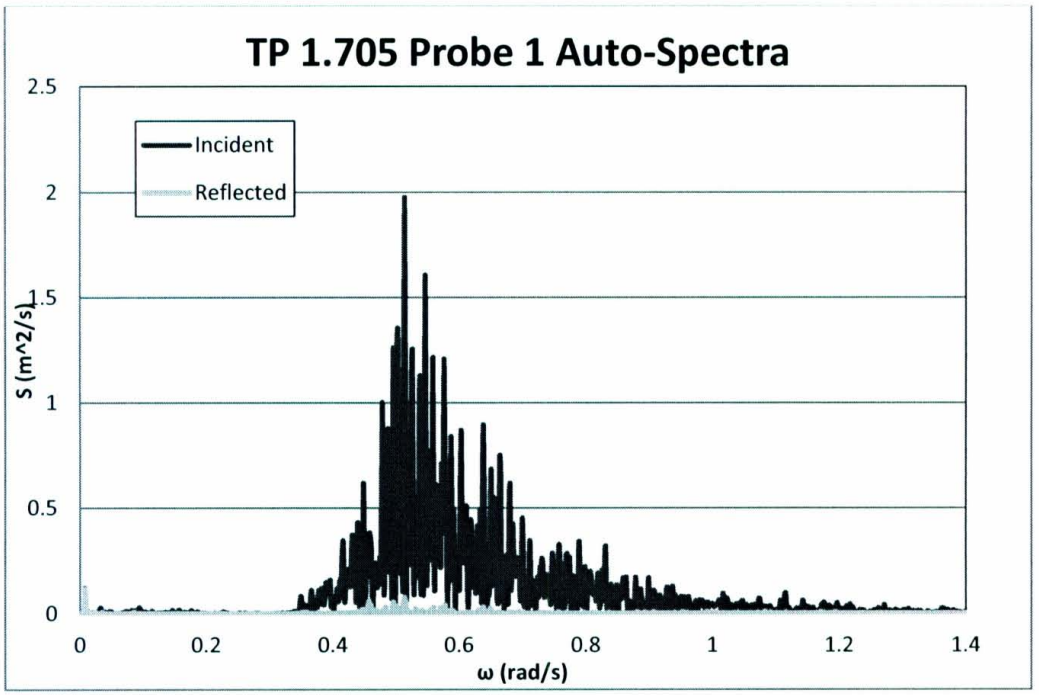
TP 1.705 Probe 1 Auto-Spectra
Incident
Reflected
S (m^2/s)
ω (rad/s)
0
0.5
1
1.5
2
2.5
0.2
0.4
0.6
0.8
1.2
1.4

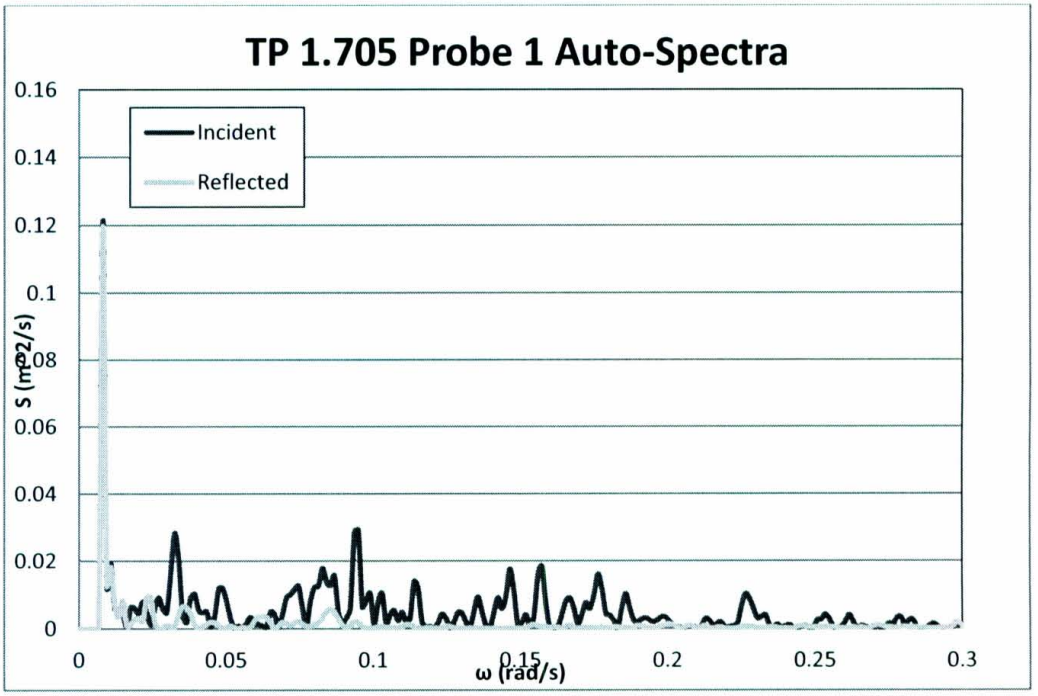
TP 1.705 Probe 1 Auto-Spectra
Incident
Reflected
S (m^2/s)
ω (rad/s)
0
0.02
0.04
0.06
0.08
0.1
0.12
0.14
0.16
0.05
0.15
0.2
0.25
0.3

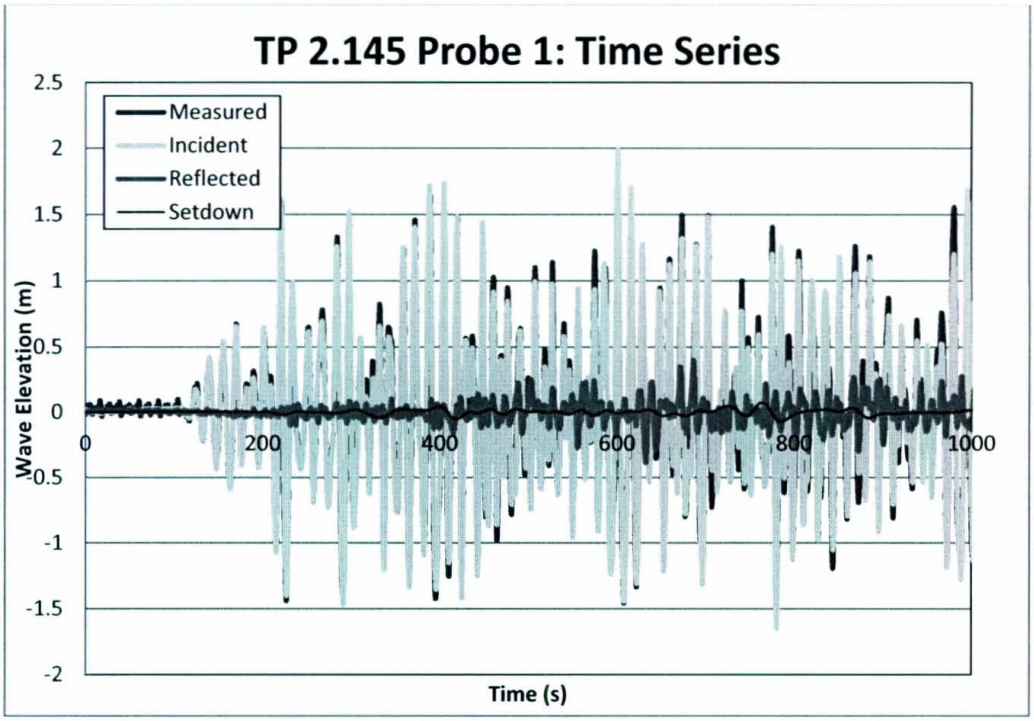
TP 2.145 Probe 1: Time Series
Measured
Incident
Reflected
Setdown
Wave Elevation (m)
Time (s)
2.5
2
1.5
1
0.5
0
-0.5
-1
-1.5
-2
0
200
400
600
800
1000

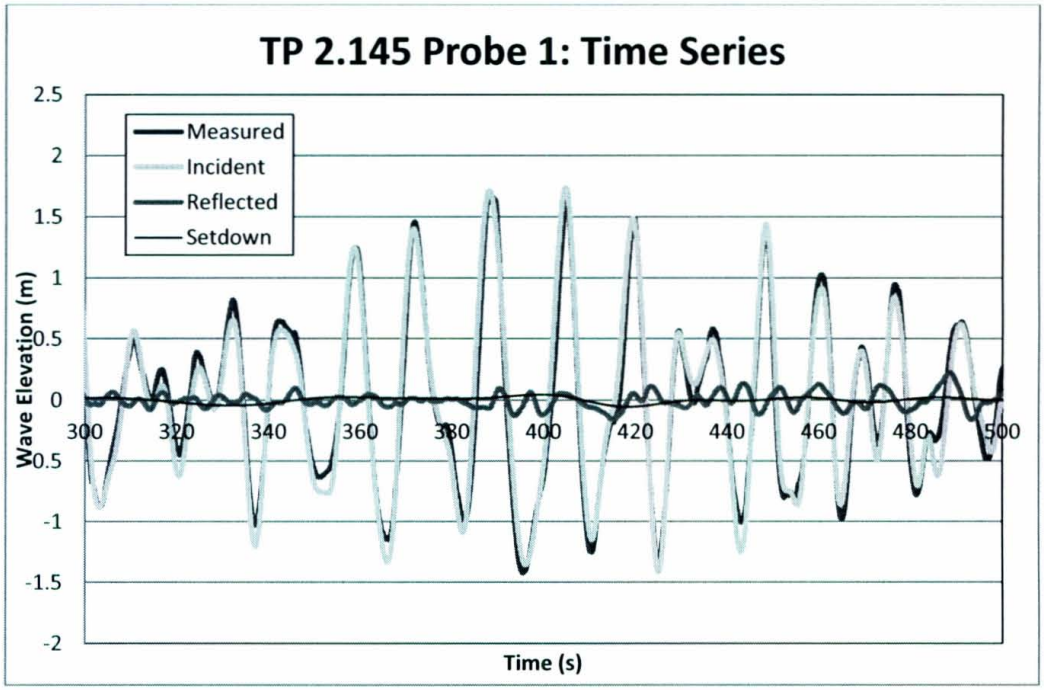
TP 2.145 Probe 1: Time Series
Measured
Incident
Reflected
Setdown
Wave Elevation (m)
Time (s)
2.5
2
1.5
1
0.5
0
-0.5
-1
-1.5
-2
300
320
340
360
380
400
420
440
460
480
500

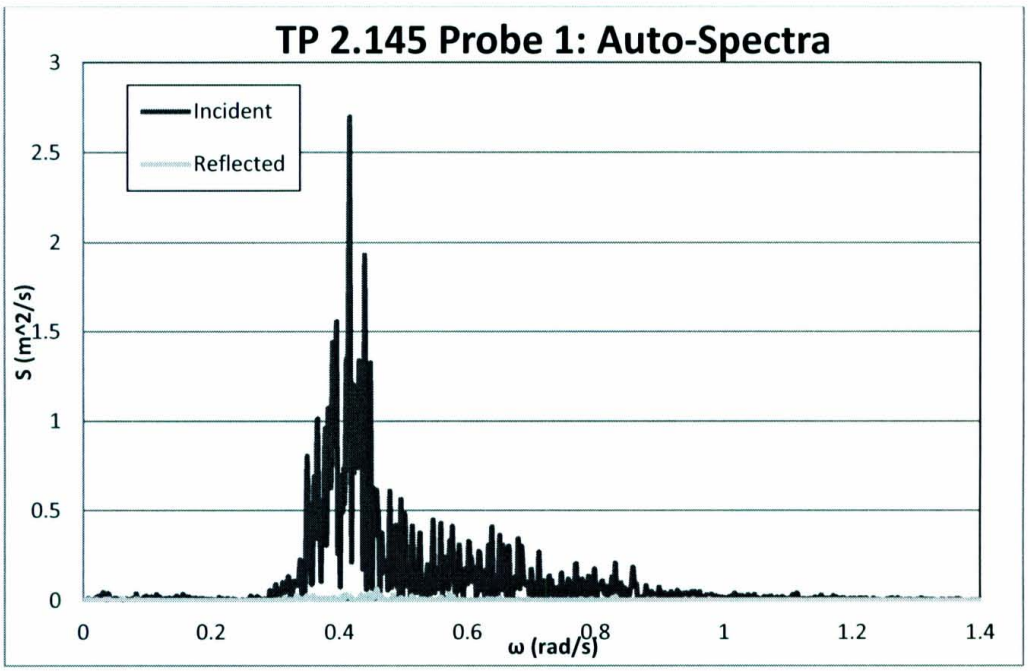
TP 2.145 Probe 1: Auto-Spectra
Incident
Reflected
S (m^2/s)
ω (rad/s)
0
0.5
1
1.5
2
2.5
3
0.2
0.4
0.6
0.8
1.2
1.4

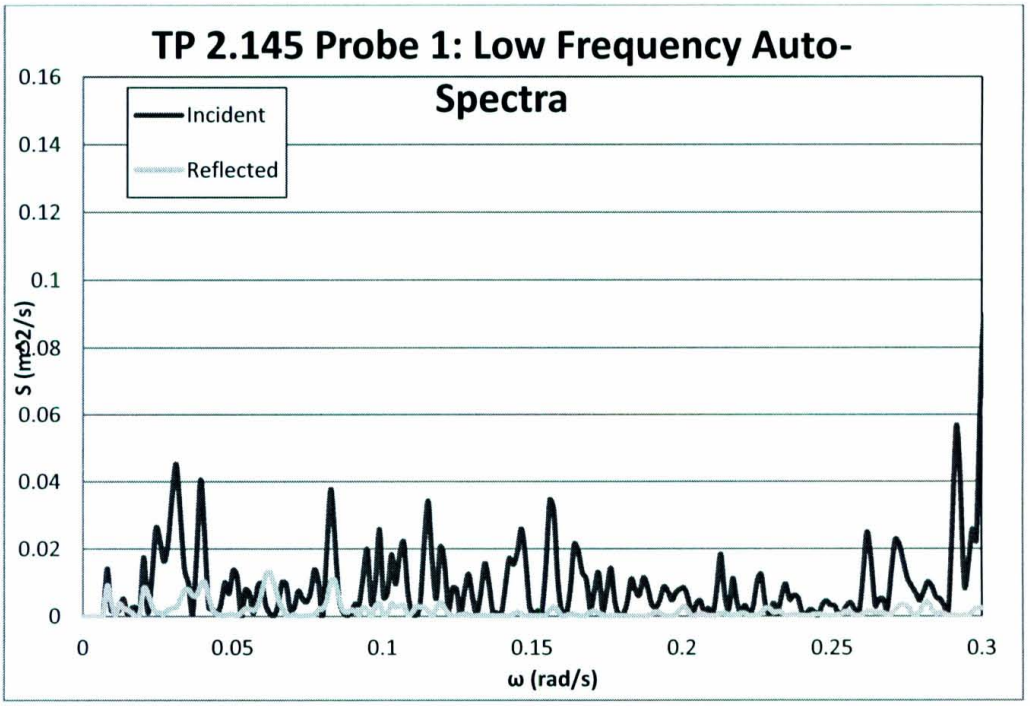
TP 2.145 Probe 1: Low Frequency Auto-Spectra
Incident
Reflected
S (m^2/s)
ω (rad/s)
0
0.02
0.04
0.06
0.08
0.1
0.12
0.14
0.16
0.05
0.15
0.2
0.25
0.3